Tampere University

LAURA SALO

Characterization and Development of Electrical Methods for Aerosol Measurement

LAURA SALO

Characterization and Development of Electrical Methods for Aerosol Measurement

ACADEMIC DISSERTATION
To be presented, with the permission of
the Faculty of Engineering and Natural Sciences
of Tampere University,
for public discussion in the auditorium TB104
of Tietotalo, Korkeakoulunkatu 1, Tampere,
on June 16th, 2023, at 12 o'clock.

ACADEMIC DISSERTATION
Tampere University, Faculty of Engineering and Natural Sciences
Finland

Responsible supervisor and Custos	Professor Topi Rönkkö Tampere University Finland	
Supervisor	Professor Jorma Keskinen Tampere University Finland	
Pre-examiners	Docent Juha Kangasluoma University of Helsinki Finland	Professor Martin Fierz University of Applied Sciences and Arts Northwestern Switzerland Switzerland
Opponent	Assistant Professor Naomi Zimmerman The University of British Columbia Canada	

The originality of this thesis has been checked using the Turnitin OriginalityCheck service.

HIILINEUTRAALI PAINOTUOTE
ClimateCalc CC-000025/FI
PunaMusta Printing

Carbon dioxide emissions from printing Tampere University dissertations have been compensated.

ABSTRACT

Aerosol particle research is motivated by the negative influence of particles on human health and air quality, as well as their impact on climate. Despite overwhelming evidence of their serious potential to do harm, only very few places have particle concentrations that do not exceed guideline values. To reduce particle pollution, we must also understand their sources. For these reasons, air quality monitoring is still of utmost importance. The World Health Organization provides guideline values for particle mass concentration, but many studies now point out that particle surface area concentration and particle number concentration may be crucial in determining the toxicity of a particle population.

This thesis presents aerosol measurement methods which are based on the electrical detection of aerosol particles, building up to the presentation of a novel electrical measurement method. The background section provides an overview of why different methods and metrics are necessary for aerosol measurement, and summarizes current knowledge on particle charging, both naturally in ambient air and through purposeful diffusion charging. The results first present electrical measurement methods in comparison to traditional filter-based techniques. Then electrical methods are employed in different surroundings to measure lung-depositing surface area (LDSA) and the LDSA concentration is compared to the particle mass concentration. Cheaper, sensor-type instruments for LDSA measurement are also evaluated in comparison to more expensive research grade instrumentation. Finally, the thesis presents the new measurement method, based on employing the natural charge of particles.

Based on the results presented in this thesis, sensor-type measurements are dependable for long-term particle monitoring; however, more intensive measurements are required as well, and sensors must be chosen to fit the monitored environment. For example, measurements in a roadside environment near Delhi and in Helsinki revealed that both particle concentrations and particle distributions differ significantly. Employing the novel measurement method in highly polluted air revealed that particle charging with a charger is unnecessary for detection, as the naturally occurring charge is enough for detection and monitoring.

TIIVISTELMÄ

Aerosolihiukkasia tutkitaan erityisesti hiukkasten haitallisten terveys- ja ilmanlaatuvaikutusten, sekä ilmastokytköksen takia. Vaikka tutkimustietoa haittavaikutuksista terveydelle on runsaasti, vain harvoilla alueilla hiukkaspitoisuudet ovat terveelliselle ilmalle vaadituissa rajoissa. Hiukkaspäästöjen vähentämiseksi täytyy myös tuntea niiden lähteet. Siksi edelleen on tarve pitkäaikaisille hiukkasten mittausmenetelmille. Maailmanterveysjärjestö WHO määrittelee toistaiseksi suositeltavia maksimipitoisuuksia vain hiukkasten massalle, mutta uusimpien tutkimusten mukaan hiukkasten pinta-ala tai lukumäärä saattavat olla terveyden kannalta ratkaisevassa roolissa.

Tässä työssä esitellään eri aerosolimittausmenetelmiä, jotka perustuvat hiukkasten sähköiseen havainnointiin. Työssä lähdetään olemassa olevista menetelmistä ja esitellään lopuksi uusi, hiukkasten luonnolliseen varaukseen perustuva mittausmenetelmä. Teoriaosuudessa taustoitetaan tarvetta erilaisille menetelmille ja mittausmetriikoille, sekä tiivistetään nykytietämys hiukkasten varautumisesta niin ilmakehässä kuin varaajissa. Tuloksissa esitellään ensin perinteisiä keräykseen perustuvia mittalaitteita ja verrataan niitä sähköisiin menetelmiin. Hiukkasten keuhkodeposoituvaa pinta-alaa mitataan sähköisesti ja tämän pinta-alan suhdetta hiukkasten massaan tutkitaan eri ympäristöissä. Lisäksi verrataan anturityyppisiä edullisia mittalaitteita kalliimpiin tutkimuslaitteisiin. Lopuksi esitellään hiukkasten luonnolliseen varaukseen perustuva täysin uudenlainen mittausmenetelmä.

Anturityyppiset mittalaitteet ovat tutkimuksen perusteella luotettavia laitteita hiukkasten pitkäaikaiseen seurantaan. Kuitenkin myös korkeampitasoisia mittauksia vaaditaan, ja sopiva anturi täytyy valita kohteen mukaan. Esimerkiksi Delhin laidalla, tienvarsiympäristössä, sekä hiukkasten pitoisuus että kokojakauma poikkeavat merkittävästi Helsingin tienvarsiympäristöstä. Uuden varaukseen pohjautuvan mittausmenetelmän käyttö hyvin saastuneessa kaupunki-ilmassa osoitti, että hiukkasten varaaminen erillisellä varaajalla tienvarsiympäristössä ei ole tarpeellista, vaan hiukkasten havaitsemiseen ja seurantaan riittää niiden luonnollinen varaus.

ACKNOWLEDGEMENTS

I thank my supervisors Professors Topi Rönkkö and Jorma Keskinen. Topi helped me see the bigger picture and find coherence where I thought there was none to be found. Discussions with Jorma helped me develop my thinking towards an instrumentalist perspective. You were always generous and kind towards me and I have felt safe to be myself and grow as a scientist. I express my sincerest gratitude to Professor Martin Fierz and Docent Juha Kangasluoma for providing thoughtful pre-examinations.

I am indebted to the wonderful and helpful members of the Aerosol Physics Laboratory—thank you for creating an atmosphere of fun and whimsy in the lab. I have gotten to know many of you very well and some of my fondest work memories are problem-solving together during measurement campaigns. Thank you also to colleagues from the Finnish Meteorological Institute, the Helsinki Region Environmental Services Authority, the University of Eastern Finland, Tallinn Technical University, the Estonian Environmental Research Centre, the Energy and Resources Institute in Delhi and Dekati.

Last but not least, I thank my friends and family. Sampsa, Nikla, Anni and Anna—thank you for days and nights spent fishing, cooking, playing board games, dancing and just hanging out. Thank you, mom and dad, and Aino-Liina and Linda, you have been so supportive of me becoming a doctor and none of you ever doubted that I could. And the very final thanks go to Taco, who showered me with

CONTENTS

List of Figures

List of Tables

SYMBOLS AND ABBREVIATIONS

ASA	Active surface area or active surface area concentration when used as a unit, $\mu m^2/cm^3$
BC	Black carbon
C_c	Cunningham slip correction factor
CPC	Condensation Particle Counter
D_p	Particle (mobility) diameter, m
DBDC	Delhi Bus Driving Cycle
DC	Diffusion Charging, Diffusion Charged
Delhi-NCR	Delhi National Capital Region
DMA	Differential Mobility Analyzer
DOC	Diesel Oxidation Catalyst
DPF	Diesel Particulate Filter
e	Elementary charge, $1.6022 \cdot 10^{-19}$ C
E	Electric field strength, V/m
ELPI	Electrical Low-Pressure Impactor
ELPI+	A newer model of the original ELPI
$F_{alveolar}$	Function for particle alveolar deposition probability
f	Function for particle charge number probability
FCAE	Faraday-cup and electrometer
$I_\pm$	Current from one polarity of particles, fA
ICP	Inherently Charged Particle
ICRP	International Commission on Radiological Protection
k	Boltzmann constant, $1.381 \cdot 10^{-23}$ J/K
L	Electrode length, m
LDSA	Lung-Deposited Surface Area concentration
n	Number of elementary charges
$n_{avg\pm}$	Average number of charges for particles of one polarity
N_{ion}	Ion concentration, $1/cm^3$ or $1/m^3$
N	Total particle number concentration, $1/cm^3$

$N(D_p)$	Particle number size distribution, $1/cm^3$
NAIS	Neutral Cluster and Air Ion Spectrometer
P	Particle penetration
PM2.5	Particle mass concentration of sub 2.5 μm particles, $\mu g/m^3$
PM10	Particle mass concentration of sub 10 μm particles, $\mu g/m^3$
PN	Particle number
Pn	Combined particle penetration and number of elementary charges
Q	Charge, C
Q_{flow}	Volumetric flowrate, lpm or m^3/s
r_i	Inner diameter, m
r_o	Outer diameter, m
SCAR	Singly Charged Aerosol Reference
SMPS	Scanning Mobility Particle Sizer
T	Temperature, K
UFP	Ultrafine particles
V	Voltage, V
v_E	Particle velocity in an electric field, m/s
WHO	World Health Organization
Z	Particle electrical mobility, $m^2/(V{\cdot}s)$
Z_0	Limiting particle electrical mobility, $m^2/(V{\cdot}s)$
Z_{ion}	Ion electrical mobility, $m^2/(V{\cdot}s)$
α	Ion recombination rate, $1/s$
β	Rate of ion attachment to aerosol particles, $1/s$
$\lambda_{\pm}$	Charge density or concentration for one polarity, fC/cm^3
μ	Dynamic viscosity, Pa·s
Φ	Ion production rate $1/s$

LIST OF PUBLICATIONS

Paper I   Salo, L., Mylläri, F., Maasikmets, M., Niemelä, V., Konist, A., Vainumäe, K., Kupri, H. L., Titova, R., Simonen, P., Aurela, M., Bloss, M., Keskinen, J., Timonen, H., & Rönkkö, T. (2019). Emission measurements with gravimetric impactors and electrical devices: An aerosol instrument comparison. Aerosol Science and Technology, 53(5), 526–539. doi: 10.1080/02786826.2019.1578858

Paper II   Salo, L., Rönkkö, T., Saarikoski, S., Teinilä, K., Kuula, J., Alanen, J., Arffman, A., Timonen, H., & Keskinen, J. (2021). Concentrations and Size Distributions of Particle Lung-deposited Surface Area (LDSA) in an Underground Mine. Aerosol and Air Quality Research, 21, 1–25. doi: 10.4209/aaqr.200660

Paper III   Salo, L., Hyvärinen, A., Jalava, P., Teinilä, K., Hooda, R. K., Datta, A., Saarikoski, S., Lintusaari, H., Lepistö, T., Martikainen, S., Rostedt, A., Sharma, V. P., Rahman, M. H., Subudhi, S., Asmi, E., Niemi, J. V., Lihavainen, H., Lal, B., Keskinen, J., Kuuluvainen, H., Timonen, H., Rönkkö, T. (2021). The characteristics and size of lung-depositing particles vary significantly between high and low pollution traffic environments. Atmospheric Environment, 255(March). doi: 10.1016/j.atmosenv.2021.118421

Paper IV   Salo, L., Rostedt, A., Kuuluvainen, H., Teinilä, K., Hooda, R.K., Rahman, Md. H., Datta, A., Sharma, V.P., Subudhi, S., Hyvärinen, A., Timonen, H., Asmi, E., Martikainen, S., Karjalainen, P., Lal, B., Keskinen, J., Rönkkö, T. (2023). Inherently Charged Particle (ICP) Sensor Design. IEEE Sensors. doi: 10.1109/JSEN.2022.3232509

AUTHOR'S CONTRIBUTION

This thesis consists of four scientific papers detailing original experimental research. Each paper is the result of scientific collaboration between universities, science institutes and companies. My contribution to each paper along with that of other doctoral researchers from Tampere University is detailed below.

Paper I   The measurements for this Paper were performed in Tallinn, Estonia in collaboration with Tallinn University of Technology, Estonian Environmental Research Centre, and the Finnish Meteorological Institute. I participated in the measurement campaign, wrote the first draft of the paper, handled part of the data, analyzed the results, and created the figures for the paper. Pauli Simonen also participated in the campaign and edited the final manuscript.

Paper II   The measurement campaign for this Paper was in Kemi, in an underground mine. The mining company provided the facilities, and research was conducted in collaboration with the Finnish Meteorological Institute. I participated in the measurements, handled the data from the sensors, and analyzed all of the data. I wrote the experimental section, the results and conclusion of the first draft of the manuscript and created all of the figures.

Paper III This paper involved two intensive campaigns: one in India near Delhi and one in Helsinki, Finland. The measurements in India were facilitated by the Indian Oil Corporation in Faridabad and involved collaboration with The Energy and Resources Institute as well as the Finnish Meteorological Institute. The campaign in Finland was facilitated by Helsinki Regional Services and The Finnish Meteorological Institute. I organized parts of both campaigns, participated in the measurements, handled most of the data, and wrote most of the original manuscript. Henna Lintusaari and Teemu Lepistö organized and participated in the campaign in Helsinki. Teemu calculated the air mass trajectories included in the supplement, validated the ELPI+ data from Helsinki and provided

the code for calculating the LDSA. Sampsa Martikainen participated in organizing the measurement campaign in India. All three edited the final manuscript.

Paper IV   This Paper contains data from the same campaign in India as Paper III, as well as data from an engine laboratory measurement in the Indian Oil Corporation facilities. Again, The Energy and Resources Institute as well as the Finnish Meteorological institute collaborated on this research. I created the CAD-model and technical drawings of the mobility analyzer. I performed the calibration measurements and participated in the two campaigns mentioned above. I handled all of the data analysis and wrote the first draft of the manuscript. Sampsa Martikainen had a major role in the measurements for the engine laboratory campaign and edited the final manuscript.

1   INTRODUCTION

The ambient air all around us is an aerosol. Aerosol particles occur both naturally and due to human activity. In urban areas, the most important anthropogenic sources of aerosol particles are traffic (road dust and engine exhaust), biomass combustion and industry (Hopke et al., 2020). Inhaling one breath of air introduces millions of tiny particles into your respiratory tract, and about half of those are released back into the air as you breathe out, but the rest are deposited into your nasal cavity, throat, mouth, and lungs. While it may sound alarming, the mass of the inhaled particles is tiny, only about one millionth of one gram. Still, in large amounts or over long exposure times these particles are very harmful: globally 7.8 % of all deaths are attributable to air pollution (Ritchie & Roser, 2022).

In addition to air quality concerns, aerosol particles play a part in the global climate. Particles are required for cloud formation as they act as condensation nuclei for water vapor, and they contribute to the radiative forcing of the atmosphere (both directly and indirectly through cloud formation). Currently, aerosols are thought to have a net cooling effect; however, the margins of uncertainty are large and some compounds, such as black carbon, are estimated to have a net positive contribution (J. Li et al., 2022). Adding to the uncertainties, global warming is likely to change the makeup of atmospherics aerosols (Gettelman et al., 2016; Jacob & Winner, 2009). Increased temperatures are leading to an increase in sea salt aerosol production (Paulot et al., 2020) and more devastating wildfires (Emmerson & Keywood, 2021; Hoover & Hanson, 2021; San-Miguel-Ayanz et al., 2020; United Nations Environment Programme, 2022), while increased humidity will affect the optical properties of aerosol particles (Gettelman et al., 2016). Direct anthropogenic emissions are also changing as a result of policies meant to improve air quality or reduce climate impacts.

These two motivating factors, air quality and climate, drive research into ways to limit emissions at their sources as well as developing monitoring techniques. Electrical methods excel at measuring with a high time resolution, and they can cover many magnitudes of particle concentrations as well as a wide range of particle sizes. In this thesis, electrical particle measurement methods are compared and evaluated,

aerosols in different environments are considered from a health perspective, and finally, a new measurement methodology is introduced.

1.1   Aerosols and their impact on air quality and health

Air pollution (fine particles and ozone) as a risk factor for death is trumped only by smoking and high blood pressure, making it the most important environmental risk factor: recent estimates for deaths due to all sources of air pollution give a range of 6.7 to 8.8 million deaths annually worldwide (data gathered by Ritchie & Roser (2022), original sources Health Effects Institute (2020) and Lelieveld et al. (2019)). These estimates have increased compared to earlier research, for example, Lelieveld previously estimated 3.3 million annual deaths (2015). The World Health Organization (WHO) guideline value for PM2.5 (mass concentration of sub 2.5 μm particles) in outdoor air is 5 μg/m³. Unfortunately, 95 % of the world's population live in areas where even the previous guideline value of 10 μg/m³ is exceeded.

An intuitive effect of inhaling too many particles is respiratory problems, but literature shows that strokes, heart attacks and other cardiovascular problems are also a major health consequence. While respiratory outcomes are a result of long-term exposure to air pollution, cardiovascular effects are usually acute, occurring within hours to days of exposure (Brook et al., 2010).

The physicochemical properties of particles matter when it comes to health effects. While mass concentration, rather than number concentration or chemical makeup, is the only metric for which there are air quality guidelines, it is not a perfect metric for predicting health outcomes. The per mass unit toxicity of particles varies from country to country (X. Li et al., 2019), and it is reasonable to think that this is due to differences in chemistry, size, or morphology.

Perhaps eventually a multivariate model incorporating all these particle attributes will be developed, but for now, there is laboratory evidence that surface area is a better predictor than particle mass or number of acute health effects, at least for insoluble particles (Oberdörster, 1996; Schmid & Stoeger, 2016). There are two ways that particle surface influences toxicity. Firstly, when a particle is deposited in the lungs, the particle surface is the site where reactions happen. Additionally, particles act as condensation nuclei for semi-volatile vapors, thus an otherwise innocuous particle can carry a toxic substance on its surface, allowing it to also enter the lungs. Particle size influences where in the respiratory tract particles are deposited (if at all).

Very small and very large particles deposit easily, the former due to diffusion and the latter due to impaction mechanisms.

1.2   A brief history of electrical methods for aerosol measurement

This section presents major milestones which led to the instruments employed in the experimental research for this thesis.

Scientists in the late 19th century, most notably John Aitken, discovered that aerosol particles were a prerequisite of fog, and that combustion created many more of these *nuclei* around which the fog was able to form (Aitken, 1881, 1895). At the time, fogs were considered a nuisance due to poor visibility, rather than a health concern, as associated deaths were blamed on cold weather instead (Russell, 1926). However, in a 1925 article ("The Measurement of Atmospheric Dust," 1925) published in The Lancet, the author writes "The importance of atmospheric dust as a cause of respiratory disease has long been recognized." The author goes on to give two other reasons for aerosol measurement: high dust concentrations can cause explosions (relevant in coal mines) and cloud formation. Although not mentioned in the Lancet article, aerosols were already known to directly affect climate as well. In a review of aerosols by Aldrich (1927), atmospheric effects of volcano eruptions are presented (Abbot & Fowle, 1913). Additionally, a book by William Humphreys (1920) presented the total effect of dust particles on Earth's temperature, calculated to have a cooling effect.

Electrical aerosol measurement began as a separate endeavor. The following advancements are summarized based on the "History of Electrical Aerosol Measurements" by Flagan (1998), original sources are cited where possible.

Quite soon after Aitken discovered particles through optical means, the same particles were discovered through an entirely different avenue. Atmospheric electrical conductivity interested scientists at the turn of the century as they sought to better understand the nature of electricity. The *coaxial condenser* was introduced for ion measurement from flames by McClelland (1898) and a similar instrument by Gerdien, the *Gerdien condenser,* for atmospheric ion measurement (1905). Aerosol particles were first observed with this method by Langevin (1950). He reported measurements of ions with surprisingly low mobilities, so-called *large ions*, which corresponded to what are now called accumulation mode particles. Interested to learn more about these low-mobility ions, McClelland and Kennedy built a huge (5.5-

m-long) rectangular condenser and measured the large ions in 30-minute intervals. They noted a large variation in measured concentrations, realizing the need for higher time resolution measurement. For decades, the coaxial condenser remained the primary measurement method of large ions. In 1970, Israël published a full ion concentration spectrum from 0.1 nm to 10 µm, recreated in Flagan's history review (1998, p. 322).

A first version of the *differential mobility analyzer* (DMA) was built in 1920. Methods for charging aerosol particles were used early on, either to bring the aerosol population to an equilibrium charge state or to simply increase the charge to allow easier detection. *Unipolar diffusion charging*, with ions produced using a corona wire or needle, is a widely used method in modern instruments targeting particles too small for optical detection (Biskos et al., 2005; Rostedt, 2018). Rohman (1923) built an instrument similar to the first DMA, but with the intention of measuring smoke particles. He incorporated a corona needle to ionize the particles. Later, the first diffusion charger was designed by Hewitt to aid particle detection (1957). Simultaneously, he also designed a DMA geometry with a sheath flow separate from the sample, and where the targeted particles would exit the condenser region through a slit instead of being collected. Some cite Hewitt's design as the first DMA. Liu and Pui improved upon Hewitt's design (1974a) for the purpose of producing monodisperse aerosol for the calibration of aerosol instruments, such as the nuclei counters introduced by Aitken.

Flagan's review of aerosol measurement history presented methods which relied on the electrical mobility of the ions and charged particles. A notable non-mobility-based instrument is the *Electrical low-pressure impactor* (ELPI) (Keskinen et al., 1992). In the instrument, particles are charged by diffusion charging, and then collected on consecutive impactor plates, each with a smaller and smaller particle cut-off size. The impactor plates are individually connected to a sensitive electrometer; hence the aerodynamic size distribution of particles can be obtained. An updated model of the original ELPI, the ELPI+ increased the number of impaction stages, allowing for a higher particle size resolution (Järvinen et al., 2014).

In recent years, electrical methods have been utilized in small, low-maintenance instruments often referred to as particle sensors. They generally employ unipolar diffusion charging and in the simplest instruments the output is the total current from the moving charge particles, while others use additional stages to classify particle by size before detection. Commercially available examples are Partector (Naneos) and AQ Indoor (Pegasor). While optical methods are able to detect

particles with diameters of 300 nm and above, electrical methods excel at a smaller size range; thus, their usage and development is likely to continue for some time.

1.3   Research objectives

The broader topic of this thesis are the various electrical detection methods available for aerosol measurement, and how they can fill in the gaps left by conventional mass-based measurements, especially when targeting exhaust emissions from road-traffic. Paper I deals with the reliability of different instruments for the measurement of particle mass concentration, and the comparison of online electrical methods with tradition offline sampling methods. Paper II and Paper III expand the usage of electrical detection methods to monitoring air quality in three different surroundings: an underground mine, a low-pollution traffic site and a high pollution traffic site. Paper IV presents a novel sensor for air quality monitoring: the Inherently Charged Particle (ICP) sensor. It is a culmination of the work and findings in the previous papers, informed by the typical particle concentrations and distributions which were measured as well as the challenges faced.

The specific research objectives can be summarized into four bullet points:

- Establish the validity of the ELPI+ as a reference instrument for particle measurement (Paper I)
- Compare results from commercially available sensors to the ELPI+, establish their strengths and weaknesses (Paper II)
- Explore the importance of different measurement metrics for characterizing different particle sizes and understanding particle sources, air quality, and health (Paper II and Paper III)
- Introduce the ICP-sensor for electrical particle detection using a novel method and investigate its performance and suitability for ambient monitoring (Paper IV)

2 TYPICAL AEROSOL PARTICLES IN TRAFFIC ENVIRONMENTS

The choice of aerosol instrumentation depends on what information is needed and how we aim to use it, as well as the properties of the aerosol itself. In this chapter we explore what is already known about aerosols originating from traffic and the concentrations and properties of aerosols found in urban air as well as in the special case of an underground mine—one of the most hazardous occupations both historically and still today, due in part to poor air quality.

Aerosol particles from traffic can be broadly divided into two groups: non-exhaust sources such as particles from the mechanical wear and tear of brakes, tires, and road surfaces and particles from engine emissions. Non-exhaust emissions contain both coarse and fine particles: road dust tends to be coarse (Fussell et al., 2022; Kovochich et al., 2021) whereas breaking can produce even nanoscale particles (Ingo et al., 2022; Kukutschová et al., 2011; Nosko et al., 2017). Exhaust emissions contain mainly fine and ultrafine particles (Kittelson, 1998; Myung & Park, 2012; Qian et al., 2019). Coarse particles are usually of lesser interest, as they deposit more easily, simply by gravitational settling, and thus have a shorter lifespan in the atmosphere than fine particles. That being said, coarse particles can become a nuisance in dry conditions, as is seen in many northern cities in the spring when the snow melts and studded tires grind paved roads causing high dust concentrations. Engine emissions produce much smaller particles (median size < 150 nm), but the concentration and exact size distribution depends on the fuel and engine lubricant as well as any after-treatment systems. For example, diesel-vehicles were previously notorious for their abundant particle emissions, but with the requirement for diesel particle filters (DPFs) and diesel oxidation catalysts (DOCs), particle emissions have dropped markedly—generally below corresponding gasoline-fueled cars (Platt et al., 2017).

Ambient urban aerosols are a mixture of primary particles and gases from emission sources, as well as products from chemical and physical processes in the atmosphere. While the precise composition varies, traffic is usually one of the main contributors to particle number concentration (Kumar et al., 2014; Rivas et al., 2020). Other direct particle sources can be emissions from factories and power plants

(Aurela et al., 2021; Mylläri et al., 2016; Pope, 1989), airports and harbors (Hudda et al., 2018; Pirjola et al., 2014), as well as smoke from biomass combustion for cooking and heating (Gustafsson et al., 2009; Krecl et al., 2008, 2023). Gaseous emissions from various sources can react chemically in the atmosphere to form new particles, while semi-volatile compounds can condense onto existing particles causing them to grow. Depending on parameters such as particle concentrations, particle sinks, weather, and climate, this secondary aerosol can linger and age, forming a steady urban background aerosol until eventually being removed by precipitation or winds.

Occupational surroundings can have high particle concentrations if the work processes require grinding or heating, and especially if the work is conducted indoors. A particularly challenging occupational environment for controlling aerosol pollution is an underground mine. Particles are released from the different mine activities, such as crushing rocks and blasting new tunnels, as well as the traffic of vehicles transporting materials and workers. The different particle emission sources lead to a variety of particle sizes and chemical compositions (Saarikoski et al., 2019) and the emissions cannot disperse properly without the help of mechanical ventilation. Ventilation requires energy and energy costs money, thus knowing when and where the air quality is poor is important for the efficient use of air exchangers (Grau III et al., 2002).

2.1   Particle sources, size distributions and concentrations

Urban aerosol particles vary in size from very tiny newly formed nucleation particles (< 30 nm) to soot mode particles (~30-300 nm) to accumulation mode particles (~200-1000 nm) all the way to coarse dust (up to 100 µm). These size ranges are guidelines rather than definitions, and different sources give slightly different ranges, as the typical modes also vary from place to place and between seasons. Additionally, the mode nomenclature differs between aerosol textbooks: the soot mode is also called the Aitken mode, and some texts refer to the soot mode as the accumulation mode. **Figure 1** illustrates an example of a three-mode urban aerosol particle distribution, in the particle size range 1 nm to 10 µm. Coarser particles have been left out, as they are outside the focus of this thesis. The total urban aerosol is the sum of the three separate modes. Note that this is an illustration, meant to convey the idea of particle modes within a wide aerosol distribution. In reality, the different modes may be closer together and much harder to differentiate, and there may also

be additional or fewer modes, depending on the different sources and atmospheric processes.
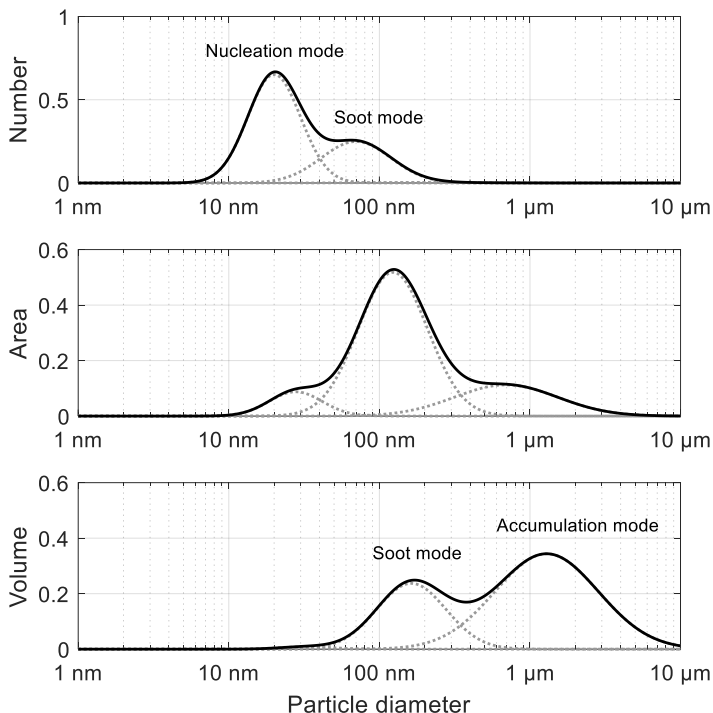
Figure 1.   An urban aerosol size distribution of three lognormal particle modes shown as a number, area, and volume distribution. The y-axis is the concentration of particles normalized by dividing by the integral of the distribution, i.e., the total particle number, area, and volume.

Nucleation mode particles form from precursor gases in the atmosphere, growing from an initially very small size of just a few nanometers up to tens of nanometers (Kulmala et al., 2004), although just a small portion of these nanoscale particles survive long enough to grow. Nanoscale particles are also emitted from combustion sources such as engine emissions (Karjalainen et al., 2014; Kittelson, 1998). Engine emissions exiting the tailpipe quickly cool and dilute which causes particles to form by nucleation from semi-volatile vapors. The particle formation happens almost instantly after emission; however, vehicles also emit some solid particles in the nucleation mode size-range which originate (in particle form) from the engine (Heikkilä et al., 2009; Saffaripour et al., 2015; Sgro et al., 2012).

Soot mode particles—also called the Aitken mode, named after John Aitken—mostly consist of particles from engine exhaust (Rivas et al., 2020; T. Wu & Boor, 2021; Z. Wu et al., 2008). Fresh soot begins its life as a fractal agglomerate of small black carbon spheres, but the large surface area allows it to quickly scavenge smaller particles and over time they become denser and more spherical. Thus, while freshly emitted engine-originated soot is roughly 50-70 nm in size, the atmospheric soot mode is closer to 100 nm (Enroth et al., 2016). Soot particles are composed of mainly black carbon, but also other exhaust pollutants such as metals and semi-volatile organic compounds. A large soot mode generally indicates large amounts of local traffic. While biomass combustion in homes also produces soot, the particles are usually larger than from engines, more in the accumulation mode size range (Leskinen et al., 2014; Pirjola et al., 2017).

The accumulation mode consists of aged particles, aerosols transported from regional sources (sometimes from far-away sources as well), as well as some mechanically produced particles. The name for the mode comes from the observation that once particles grow to be in the accumulation size range they are not easily removed from the atmosphere: they are too big to move much by diffusion and too small to settle gravitationally. Particles which begin in the soot mode can grow up to become accumulation mode particles in favorable conditions. Due to their longer lifespan, accumulation mode particles are the most likely to get transported far from their original source.

A more recent metric in aerosol science is the lung-deposited surface area (LDSA). It is the surface area distribution weighted by the lung-deposition probability of each particle. More specifically, in this thesis, it is the probability of deposition in the alveolar area of the lungs; however, sometimes in literature the same acronym is used for total deposition in the respiratory system (head airways, tracheobronchial region, and alveolar region), or the region may be denoted as A-LDSA (alveolar). Deposition in the alveoli is believed to be the most harmful, thus the LDSA distribution represents the particle distribution in a way which shows the particle size most likely to cause harm.

A good question to ask is why LDSA rather than lung-deposited number concentration or mass concentration? The scientific reason is that particle surface area has been found in toxicological studies to be the best predictor of toxicity for insoluble, spherical particles (Oberdörster, 1996; Schmid & Stoeger, 2016; Tran et al., 2000) and for ultrafine particles (UFP) (Aguilera et al., 2016). Epidemiological evidence is still scarce; however, one study on indoor air pollution found LDSA superior to PM2.5 in predicting lung function (Patel et al., 2018). This is fairly

intuitive, as it is the particle surface which reacts with the lung cells, and a high surface area concentration also means a large condensation sink, allowing particles to carry more toxic material on their surfaces. This applies especially to fresh, agglomerated soot particles released together with toxic semi-volatile compounds, such as polycyclic aromatic hydrocarbons (Polidori et al., 2008). The technical reason for the greater usage of LDSA (as opposed to lung-deposited number or mass) is that it is easy to measure. This will be discussed more in section 3.
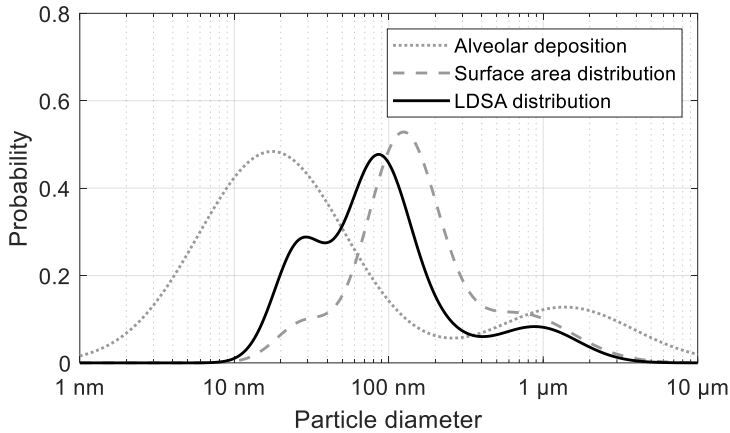
Figure 2. The surface area distribution from Figure 1 alongside the alveolar deposition curve and the product of these two: the LDSA distribution. The surface area and LDSA distributions have been normalized by dividing by the total surface area and LDSA, respectively.

Figure 2 shows the same particle surface area size distribution as in **Figure 1** along with the alveolar deposition curve and the product of these two, the LDSA curve. The deposition probability curve shown in equation (1) is an empirical fit to the ICRP (International Commission on Radiological Protection) model (1994), published in Hinds (1999) and gives the fraction of deposited particles as a function of particle size, $F_{alveolar}(D_p)$, where D_p is in micrometers.

$$F_{alveolar}(D_p) = \frac{0.0155}{D_p} e^{-0.416(\ln D_p + 2.84)^2}$$
$$+ 19.11 e^{-0.482(\ln D_p - 1.362)^2}$$

(1)

The deposition probability is highest (roughly 50 %) at 18 nm, decreasing down to a local minimum of 6 % at 250 nm. A second smaller maximum (13 %) is found at 1.4 μm. For this particle population, the nucleation and soot modes comprise most of the total LDSA (86 %, 62 % from the soot mode), and quite often LDSA is

portrayed as a metric sensitive to local emission sources, especially soot or BC (Lepistö et al., 2022). However, this is not always the case. For example, if the accumulation mode particles were to age further, they would begin to move toward the second maximum of the deposition curve, thus increasing their contribution to LDSA.

There are numerous studies which cover aerosol particle concentrations and distributions in urban air. In 2017, the average exposure-weighted PM2.5 concentration ranged from ~5 µg/m³ to ~100 µg/m³ from country to country (Ritchie & Roser, 2022, data from the World Bank). In review of aerosol size distributions, Europe, North America, Australia and New Zealand had particle number size distributions dominated by soot mode particles, whereas Asian countries tended to have larger contributions from the accumulation mode (T. Wu & Boor, 2021). The same study showed that the median particle diameter in urban background air tends to be larger than the median at traffic sites, explained by the shorter lifespan of nucleation mode particles compared to the soot and accumulation mode. Total number concentrations at urban measurement sites have high spatial and temporal variability and can range thousands to hundreds of thousands of particles per cubic centimeter (Kumar et al., 2014). The current WHO good practice statement gives 10 nm as the minimum size that must be measured in terms of number concentration (World Health Organization, 2021); however, a large fraction can be even smaller (Rönkkö et al., 2017). In terms of LDSA, outdoor urban concentrations are typically above 10 µm²/cm³ and below 100 µm²/cm³. In Europe, studies show LDSA is correlated with local combustion sources (Hama et al., 2017; Lepistö et al., 2022; Reche et al., 2015; Shah et al., 2023).

Unsurprisingly, studies of underground mine air quality are not quite as abundant as urban air studies, but there are a few, and several studies point to traffic as a central emission source (Debia et al., 2017; McDonald et al., 2003; Noll et al., 2007; Pronk et al., 2009; Saarikoski et al., 2018, 2019). In a source apportionment study by McDonald et al. (2003) over 78 % of PM2.5 in an underground mine originated from diesel exhaust. A later study by Saarikoski et al. (2019) studied five locations in a mine and found the contribution of diesel exhaust to PM1 to be 35 to 84 % and the contribution of blastings was 7-60 %. The mass size distributions of BC in the different areas were similar to those in outdoor ambient air. The particle modes were between 100-200 nm, corresponding quite well with the soot mode in the mass size distribution of **Figure 1**. The blasting-originated particles were mostly larger, sulphate peaked at ~550 nm and organics at ~450 nm. The study also reported the

overall number size distribution, which showed a significant presence of nucleation mode particles as well.

Occupational settings are not covered by the WHO air quality standards, and they have their own, often national, guidelines. In Finland, for instance, the Finnish Institute of Occupational Health recommends limiting respirable dust (particle diameter smaller than ~4 µm) to 500 µg/m³ (Hyytinen et al., 2016) and soot (elemental carbon) to 20 µg/m³ (8-hour mean) at underground occupation locations such as mines, although the law only requires 100 µg/m³ (Taxell et al., 2015). Compare these to the WHO guideline for 24h-PM10, which is 45 µg/m³. Not only are these guideline values astoundingly large, but there are also no guidelines or limitations on the number of UFP.

In addition to illustrating a particle size distribution, **Figure 1** shows one reason for the many measurement metrics employed for understanding aerosols. The number size distribution emphasizes small particles while the mass size distribution emphasizes large particles. In fact, the urban aerosol portrayed only has three visible modes in the middle panel, displaying the surface area distribution. As was explored in the introduction, we do not have a full understanding of what metric or metrics should be measured to best predict health outcomes, and clearly measuring either purely the total number or mass concentration leaves out a lot of information. As is also portrayed in **Figure 1**, particle modes from various sources and in various surroundings tend to be lognormal (Kulkarni et al., 2011), meaning they appear as normal distributions when viewed on a logarithmic x-axis.

2.2   Section summary

Like the size of particles, ambient particle concentrations also span several orders of magnitude, especially if measured with a high time-resolution. To summarize this section and give context for the results later shared in this thesis, **Table 1** gives some examples of measured values for mass, number and LDSA in recent studies.

Table 1. Particle concentrations in several metrics for different locations. The first row gives guideline values provided by WHO. The purpose of this table is to show the range of typical values; the locations cannot be compared as the measurement times differ.

	PM10 µg/m^3	PM2.5 µg/m^3	PN 1/cm^3	LDSA µm^2/cm^3	Reference
WHO 24 h average guideline value	45	15	10 000[i]	-	(World Health Organization, 2021)
Beijing	110	37	-	-	https://www.iqair.com/china/beijing, January 18th, 2023
Delhi	-	270	67 000	330	Paper III
Helsinki	9.9*	6.4	26 000	27	Paper III *(European Environment Agency (EEA), 2021)
Helsinki (long-range transport episode)	20*	19	21 000	40	Paper II *(European Environment Agency (EEA), 2021)
Vienna	17	9.5	18 000	35	(Strasser et al., 2018)
Underground mine maintenance area	49	46[ii]	34 000	79*	(Saarikoski et al., 2019) *Paper II
Helsinki subway station	-	60	31 000	-	(Aarnio et al., 2005)

The values for different cities are mean values for at least some hours of measurement, up to days of measurements. In addition to giving a range of possible values, **Table 1** shows that knowing the value for one metric is not enough to guess another. For example, LDSA and PM2.5 in Delhi are very high, but PN is quite comparable with the other locations. Comparing the values to WHO guidelines shows exceedances especially in PM2.5; however, the 2021 WHO guidelines were not in effect yet when these measurements were conducted, and the previous limit was 25 µg/m^3 (World Health Organization. Occupational and Environmental Health Team, 2006).

---

[i] While not worded as a guideline value, 10 000 1/cm^3 is given as the lower limit for "high PN" in the Best Practice Statements

[ii] This value is for PM2, the study did not report a PM2.5 value.

3   PARTICLE CHARGE

Many aerosol instruments employ charging as an initial step for particle detection or classification. As this thesis deals with electrical measurement, we wish to understand the typical charge distributions found in ambient air and the charges which result from charging for classification or detection. In ambient air, roughly half of all particles are either positively or negatively charged. In electrical aerosol instruments, the typical charging method for detection is diffusion charging with unipolar ions, usually positive ions, which results in almost all particles becoming positively charged.

Both charging methods involve the *Fuchs limiting sphere*, which describes a region around a particle with a radius dependent upon the mean free path (Fuchs, 1963). Outside the sphere, ions behave as they normally would, moving in random motions due to diffusion. Inside the sphere, ions are no longer bumping into gas molecules, and instead they move according to their initial velocity and the electric field. The limiting sphere is relevant for particles which are smaller than the mean free path, 66 nm for the average air molecule at ambient conditions.

3.1   Ambient ions

The word ion is often used for any kind of charged particle. In this thesis, ions refer to gaseous ions (also called small ions), while charged aerosol particles (either in the liquid or solid phase) are referred to as charged particles. Charged clusters of molecules at a size of ~1 nm can be called cluster ions, and indeed the difference between ions and particles in this size range is difficult to define. Most atmospheric ions form from air molecules ionized by radiation. When a neutral molecule hit by radiation gains enough energy to eject an electron it becomes positively charged and the free electron quickly finds a new neutral molecule, causing it in turn to become a negatively charged ion (Fleagle & Businger, 1980, p. 134). These single-molecule *primary ions* are unstable and become small ions in just few microseconds (Hirsikko et al., 2011). The end result is positive and negative *small ions* or *cluster ions*, which can

ionize aerosol particles by being scavenged by existing particles, or they can act as condensation nuclei and form new particles.

A typical ionization rate is 10 ions/cm^3·s (Jokinen, 1995) and ambient small ion concentrations typically range from 10^2/cm^3-10^3/cm^3 (Ling et al., 2010). Ion concentrations depend on many factors, namely local ion sources and sinks. Examples of ion sources (in addition to the air ions described above) are waterfalls (Laakso et al., 2007), powerlines (Jayaratne et al., 2015), and combustion generated aerosol, such as vehicle exhaust (Jayaratne et al., 2014; Yu et al., 2004). The main small ion removal methods are recombination with other ions of opposing polarity and deposition on aerosol particles and other surfaces (Hõrrak et al., 2008). Concentrations of ions in heavily polluted air are generally lower than the corresponding background level, as ions are quickly scavenged by particles (Jokinen, 1995). A simple mathematical balance equation for ion concentrations is

$$\frac{dN_{ion}}{dt} = \Phi - \alpha N_{ion}{}^2 - \beta N N_{ion}, \tag{2}$$

where N_{ion} is the ion concentration, N is the aerosol particle concentration, Φ is the ion production rate, α is the recombination rate and β is the rate of attachment to aerosol particles. This equation, presented originally by Hoppel and Frick (1986), assumes equal amounts of the two polarities of ions and the attachment rate is an average for the total aerosol particle distribution. The term βN is sometimes referred to as the ion sink from particles (Tammet et al., 2006), and can be thought of as a property of the aerosol particle population, as in how much particle surface area is available for ion attachment.
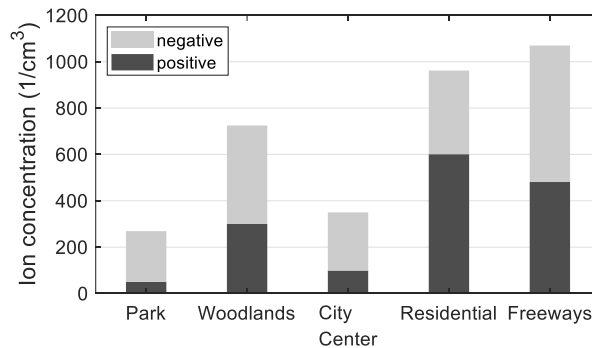
Figure 3.   Total small ion concentrations in various environments. Data is from Ling et al. (2010), measured in an Australian city.

As an example of measured ion concentrations in urban areas, **Figure 3** shows measured values from different environments within an Australian city. The park ion concentrations can be considered equivalent to background concentrations. The other areas show higher concentrations. The study found low ion to particle ratios in the city center and the freeway despite the local ion sources, indicating a large ion sink. (Ling et al., 2010).

3.2   Bipolar particle charge distributions

Particles can become charged by scavenging gaseous ions or the small gaseous ions can act as condensation nuclei for semi-volatile vapors, therefore growing into charged aerosol particles (Hirsikko et al., 2011). Larger particles can reach higher charge numbers than small particles and higher temperatures also increases charge numbers due to more diffusional movement increasing the chances of particle-ion collisions. Over time, ambient particles reach a state of quasi-equilibrium, where particles gain positive and negative charges at equal rates. This steady state is approximated by the *Boltzmann equilibrium charge distribution*. It gives the fraction of particles f_n of a certain size with a given number of charges n (either positive or negative) (Flagan, 2011, p. 351; Hinds, 1999, p. 335).

$$f(n, D_p) = \frac{\exp\left(-\frac{n^2 e^2}{D_p kT}\right)}{\sum_{i=-\infty}^{\infty} \exp\left(-\frac{i^2 e^2}{D_p kT}\right)} \tag{3}$$

In eq. (3) e is the elementary charge, k is the Boltzmann constant ($k = 1.381 \cdot 10^{-23}$ J/K) and n is the number of elementary charges. The Boltzmann distribution is applicable when ion attachment rates are high, either due to high temperature or large particle size. Experimentally, it has been found to fit many measurements (Forsyth et al., 1998; Liu & Pui, 1974b; Maricq, 2006; Sgro et al., 2011), and its simplicity makes it attractive. Unfortunately, the Boltzmann distribution underestimates the number of charges carried by small particles (< 30 nm) at ambient temperatures (Flagan, 2011, p. 352). Also, negative ions have slightly higher mobilities than positive ions, increasing their chances of colliding with particles. Thus, negatively charged particles are slightly more common than their positive counterparts. For example, J-Fatokun et al. reported a mean net charge of -478 elementary charges/cm^{3} measured outdoors.

Another approach to particle charging is the Fuchs model, based on the limiting sphere theory (Fuchs, 1963; Hoppel & Frick, 1986). It is only solvable numerically. Wiedensohler (1988) has formulated a parameterization, eq. (4), which fits ambient equilibrium particle charge distributions, and can be combined with Gunn's charging theory (Gunn & Woessner, 1956), eq. (5), to calculate the charged fraction of particles at ambient temperatures. The first equation is for charge numbers from -2 to 2, while the second equation gives the fraction of particles with (absolute) charge numbers of three and above.

$$f(n, D_p) = 10^{\sum_{j=0}^{5} a_{j,n}(\log_{10} D_{p,nm})^j}, |n| < 3 \tag{4}$$

$$a_{j,n} = \begin{bmatrix} -26.3328 & -2.3197 & -0.0003 & -2.3484 & -44.4756 \\ 35.9044 & 0.6175 & -0.1014 & 0.6044 & 79.3772 \\ -21.4608 & 0.6201 & 0.3073 & 0.4800 & -62.8900 \\ 7.0867 & -0.1105 & -0.3372 & 0.0013 & 26.4492 \\ -1.3088 & -0.1260 & 0.1023 & -0.1553 & -5.7480 \\ 0.1051 & 0.0297 & -0.0105 & 0.0320 & 0.5049 \end{bmatrix}$$

$$f(n, D_p) =$$

$$\frac{e}{\sqrt{4\pi^2 \varepsilon_0 D_p kT}} \exp \frac{-\left[n - \frac{2\pi\varepsilon_0 D_p kT}{e^2} \ln\left(\frac{N_{ion+} Z_{ion+}}{N_{ion-} Z_{ion-}} \right) \right]^2}{\frac{4\pi\varepsilon_0 D_p kT}{e^2}}, |n| \geq 3 \tag{5}$$

In eq. (5), N_{ion+} and N_{ion-} are the concentrations of negative and positive small ions and Z_{ion+} and Z_{ion-} are their respective mobilities. If these values are unknown, the ratio of ion concentrations can be taken as one, and the ratio of mobilities as 0.875 (Wiedensohler, 1988). The particle diameter in eq. (4) must be given in nanometers. Note, the original coefficients in matrix $a_{j,n}$ given by Wiedensohler have been revised (Flagan, 2011, p. 352).

The absolute mean charge per particle for one polarity, $n_{avg}(D_p)$, can be calculated by summing the probabilities multiplied by the respective charge numbers.

$$n_{avg+}(D_p) = \sum_{n=0}^{\infty} n \cdot f(n, D_p)$$

$$n_{avg-}(D_p) = \sum_{n=-\infty}^{0} n \cdot f(n, D_p) \tag{6}$$

The Boltzmann distribution is symmetrical and $n_{avg+} = |n_{avg-}|$, whereas the Wiedensohler distribution is not.

As shown by eq. (3) and eq. (5), temperature also plays a role in particle charging. Higher temperatures increase ion diffusion, leading to an increase in the average charge. As a result, soot particles emitted from combustion engines are expected to have more charges than similarly sized particles of other origins in a traffic environment, and studies confirm this (Jayaratne et al., 2015). Based on charge distribution experiments directly on engine exhaust, combustion-originated soot-mode particles are well-described by the Boltzmann distribution (Jung & Kittelson, 2005b; Lähde et al., 2009; Maricq, 2006) at temperatures of roughly 800 K to 1100 K (Maricq, 2006). This result could hint that the processes affecting particle size end before ions are depleted; however, Maricq has shown that an alternative theory in which particles are first charged and then undergo coagulation results in a very similar charge distribution. In contrast to soot mode particles from exhaust, nucleation mode particles tend to be neutral, as they form from gaseous compounds after the exhaust cools and dilutes in atmospheric conditions (Jung & Kittelson, 2005b; Sgro et al., 2011).

3.3   Unipolar diffusion charging of particles

In instruments designed for particle detection, diffusion charging is a common solution. Ions are produced from a needle or wire electrode, called a corona needle, by connecting a high-voltage source to the electrode. The simplest charger design employing a corona needle is to direct the sample aerosol flow past the corona needle (Rostedt, 2018, p. 14), where the ions will then attach to the particles by diffusion. Unipolar charging by diffusion is described by the limiting sphere approach (Dhaniyala et al., 2011, p. 394). A particle and an ion will always have the same polarity and the two will therefore repel each other. This means that inside the limiting sphere of small particles there is a decreased probability of collision between the ion and the particle. Diffusion charged particles smaller than ~30 nm have less than one elementary charge on average.

Compared to ambient charge distributions, higher charge numbers are possible with unipolar diffusion charging, because any ion attachment will result in an increased charge. The average charge per particle can be derived from the product of the ion concentration and the charger residence time. Experimentally, diffusion chargers are characterized by their Pn-curves, where P is the particle penetration

through the charger and n is the average charge per particle. For most diffusion chargers, the following relationship to particle size has been observed:

$$Pn = aD_p{}^b, \tag{7}$$

where a and b are constants specific to the charger. The exponent tends to be between 1.1 to 1.9 (Dhaniyala et al., 2011, p. 397).
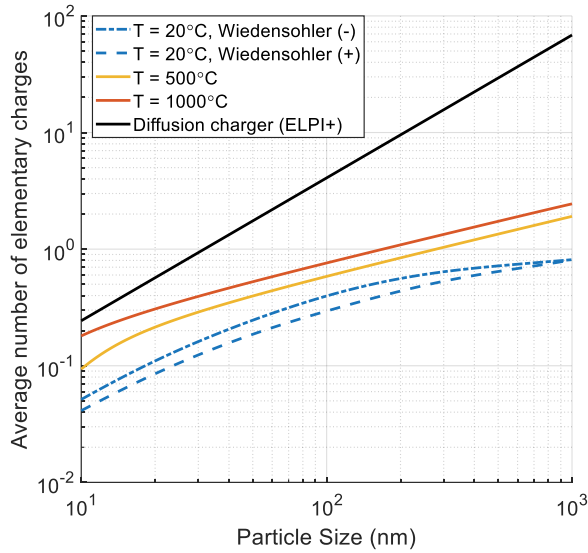
Figure 4. Comparison of the average charge achieved by unipolar diffusion charging and naturally occurring charge distributions. Figure from Paper IV.

Figure 4 shows the average charge number as a function of particle size for naturally occurring charge distributions and as a result of unipolar diffusion charging. The diffusion charging curve is the Pn-curve for the ELPI+ (Järvinen et al., 2014). The two curves at higher than ambient temperatures are the average charge numbers based on the Boltzmann distribution. Only one curve is shown for each, as the negative and positive charge numbers are the same, whereas two curves are shown for the ambient temperature based on the Wiedensohler approximation. The number of charges is slightly larger for negatively charged particles.

3.4   Relationship between particle charge concentration and other metrics

Particle charge concentration is the charge contained in a volume. As a metric, it is perhaps more often used in relation to ambient ion concentrations. In relation to particles, the net particle charge concentrations have been previously measured in ambient air using an electrometer connected to a filter (J-Fatokun et al., 2008) and the number concentration of charged particles has been reported in ambient air based on measurements with the Neutral Cluster and Air Ion Spectrometer (NAIS) (Jayaratne et al., 2014). In this thesis, charge concentration refers to the total charge carried by particles of one polarity in a volume of air. If the average charge per particle is $n_{avg}(D_p)$, as given in section 3.2, then the charge concentration $\lambda_{\pm}$ for a particle number distribution $N(D_p)$ is

$$\lambda_{\pm} = \int Nen_{avg\pm}\,\mathrm{d}D_p$$

(8)

In this form, the charge concentration relays information on the particle concentration and the charge state of the particle population. As the charge distribution depends on temperature in addition to particle size, an accurate calculation might include information on the source of the particle mode, such as applying a high-temperature distribution to soot mode particles, assuming they originated from engine exhaust.

It is interesting to know how the charge concentration relates to other, more established metrics. Particles which have undergone charging with a diffusion charger have lost the information of their initial charge, thus reporting the charge concentration seems irrelevant in this case.

Figure 5 shows the average charge number as a function of particle size divided by its different moments. The purpose of viewing the charge distribution this way is to understand what metric or metrics the charge concentration is associated with. The curves have been normalized to equal one at 100 nm to allow for easier comparison, and the average number of charges has been calculated with equations (5) & (4) for negatively charged particles. The solid line simply shows the average charge number dependency on size. Based on the plot, the charge concentration of an ambient aerosol is most closely related to the particle length concentration of UFP and to the particle number of particles larger than 100 nm. In an instrument created for charge measurement, different sampling methods and analyzer

geometries can be used to modify the particle detection efficiency to better correlate with a targeted output metric.
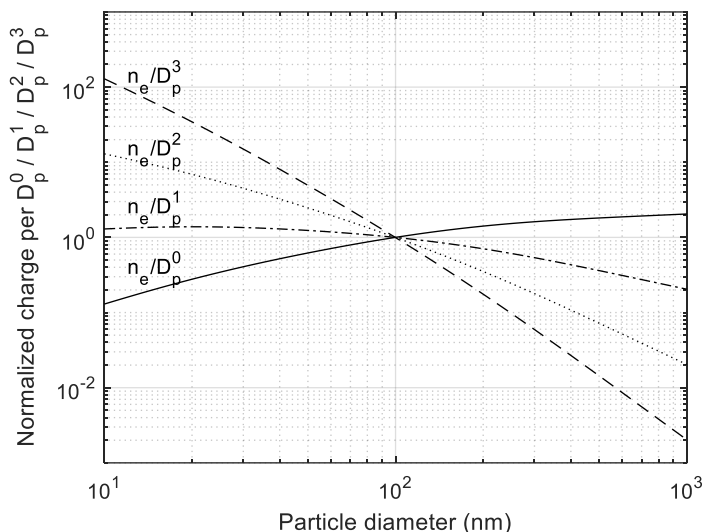
Figure 5. The relationship between the average ambient charge, calculated from the empirical equation by Wiedensohler (1988), to different moments of particle size. Each line has been normalized to equal one at 100 nm for easier comparison.

Along with LDSA, other surface-based metrics have been proposed for the calibrated output of charge-based measurement. Particle surfaces can be thought of as sinks for gaseous ions or semi-volatile molecules; hence the terms *ion sink,* as in eq. (2), or *condensation sink.* Diffusion-charged particles are well-correlated with these metrics (Kuuluvainen et al., 2010). The *Fuchs Surface Area,* also called the *Active Surface Area* (ASA), is a term to describe the portion of the total geometric surface area which is available for surface interactions. It has also been used, for example, as the quantity measured by a device where aerosol particles are detected via attached radioactive lead isotopes, called an epiphaniometer, whose signal closely followed Fuchs coagulation theory (Baltensperger et al., 1991; Pandis et al., 1991). The ASA of a particle is a function of its diameter to a power of 1 to 2: for small particles (< 100 nm), it is proportional to the geometric diameter ($ASA \propto D_p^2$) and for larger particles it decreases with increasing particle size. Later studies began using ASA to describe the surface available for ion attachment in diffusion chargers (Keller et al., 2001; Siegmann & Siegmann, 2000), although it is not entirely equivalent to the ASA measured by the epiphaniometer due to the repulsion between unipolar-charged

particles. Experimentally, the response of diffusion-charging based instruments has been found to equal the ASA (or Fuchs Surface area) at least for some cases (Jung & Kittelson, 2005a).

The sensor response for diffusion charging based sensors is close to $D_p{}^1$, the sum of particle diameters, both according to Fuchs' theory and experimental results (Dhaniyala et al., 2011, p. 396). Due to the focus on particle mass and number concentration, this may seem unfortunate at first, but somewhat coincidentally LDSA $\propto D_p{}^1$, for particles in the size range 20 nm to 300 nm. This is the result of the deposition curve in this size range following a curve of approximately $\propto D_p^{-1}$, which is then multiplied by particle surface area, D_p^2, to achieve LDSA, $D_p^{-1} D_p^2 = D_p^1$. This has led several diffusion-charging based instruments to report the measured current as LDSA, needing only a single calibration factor (Fierz et al., 2014; Fissan et al., 2007; Wilson et al., 2007). The benefit of reporting LDSA as opposed to another surface-related quantity is the weighting towards health-relevant particles, while a slight negative is the dependency on an empirical model of lung-deposition. Deposition of course varies depending on the biology of a specific individual, as well as the hygroscopicity and density of the particles, neither of which are usually known. Nonetheless, LDSA has gained popularity especially with sensor-type electrical measurement.

Continuing with the same particle population as in **Figure 1** and **Figure 2**, **Figure 6** shows how the particle distribution would look based on the average ambient charge compared to other metrics related to particle surface area.
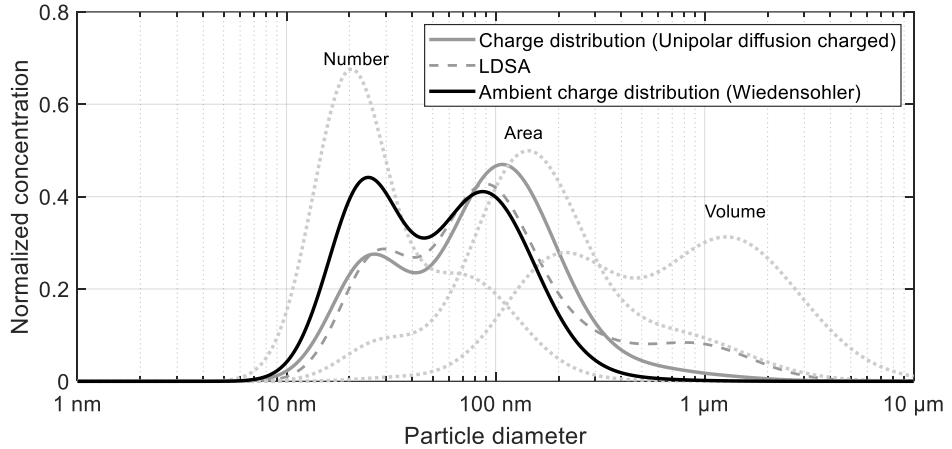
Figure 6.   The ambient particle charge distribution alongside the unipolar diffusion charged distribution, and LDSA, number, surface area and volume distributions. This example particle distribution is the same three-mode population as in **Figure 1** and **Figure 2**.

The ambient charge distribution gives more weight to the nucleation mode particles than the LDSA or diffusion charged distributions, although its modes are quite close to those two. While LDSA has a clear mode for accumulation mode particles, it is not seen in either the ambient or the diffusion charged particle size distribution. Compared to the surface area distributions, the soot mode peak is shifted to smaller sizes, while the nucleation mode is in a similar size range. This shows in practice how the ion attachment goes from following a relationship to D_p^2 for small particles to D_p^1 for larger particles, although the soot mode particles belong to a transition regime, where the power is somewhere in between. The high sensitivity to smaller particles indicates that the ambient charge concentration should be a good metric for UFP as well as soot mode particles.

4 METHODS

This thesis consists of articles and results which have involved several months of experimental research in laboratory settings, in an underground mine, in an engine laboratory, in ambient air, in a powerplant test facility and a laboratory wood fireplace. This chapter gives an overview of electrical methods in general, then summarizes instruments and data handling which is common to all (or most) of the thesis papers, and finally gives more specific information regarding each paper. The detailed methodology is found in each corresponding Paper, and thus only short summaries are presented here.

4.1 Electrical particle measurement

Electrical particle measurement excels when particles are small, numerous and high time resolution is required. UFP are too small to be measured optically, and they have very little mass (as discussed previously), but they can be charged (either by ions in the atmosphere or ions created with a charging device), and in large enough quantities that charge becomes detectable with an electrometer. Electrical methods are employed both in expensive instruments for intensive research and cheaper, sensor-type instruments for monitoring purposes. Electrical methods are also employed for particle classification, most notably the Differential Mobility Analyzer (DMA), which is a second order mobility analyzer (Knutson & Whitby, 1975). This section presents an analyzer for measuring charged particles as well as diffusion charging, as it is used in many commercial measurement devices.

The particle size which can be inferred from electrical mobility is the mobility diameter, D_p. Charged particles can be categorized by their drift velocity v_E in an electric field of a given strength E, this is called the electrical mobility of the particle, Z.

$$Z = \frac{v_E}{E} \tag{9}$$

Electrical mobility is a property of a particle moving in a fluid, and can also be written using physical parameters, eq. (10). It depends on the particle diameter D_p, the

number n_e of elementary charges e, the Cunningham slip correction factor $C_C(D_p)$ and the dynamic viscosity of the surrounding fluid μ, usually air. The SI-unit of electrical mobility is m²/(V·s). When particles are small and highly charged, they have a high mobility, whereas larger and less charged particles have lower mobility. When particle diameter is determined from mobility, the number of charges must be known, otherwise large, highly charged particles can be mistaken for smaller, less charged particles.

$$Z = \frac{ne C_c(D_p)}{3\pi\mu D_p} \tag{10}$$

Zeroth order mobility analyzer

One of the first electrical instruments for atmospheric studies is the *Gerdien condenser,* which measures atmospheric conductivity by collecting and measuring gaseous ions, presented in detail in, e.g., Aplin (2005). The general equations for mobility analyzers were first derived by Tammet (1970), although he uses the term *aspiration counter*. In this section, we examine a similar concept from the perspective of charged aerosol particles, which have much smaller mobilities than their gaseous counterparts.

Mobility analyzers are devices used to separate particles based on their electrical mobility. The simplest mobility analyzer consists of two electrodes of length L opposing each other. One of the electrodes is grounded and the other connected to a voltage source, creating an electric field of in between the two. A common geometry is two concentric cylinders. Charged particles in an aerosol flowing through the analyzer will begin moving in the direction of the electric field (in addition to moving with the fluid). Particles with a high enough mobility will always reach an electrode surface, while particles with lower mobilities will sometimes travel through the analyzer, depending on how far from the electrode they are to begin with. An important parameter of a mobility analyzer is the limiting mobility Z_0, defined as the lowest mobility for which all particles are collected.

The derivation of the limiting mobility and collection efficiency of a coaxial condenser was first presented by Tammet (1970). It depends on the radii of the outer r_o and inner r_i electrodes, the volumetric flow Q_{flow} through the instrument, the voltage V applied across the electrodes and the length L of the collection area.

$$Z_0 = \frac{\ln\frac{r_o}{r_i} Q_{flow}}{2\pi VL}. \tag{11}$$

The limiting mobility is a very useful concept. It incorporates all the analyzer geometry as well as the adjustable variables into a single variable. It also allows for the determination of collection efficiency. The mobility analyzer can be used to separate high mobility particles from low mobility particles, or with a high enough collection voltage, all charged particles can be collected. By attaching an electrometer to the electrode, the current $I_\pm$ from the deposited particles can then be measured

$$I_\pm = \lambda_\pm Q_{flow}, \tag{12}$$

where $\lambda_\pm$ is the charge concentration of either positive or negative polarities, the subscript symbolizing one of the two polarities. The measured polarity is the same as the polarity of the applied voltage. If the applied voltage is not high enough to capture particles of all electrical mobilities; however, the deposited particles and the resulting current are dependent on the collection efficiency $\eta(Z)$. For high mobilities, i.e., mobilities larger than Z_0, the efficiency is 1, simply from the definition of the limiting mobility. For a smaller mobility Z^*, only the particles entering the analyzer close enough to the measuring electrode are collected. Letting the flow through this surface be Q_{flow}^*, the collection efficiency is the ratio of the two flows.

$$\eta(Z^*) = \frac{Q_{flow}^*}{Q_{flow}} \tag{13}$$

and the collection efficiency can then be written as

$$\eta(Z^*) = \frac{Z^*}{Z_0}. \tag{14}$$

The theoretical collection efficiency for a particle of any mobility is therefore

$$\eta(Z) = \begin{cases} 1, Z \geq Z_0 \\ \frac{Z}{Z_0}, Z < Z_0 \end{cases}, \tag{15}$$

and the measured current is

$$\begin{aligned} I_\pm &= \int \eta(Z)\lambda_\pm(Z)Q_{flow}dZ \\ &= Q_{flow}\left(\int_0^{Z_0} \frac{Z}{Z_0}\lambda_\pm(Z)dZ + \int_{Z_0}^{\infty} \lambda_\pm(Z)dZ\right) \end{aligned} \tag{16}$$

Particle mobility is a continuous variable: although the charge is limited to multiples of the elementary charge, particle size varies continuously. The true collection efficiency can deviate from the theoretical one for several reasons: the aerosol isn't sufficiently mixed at the entrance, losses caused by diffusion, interactions between particles (coagulation, repulsion/attraction, etc.) and nonuniform flowlines from bumps and edges.

Diffusion charging based measurement

Electrical measurement methods often employ a charging mechanism in order to increase the number of charges per particle or create a known charge distribution. Ideally, the new charge distribution is independent from the initial charge distribution. For particle detection, unipolar chargers are more common, whereas classification uses bipolar charging.

Diffusion chargers are characterized using Pn rather than each variable separately. Without removing the charger from its surroundings, it is impossible to measure the particle penetration, and secondly, it is not even necessary to know each one separately to be able to process the measurement data into particle concentrations. For example, if the Pn for a certain particle size is 0.5, it can mean (for example) that there are no particle losses, but only half are (singly) charged, or that all particles are singly charged but only half of them penetrate the charger. In either case a correction factor of two is necessary to compensate for uncharged or depositing particles. The output current I is determined similarly to eq. (12), where the charge density can now be replaced the number concentration of particles multiplied by the average charge of a single particle, $Pn \cdot e$.

$$I = N \cdot Pn \cdot e \cdot Q_{flow} \qquad (17)$$

Diffusion charged particles can be detected by collecting them on an electrically conductive surface and measuring the incoming charge as a current with an electrometer. Collection can be done using a filter, a mobility analyzer, a diffusion battery, an impactor, or some combination of these. For an instrument with several particle collecting stages, where the particles are separated according to their size, the average Pn can be determined for each particle size bin. For size ranges which are narrow enough, this allows the calculation of particle number concentration by rearranging eq.(17):

$$N = \frac{I}{PneQ_{flow}} \cdot \qquad (18)$$

If the shape of the particles is known, then also the surface area and volume concentration can be determined, and furthermore, if the density is also known, then the mass concentration can also be calculated. Often particles are assumed to be spherical, and a density is assumed based on knowledge of the particle composition, or if the composition is mixed or unknown, then unit density may be used (1 g/cm^3). Of course, the more assumptions and simplifications are made, the larger the error bars are for the result.

4.2   Measurement instruments

Paper I introduces two offline instruments. The first is a cascade impactor (commercial name Dekati PM10 Impactor, by Dekati Ltd.), which collects particles between 2.5 to 10 μm, 1 to 2.5 μm and below 1 μm. The first two size ranges are collected using impaction and the final stage is a filter. The cascade impactor flow rate needs to be 10 lpm for the above-mentioned cut-offs. The collected particles are weighed, and the volume of aerosol sampled is recorded to allow calculation of the mass concentration.

The second is only partially offline, as the eFilter (Dekati Ltd.) simultaneously collects particles on a filter and houses a diffusion-charging based sensor. This allows for more information on the temporal nature of a measurement than a purely offline device. The eFilter Pn curve was characterized by Lassila (2018), and the resulting exponent b, as in eq. (7), was 1.47 for particles between 25 nm to 570 nm. The main flow through the instrument can be set to 10 to 30 lpm, and the flow through the electrical detection is 0.5 lpm. For one eFilter sample, the matching charge or current can be taken as an integral of the collection time, then dividing the total mass by the total charge gives a factor for converting the charge to mass. An approximation of the mass concentration can be determined for any period within the original sample. The quality of the approximation depends on the stability of the particle size distribution (median size, distribution width).

Paper I also introduces an online measurement method, and one of the main instruments in this thesis, the ELPI+ (Electrical Low-Pressure Impactor, manufactured by Dekati Ltd.), it is an important part in all Papers I to IV. Like its predecessor ELPI (Keskinen et al., 1992), it consists of a diffusion charger for charging incoming particles, followed by an ion trap to remove excess ions, then a cascade impactor followed by a filter to collect the charged particles. The current from the collected particles is detected with an electrometer. There are altogether 14

measurement stages, thirteen impactor stages and one filter stage, and one additional pre-impactor stage for removing coarse particles (> 10 μm). The measurable particle size range is from 6 nm to 10 μm. Whereas the largest size is limited by the pre-impactor, the smallest measurable size is limited by the diffusion charging efficiency. The minimum measurable concentration depends on the particle size (fewer large particles are needed to create enough current compared than small particles). The stage at which each particle impacts is determined by its aerodynamic size; thus, the size distribution may not always match a distribution obtained using electrical classification (for example, the Scanning Mobility Particle Sizer, SMPS). A low-density particle would reach a lower stage (corresponding to a smaller aerodynamic diameter) in a cascade impactor than an equal size high-density particle would, whereas the electrical mobility is independent of particle density. The ELPI+ requires a downstream pressure of 40 mBar. The low-pressure environment allows for the impaction of very small particles; however, small particles also undergo significant movement due to diffusion, which can cause them to deposit earlier.

The ELPI+ has been previously characterized by Järvinen et al. (2014). Particle deposition by diffusion is corrected in the data handling by moving current from the upper stages to the lower stages (from larger particles to smaller particles), according to the collection efficiency determined by Järvinen et al. The Pn of the charger is given separately for three particle size ranges: for sub 1.035 μm particles the exponent b, eq. (7), is 1.225 and up to 4.282 μm particles it is 1.515. The current measured with the ELPI+ is converted into a number size distribution by using eq. (17) for each impactor stage (and the final filter stage). If the shape and density of the particles is known, then also the mass size distribution can be calculated. It is a reasonable assumption in most cases that particles are close to spherical. In ambient measurements, the particle population is a mixture of chemistries, morphologies, and sizes, thus in this thesis all particles are treated as spheres of unit density, unless otherwise noted.

Papers II and III explore the uses of the ELPI+ for LDSA measurement. As it is a diffusion charging based instrument, the measured current can be converted into LDSA. Furthermore, this can be done using stage-specific calibration factors (Lepistö et al., 2020), increasing the accuracy of LDSA-measurement. As discussed in section 3.4, the linear relationship between diffusion charged particles and LDSA is generally limited to particle diameters between 20 – 300 nm, but the stage-specific calibration expands this range to 10 nm – 10 μm. An SMPS was also employed in these measurements and could have been used to assess LDSA by multiplying the

surface area concentration with the deposition curve; however, the SMPS measurable particle size range is much narrower than that of the ELPI.

In addition to the ELPI+ measurement of LDSA, LDSA is also measured with several commercially available sensors in Paper II: Partector (Naneos GmbH), AQ Indoor (Pegasor Oy), DiSCmini (Testo). These sensors all employ diffusion charging and particle concentration is given as the LDSA concentration, using a calibration factor inserted by the manufacturer. There are some differences in how the particles are collected: the Partector does not collect the particles at all, rather it uses pulsed charging and measures the current induced by the changing charge. The DiSCmini uses two-stage collection, the first collector employing diffusion and the second a filter to collect any remaining particles. The two stages allow a rough estimate of the mean particle size. The AQ Indoor also estimates particle size. It only has one collection area, but the collection voltage is varied, and the particle size inferred from the changes in the resulting current. To keep the insides free of accumulating coarse particles, the DiSCmini has an impactor before the sample inlet, and the AQ Indoor has a cyclone. These instruments are expected to work best within the 20 to 300 nm size range.

In Papers II and III, the campaigns also included other instruments, such as CPC's (Condensation Particle Counters), aerosol mass spectrometers and aethalometers. The data from these instruments is touched upon only briefly in these papers and are outside the scope of this thesis.

4.3   Instrument comparison

Paper I concerns the comparison of three different instruments for the measurement of particle concentration: two ELPI+ instruments, one eFilter and two cascade impactors.

The first measurements were at an oil shale test facility, located on the Tallinn University of Technology campus. The second comparison measurement employed a brick fireplace in a laboratory setting, where wood and garbage were burned. The cascade impactors measured the raw exhaust, whereas the ELPI+ and eFilter received aerosol samples diluted with ejector diluters (Dekati Ltd.), as shown in the schematic in **Figure 7**. Although the measurements were conducted with combustion-originated aerosol, the results should apply to ambient aerosols (of similar particle sizes and concentrations) as well.
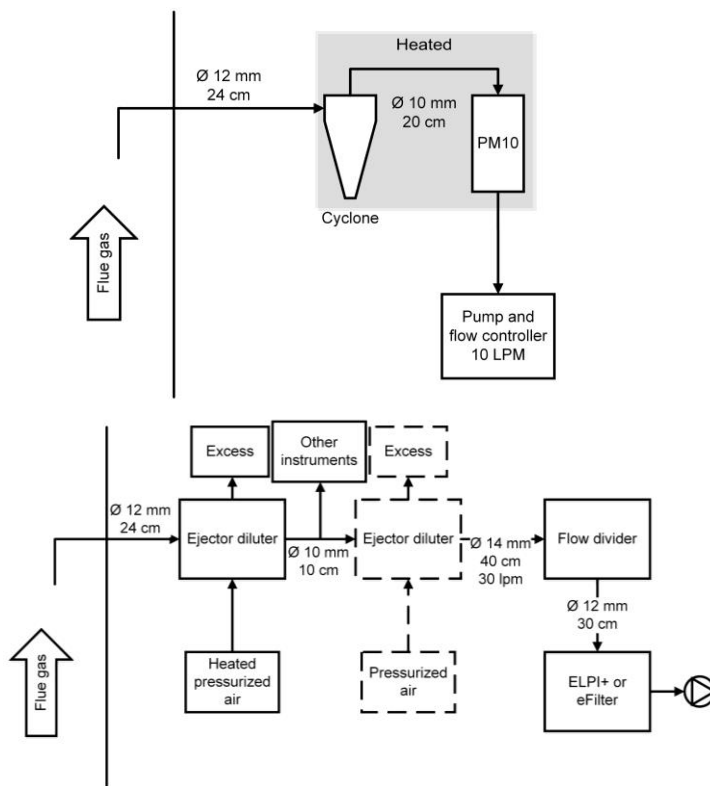
Figure 7. Schematics of the sampling systems used in the exhaust measurements for Paper I. The top schematic shows the sampling setup for the PM10 cascade impactors, while the lower one shows the setup for the two ELPI+ units and the eFilter.

The data handling for the PM10 cascade impactors involved weighing the samples and calculating the mass per volume based on the sampled aerosol volume. The eFilter samples were also weighed; however, these samples were collected over longer sampling times, and the mass concentration was calculated as described in the instrument sections. For the ELPI+ mass concentration, only stages which sampled at least 2.5 % of the total current were included in the calculated mass. This is because very small errors in the correction of diffusion collected particles could result in a large mistake in the calculation of the total mass. Particles were assumed to be spherical and have unit density.

4.4 LDSA measurement in an underground mine

Paper II concerns LDSA concentrations and size distributions in different areas of an underground mine. To begin with, the different sensors were tested in the maintenance area of the mine with the ELPI+ as the reference. The other measurement locations were near different mining operations: dumping, crushing, a transfer belt and blasting. A mobile laboratory was used to move around the mine and measure the LDSA distributions with the ELPI+; unfortunately, some areas did not have electricity available, limiting the measurement time.

After the main measurement campaign, two sensors (the AQ Indoor sensors) were left to measure for about a month at two mine locations. The purpose was to monitor the LDSA concentration for a longer period, and to determine whether the sensors were suitable for long-term measurements in an underground mine environment.

4.5 Ambient measurements of LDSA in Delhi and Helsinki

Paper III concerns ambient measurements in two cities: Delhi-NCR and Helsinki. The aim of the measurements was to establish the similarities in the aerosol population between two cities: one relatively clean city (Helsinki) and one polluted city (Delhi). In both Delhi-NCR and Helsinki, ambient air LDSA concentration was measured from a roadside container or mobile laboratory. The sampling system consisted of a PM2.5 impactor and tubes leading to each instrument: an ELPI+, the ICP-sensor (results presented in Paper IV), an aethalometer, an SMPS, and an ACSM (Aerosol Chemical Speciation Monitor). The inlet was placed at roughly 3 m above ground and horizontally just a few meters from driving lanes. The traffic rates were similar on the two roads, approximately 1000 vehicles/hour.

The measurements lasted several weeks in Delhi-NCR, and about one week in Helsinki. In total, four days of the Delhi-NCR data was valid, the rest was affected by the accumulation of particles in the ELPI+ instrument, despite feeding clean air into the line with a compressor to dilute the aerosol (dilution factor 2)—the ambient particle concentration was even higher than anticipated. The Delhi-NCR measurement campaign was in December 2018 and the Helsinki campaign in September 2019. Although the two are compared to point out the extent of the differences between the particle distributions, both represent only snapshots of the total variation (both spatially and temporally).

4.6 Characterization of a new electrical sensor

Paper IV details the measurement method, characterization, and testing of a novel electrical sensor, the ICP sensor. The sensor measures the charge concentration of particles in an aerosol flowing through it, one polarity at a time. I designed the sensor using Solidworks software and the sensor was built by the workshop staff at Tampere University. Dimensions were selected to target particles in a size range found in traffic environments, but also to keep the sensor small in size. The sensor was characterized in the Aerosol Physics calibration laboratory, while the test measurements were in an engine laboratory and ambient air. The ambient air tests were conducted in the same measurement campaign as the LDSA measurements in Delhi-NCR for Paper II.

Sensor components

The sensor consists of an ion trap, a mobility analyzer with one electrode connected to a voltage source and one electrode connected to an electrometer, a critical orifice, and a pump. The ion trap removes gaseous ions to avoid mistakenly measuring them as particles. The data output is the current measured by the electrometer.

The mobility analyzer consists of concentric cylinders with an electrical field applied between them. It is similar to the *Gerdien condenser*, used in atmospheric studies to measure air conductivity by collecting gaseous ions. The outer electrode collects particles which have the same polarity as the applied field and the current from the particles is measured with an electrometer. The inner electrode, where the voltage is applied, collects particles of the opposing polarity; however, they are not measured. Neutral particles and charged particles with low mobilities penetrate the mobility analyzer. This allows for the possibility to also measure the penetrating particles. Finally, the critical orifice controls the flow rate through the sensor to the pump.

The geometry of the mobility analyzer is shown in **Figure 8**: a cross-section of the model produced with computer software. The most important dimensions are the distance between the two electrode surfaces (2 mm) and the length of the collecting area (48 mm). The outer electrode is slightly longer at each end, 1mm each way, adding to a total length of 50 mm. This is to decrease electrical losses caused by edge effects on the electric field. The top of the mobility analyzer is connected to the rest of the sensor with screws through the flange.

The collection voltage was chosen as -500 V and the flow rate as 1 LPM. The flow was chosen to be large enough that particle diffusion does not reduce efficiency too much, but on the other hand it should be small enough that the flow stays laminar. The voltage was then chosen to be large enough to capture all charged soot mode particles. These parameters equal a limiting mobility of $1.466 \cdot 10^{-4}$ cm²/(V·s), or in terms of particle size, a singly charged 140 nm particle or doubly charged 220 nm particle.
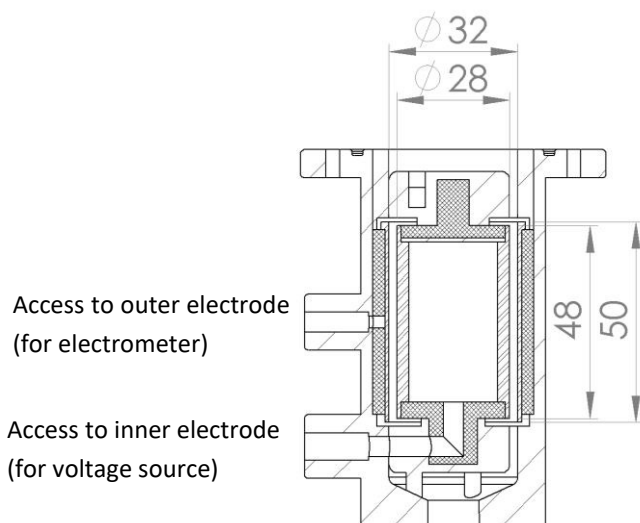
Figure 8. The mobility analyzer portion of the sensor. The aerosol enters from the top and exits through the bottom. The main body of the sensor is stainless steel, the tightly cross-hatched sections are an electrically insulating material. Figure adapted from Paper IV (supplementary material).

Laboratory characterization

The laboratory characterization was conducted with the setup shown in **Figure 9**. The dotted line encapsulates SCAR (Singly Charge Aerosol Reference), a system for producing singly charged monodisperse particles (Yli-Ojanperä et al., 2010). The reference instrument is an FCAE (Faraday cup and electrometer, Keithley 6430 Sub-Femtoamp Remote SourceMeter, Keithley Inc.). To measure the penetration of particles through the ICP-sensor, a CPC (model 3750 by TSI Inc.) was placed after the sensor.
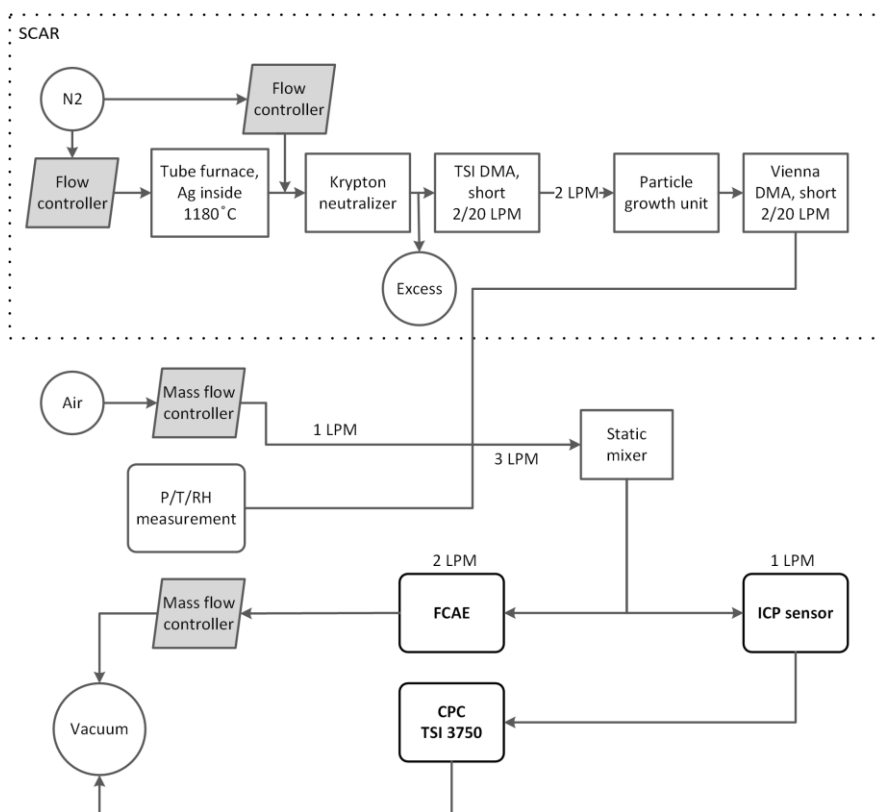
Figure 9. The schematic for laboratory characterization of the ICP-sensor. Figure adapted from Paper IV.

The basic principle of the ICP sensor is that it uses an electric field to collect charged particles onto two opposing surfaces, one of which is connected to electrometer allowing current created by collected charged particles to be measured. The theoretical detection efficiency was calculated based on eq. (15), using eq. (11) to determine the Z_0 value and eq. (10) for the Z value. **Figure 10** shows the measured detection efficiency for two particle sizes: 25 nm and 100 nm. To achieve different Z to Z_0 ratios, the collection voltage was altered, thereby changing the Z_0 value. Other options were to change the sample flowrate, the test particle size, or the number of elementary charges on the particles, but the collection voltage is the easiest and fastest to control. The measured efficiency of the sensor is the percentage of particles detected compared to the reference FCAE.
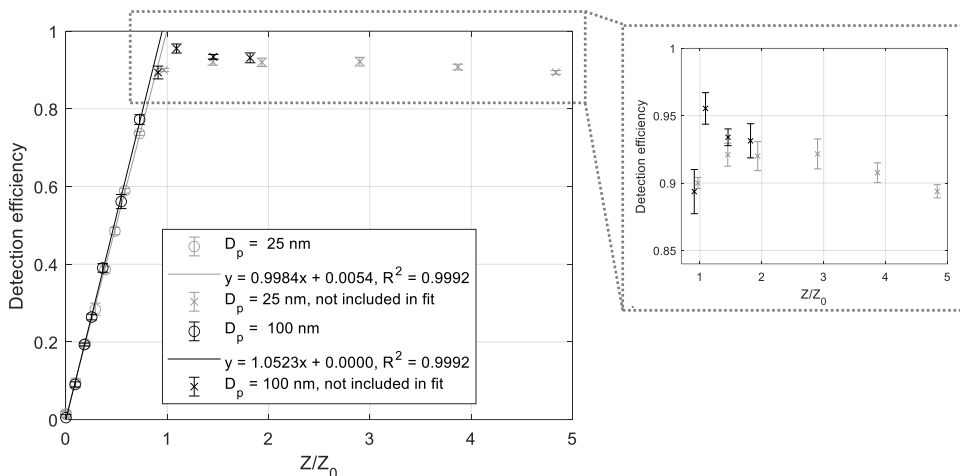
Figure 10. Characterization of the ICP sensor's mobility analyzer's detection efficiency. Figure adapted from Paper IV.

Judging by the coefficients shown in **Figure 10**, the effective length is almost equal to the physical length of the collection electrode. It should be noted that the electrode collecting particles for current measurement is longer (50 mm) than the opposing electrode (48 mm, connected to a voltage source), and for this calculation the shorted length electrode was used. The fit for 100 nm was slightly steeper than for 25 nm particles, possibly due to increased diffusional losses for the 25 nm particles. Zooming into the area where the detection efficiency is at its maximum, it nears one and begins to slowly decrease at higher ratios. As the ratio was controlled with the collection voltage, which increases towards the right, the electrical losses due to edge effects from the electrical field may be the cause for the decrease in detection efficiency. The sensor diffusion losses were measured as a function of particle size. The measurements matched the theoretical losses of a 4.263 m tube, calculated according to Gormley & Kennedy (1948). For 25 nm particles the losses were between 6 % to 12 %, whereas the losses for 100 nm particles were essentially zero.

Additional measurements were made with different particle number concentrations and the detection efficiency was found to be higher for lower concentrations. I also tested the sensor for losses in its full configuration, the efficiency peaked at 0.92 compared to 0.95 for just the mobility analyzer. The additional losses came simply from the ion trap and additional tubing required to attach the ion trap to the mobility analyzer.

Test cases

The two test cases were 1) engine exhaust from a heavy-duty vehicle and 2) ambient air at a roadside in Delhi-NCR. The engine exhaust measurements were in an engine laboratory, where the exhaust was sampled using a Constant Volume Sampler, CVS. The vehicle was a typical heavy-duty truck with a diesel oxidation catalyst (DOC) but no particulate filter. The vehicle was driven following the Delhi Bus Driving Cycle (DBDC), which is designed to mimic typical Delhi traffic. The highest speed in the cycle is 50 km/h. The test matrix included different fuels and oils, as well as cold and warm starts, in-depth information has been published by Martikainen et al. (2023). The ICP-sensor was operated mostly with a positive voltage (therefore measuring positively charged particles), but a few cycles were also measured with a negative voltage for comparison.

As mentioned previously, the ambient tests were done alongside the measurements for Paper III. A negative voltage was applied to the sensor to measure negatively charged particles, which are (in theory at least) slightly more numerous than positively charged particles.

For both test cases, a theoretical charge concentration was calculated based on measurements with the ELPI+ and using eq. (3), the Boltzmann distribution (T = 500°C), to approximate the charge distribution for engine exhaust particles, and eq. (4) and eq. (7) to approximate the ambient charge distribution. The diffusion losses of the ICP were also noted, and the ELPI+ currents were adjusted accordingly.

5   RESULTS AND DISCUSSION

Together the four Papers included in this thesis build a picture of the current electrical measurement methods, aerosol distributions in traffic-influenced environments, and the types of challenges faced. This section presents the most relevant results from each paper regarding the broader topic of this thesis.

5.1   Comparison of online and offline results for mass concentration

The purpose of the Paper I study was to compare online electrical instruments to offline aerosol sampling. The main metric for comparison was the particle mass concentration each instrument measured, as the offline method, sampling with the PM10 cascade impactors, cannot be easily employed for other metrics. **Figure 11** presents the mass concentration in flue gas samples taken from oil shale and wood combustion, as well as the intercorrelation between two ELPI+ units and two PM10 cascade impactor units. Each sample is the duration of a sample taken with the PM10 cascade impactors. The corresponding time was averaged from the ELPI+ and eFilter. Although the eFilter also contains a filter, the samples taken with it do not match the PM10 samples—the mass concentration for the correct time period was inferred from the online current measurement.
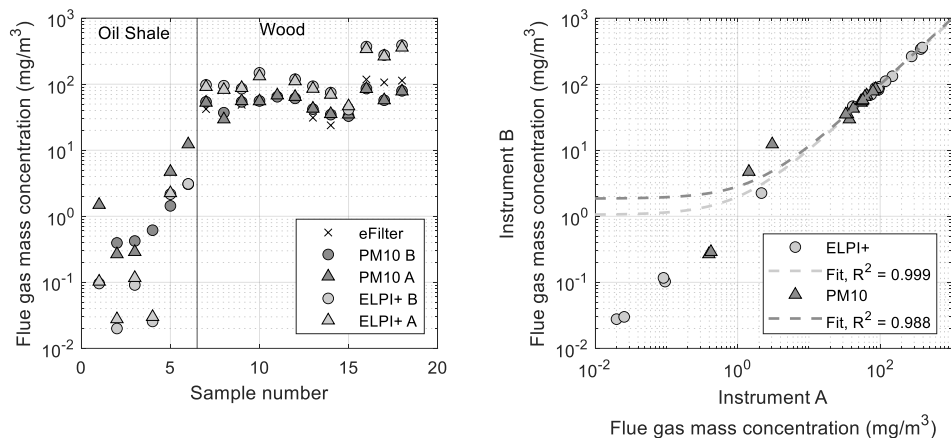
Figure 11. Mass concentration of particles measured from two combustion emission sources, covering a large range of concentrations. Figure adapted from Paper I with permission from Taylor & Francis.

The oil shale combustion aerosol had far less particle mass than the wood combustion aerosol (measured from the flue gas), thus the instruments were tested both at low and high concentrations. In some of the oil shale measurements the PM10 cascade impactor samples resulted in negative masses, and they are missing from these logarithmic plots. The ELPI+ instruments reported lower concentrations than the PM10 cascade impactors at low concentrations (oil shale), and vice versa when the measured concentration was high. The difference for the high concentration measurements is attributed in part to semi-volatile particles, such as polycyclic aromatic hydrocarbons, which are released in abundance from wood combustion (Shen et al., 2017). Some semi-volatiles may still have been in gaseous form when passing through the PM10 impactors, as they were at a higher temperature than the ELPI+, or the collected particles may have evaporated from before weighing. The eFilter was only included in the wood combustion study, where it reported results similar to the PM10 cascade impactors. The correlation plot shows that both the PM10 cascade impactors and the ELPI+ are very well intercorrelated. The two diverging points in the PM10 results were most likely due to a misaligned sampling nozzle.

In Figure 5 of Paper I, the size distributions of particles measured by ELPI+ in terms of current, number and mass are compared. The difference in the raw current distributions is very small; however, small differences in current become large

differences in the number concentration of the smallest particles (< 10 nm) and mass concentration of the largest particles (< 2 μm). Additionally, the presence of large amounts of sub-10 nm particles may cause errors if the correction for deposition by diffusion is not sufficient. The most reliably measured particles are the midrange stages.

Overall, Paper I showed the ELPI+ to be a robust and reliable instrument, although care must be taken especially with mass concentration, where the deposition of small particles by diffusion may have a significant effect on the total mass concentration.

5.2   LDSA in the underground mine

Underground mines require mechanical ventilation to circulate air, and it is very important for occupational hygiene that exhaust fumes are quickly removed. The two main aims of Paper II were to investigate the LDSA distributions inside an underground mine and establish whether LDSA sensors are a suitable option for monitoring air quality in the underground mine. The ELPI+ is the reference instrument for the sensor. As shown in Paper I, the midrange stages, around 10 nm to 1 μm, which correspond to most of the surface area concentration in traffic-influenced environments can be reliably measured with the ELPI+, additionally, it measures the LDSA for a large size range of particles.

Figure 12 shows a timeseries of the sensor comparison, as well as a correlation plot of each sensors' measurement results against the LDSA measured with the ELPI+. The lines show fits for each data set and the corresponding equations are in the legend. The AQ Indoor sensors achieved the best correlation factors; however, the equations reveal that these sensors reported 50 % higher concentrations than the ELPI+. Overall, all the sensors report higher concentration than the ELPI+ on average, and looking at the timeseries, the discrepancy was especially large at the end. The end of the measurement period had a particularly wide particle size distribution, with a large concentration of small and large particles. An examination of the sensor to ELPI+ LDSA variation in relation to the presence of either large or small particles revealed that small particles (sub 30 nm) caused an overestimation of LDSA. Most likely this is due to the sensors being calibrated for a larger median particle size. The closest to a one-to-one relationship was the Partector$_A$.

While the larger particles did not seem to significantly distort the measurement results, they did cause problems by depositing inside the sensors. The DiSCmini and

Partectors had to be cleaned several times (the DiSCmini impactor and the Partector corona wire chambers). A qualitative result of this study is that a cyclone significantly increases the maintenance-free operation time of a sensor-type instrument in this environment.
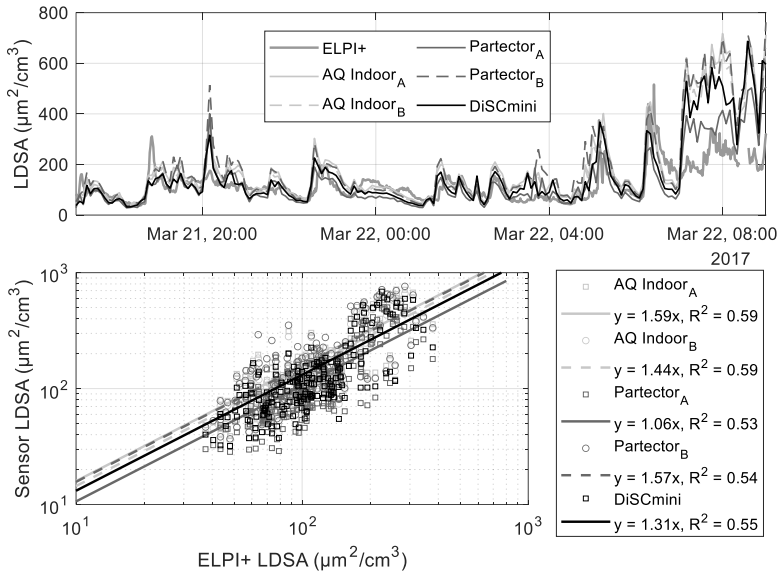
Figure 12. Comparison of LDSA measured with electrical particle sensors to LDSA measured with the ELPI+ in the maintenance area of an underground mine. The original data was averaged into 5-minute time bins. Figure adapted from Paper II.

Figure 13 shows LDSA size distributions measured at the various mine locations. Several locations show a mode at roughly 100 nm, which corresponds to the soot mode of diesel exhaust. Several locations have a second mode at a larger particle size, which could indicate mechanically produced particles (dust). The only location with a larger mode size is the blasting area, influenced by dust from the blast. The lowest measured concentration is at the maintenance area. Although not pictured here, brief measurements were conducted inside the mine canteen (located near the maintenance area); however, there were essentially no particles there, showing that air can be kept clean with filters and ventilation, even in challenging areas. **Figure 13** includes two lines measured at the conveyor belt, as the particle levels were very different for two measurements (at different times).

The overall LDSA concentration in the maintenance area is high in comparison to typical urban concentrations; however, it is comparable to a previous study on

mine LDSA (Huynh et al., 2018). Also importantly, the LDSA concentration was low inside the canteen and offices, where workers spend a lot of time without any barriers to the ambient air. At the other locations, most of the work was done inside vehicles.
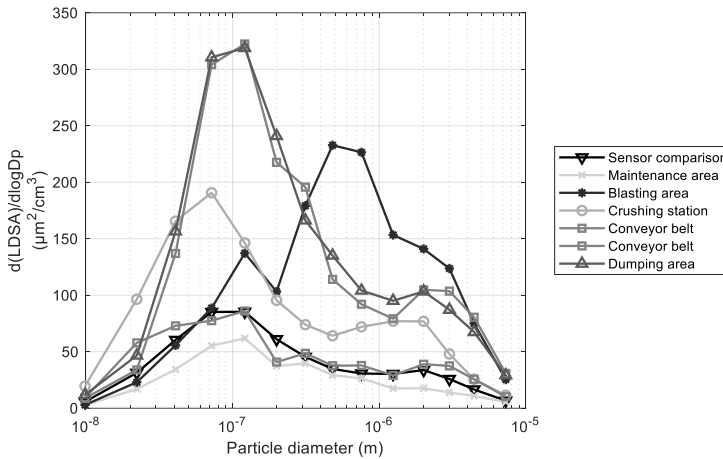
Figure 13. LDSA size distributions in different areas of the studied underground mine. Figure adapted from Paper II.

Very little LDSA in the mine was contributed by particles larger than 2.5 μm (less than 13 % for all areas), and there was large variation in the LDSA to mass ratios: 0.9 in the blasting area and 1.6 in the maintenance area (units μm²cm⁻³μg⁻¹m³). These observations show that mass-based monitoring and guideline values are not sufficient for ensuring good air quality.

5.3 Particle size distributions in urban air

In Paper III the contrasting air quality of two cities, Helsinki, and Delhi-NCR, was measured with the same instrumentation to determine particle size distributions.

Figure 14 shows the particle number, LDSA and mass size distributions measured in Helsinki and in Delhi-NCR. The top row distributions are normalized to a maximum concentration of 1 to allow for easier comparison of the mode sizes. The bottom row shows the distributions with the absolute concentrations. Particle modes described in section 2.1 and **Figure 1** can be identified in these measured

results. Nucleation mode particles dominate each of the number size distributions, and the soot mode particles form a second smaller mode. The mass size distributions each have a dominant mode in the range of the accumulation mode particles.
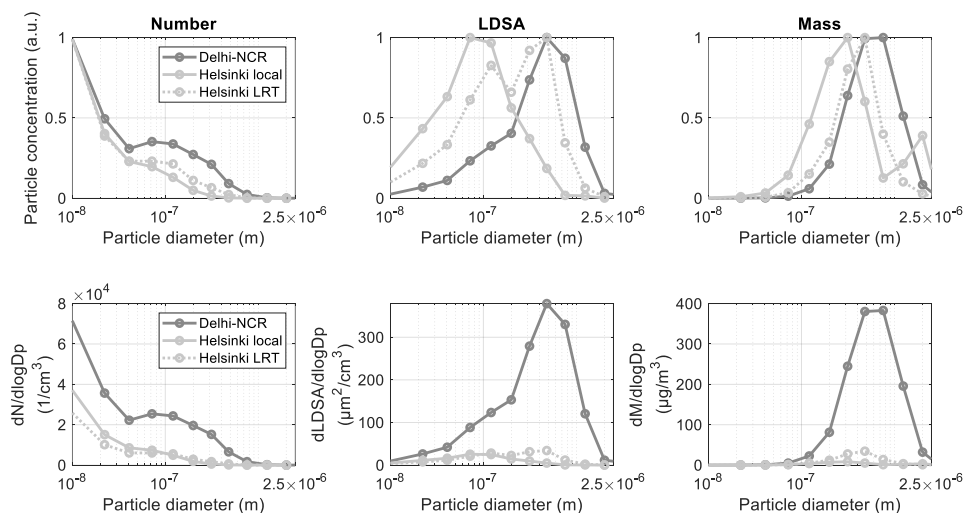
Figure 14. Number, LDSA and mass size distributions measured in Delhi-NCR and Helsinki. Figure adapted from Paper III.

The most interesting result is the LDSA distribution modes. The Helsinki local LDSA distribution shows that the soot mode contributes most to the lung-depositing particles, whereas the highest mode of the Delhi-NCR distribution is firmly within the accumulation particle size range—although the soot mode particles create a "shoulder" in the distribution. Finally, the LRT-episode in Helsinki includes the same soot mode as the local distribution, but also an approximately equal height accumulation particle mode. The contrast between the different size distributions (when viewing the normalized distribution) is small for number and mass, whereas the LDSA distributions have profoundly different modes. Other studies in Europe have found a local emissions to be the largest contributor to LDSA (Hama et al., 2017; Lepistö et al., 2022; Shah et al., 2023), and one other study in Asia (in Taipei) also found that LDSA consisted mostly of accumulation mode particles (Chen et al., 2023).

As was the case between locations in Paper II, the LDSA to mass concentrations were inconsistent between Helsinki Local and Helsinki LRT and Delhi-NCR. Whereas in Delhi-NCR mass concentration and LDSA concentration are highly

correlated, there is almost no correlation between the two in Helsinki, especially when the particles are from the local sources. The LDSA to mass ratio in Helsinki (local emissions only) was more than twice the amount in Delhi-NCR. These results hint at one reason why $PM_{2.5}$ toxicity depends on location: the particles lungs are exposed to are of different sizes and therefore of different origins and chemical compositions as well. Again, this result emphasizes the need for more than a single particle concentration metric.

5.4   Measurements with the novel electrical sensor

Paper IV presents the novel ICP-sensor for particle measurement. The characterization results were presented in section 4.6 and this result section covers the two test cases: engine exhaust measurements in a laboratory and ambient roadside measurements in Delhi-NCR.

The measured charge concentration inside the CVS in the engine exhaust tests was between $0 \, fC/cm^3$ to $60 \, fC/cm^3$. The ambient charge concentration was between $1 \, fC/cm^3$ to $6 \, fC/cm^3$. **Figure 15** shows that the ICP-sensor results correlated very well with the theoretical charge concentration, as calculated from the ELPI+ particle number size distribution.
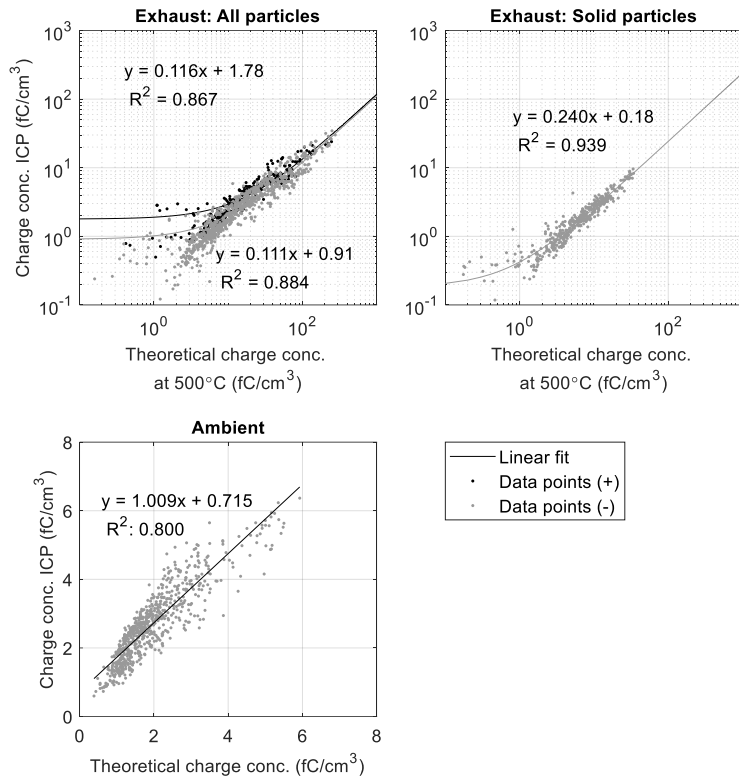
Figure 15. The measured charge concentration (ICP) versus the theoretical charge concentration based on the number distribution from the ELPI+ and the equilibrium charge distribution predicted by the Boltzmann distribution (engine exhaust, top) or Wiedensohler formulation (ambient air, bottom). Figure adapted from Paper IV.

In **Figure 15**, the engine exhaust charge concentration is compared to the Boltzmann distribution at 500°C while the ambient concentration is compared to the Wiedensohler distribution for negative charge. In the engine exhaust case, while the measured and theoretical charge concentrations correlated well, the measured concentration was much lower, only 10 % for "all particles" and 20 % for "solid particles". Previous research has found engine exhaust charge distributions to correspond to Boltzmann distributions between temperatures of 500°C to 800°C (Maricq, 2006)—the reason for this different result remains uncertain.

In the ambient case there was more variation, but the best fit line was almost one to one. Investigation of the residuals of the fitted line revealed that soot mode particles were associated with a higher measured than theoretical charge concentration, whereas the opposite was true for nucleation mode particles. This

result is in line with previous research, which has found that nucleation particles emitted with exhaust are uncharged (Jung & Kittelson, 2005b; Sgro et al., 2011), and that soot particles retain the higher charge numbers incurred in the engine for some time after emission into ambient air (Jayaratne et al., 2014).

Number

$y = 0.15x + 8.75$
R^2: 0.774
$y = 0.59x + 3.94$
R^2: 0.819

Surface area

$y = 0.26x + -4.78$
R^2: 0.874
$y = 0.16x + 0.65$
R^2: 0.739

Mass

$y = 3.08x + 11.00$
R^2: 0.224
$y = 2.14x + 9.63$
R^2: 0.108

$y = 1.993x + 1.482$
R^2: 0.493

$y = 0.069x + -0.180$
R^2: 0.800

$y = 0.684x + 0.204$
R^2: 0.555
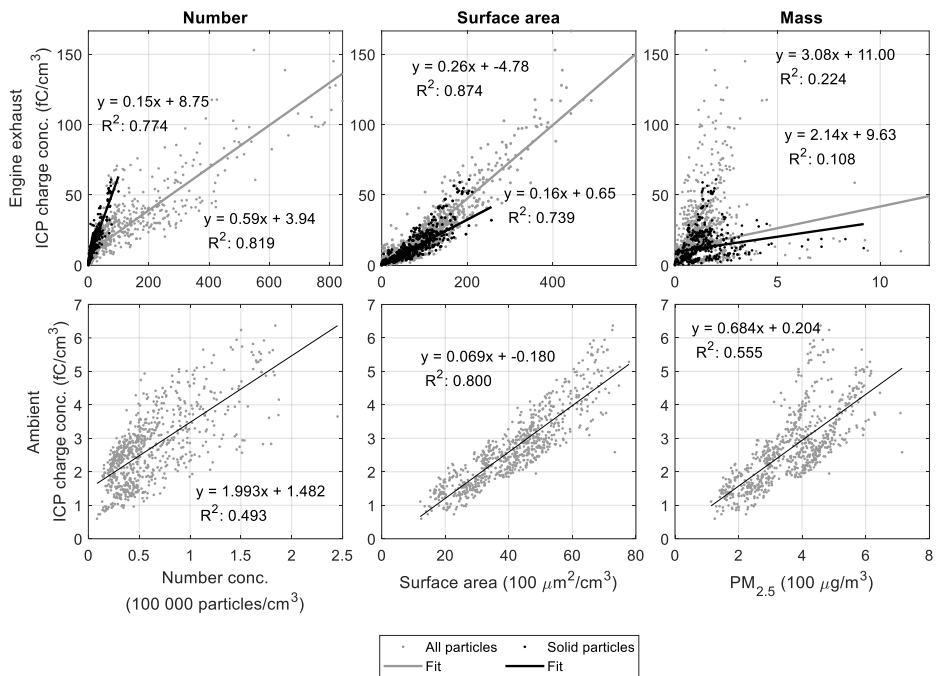
Figure 16. Charge concentration measured with the ICP-sensor compared to number, surface area and mass concentration from the ELPI+, measured from engine exhaust (top row) and ambient air (bottom row). Figure adapted from Paper IV.

Because charge concentration is not a widely used metric, it is interesting to see whether it correlates with any more common particle concentration metrics. **Figure 16** shows the correlation between the particle charge concentration and the number, surface area and mass concentration. The top row is for engine exhaust and the bottom row for ambient measurements. The particles size distributions for the engine study are reported by Martikainen et al. (2023) and the ambient size distributions are the same as in Paper III (Delhi-NCR).

The exhaust data is separated into "All particles" and "Solid particles", and for the number concentration the two groups have very different fits, showing that the solid particles are much more highly charged on a per particle basis. This is the expected result, as previous research has demonstrated that combustion-originated

nucleation particles are uncharged (Maricq, 2006; Sgro et al., 2011). The correlation with surface area is good for both particle groups, and there is less difference between the groups. There is little correlation with particle mass concentration (for either group).

In the ambient cases, the charge concentration is well-correlated with all three metrics, but the correlation coefficient is the highest for the surface area concentration (R^2=0.800). Based on **Figure 5**, the correlation for number and surface area concentrations is expected to be about the same; however, the nucleation mode particles, which make up a large portion of the number concentration, tended to be less charged than the ambient equilibrium predicts, hence the poorer correlation with number (R^2=0.493). The relatively good correlation ($R^2 = 0.555$) with the mass concentration is the most surprising result; however, LDSA and mass concentration were also found to be well-correlated in Paper III.

In a previous study by Y. Li et al. (2022), they reported that measurements with an SMPS (Scanning Mobility Particle Sizer) can be conducted without using a neutralizer, and still achieve reliable results, simply by using the inherent particle charge for classification. In analyzing the results in Paper IV, I noted a similar result: an excellent correlation between charge concentration measured from inherently charged particles and diffusion charged particles. The result was almost the same between the engine laboratory and the ambient measurement results, including the correlation coefficient and the slope of the fit (R^2=0.92 and R^2=0.87, slope = 0.63 and slope = 0.76, when adjusted to the same flow rates). Research regarding this finding is currently ongoing. If this relationship holds in other environments as well, the use of DCs could be unnecessary in cases where the inherent particle charge concentration is high enough for detection and the price of the sensor is an important factor.

Overall, the sensor's performance in both applications showed it to be a suitable option for particle monitoring, especially for high pollution environments. On its own, it can be used to measure particle pollution as charge concentration—or possibly surface area; however, one should be careful to note that sensitivity was poor for nucleation mode particles. Combined with the ELPI+ data, the sensor data showed that ambient particles in the soot mode size range were highly charged whereas nucleation mode particles were less charged than the theoretical equilibrium state.

6   SUMMARY

One important measure of good air quality is low aerosol particle concentration, but should the concentration be measured as mass, number, surface area or something else? The results from this thesis show that low particle mass concentration is not an exhaustive criterion, despite being the only widespread ambient air quality particle metric. UFP are barely detectable by mass, yet their small size allows them to easily bypass barriers meant to keep toxins outside of our bodies and organs. Furthermore, toxicological studies have found the surface area of solid particles, rather than mass, to better correlate with health effects. This thesis gives an overview of the current knowledge of particle populations in different traffic-influenced surroundings and discusses both commercially available electrical measurement methods and the potential of the newly developed ICP-sensor.

Paper I established the ELPI+ as a reliable instrument, based on the high correlation of results between two ELPI+ units. That being said, mass concentrations measured with the ELPI+ should be reported with caution, paying close attention to the contribution from higher stages. A simple test for whether the mass of a given stage should be included, is to check if the current from that stage is at least 2.5 % of the total measured current. Overall, the ELPI+ is a highly useful instrument, as it enables high time resolution measurement of a wide particle distribution.

In Paper II, four of the five sensors included in the test significantly overestimated the LDSA concentration, especially when the measured particle distribution contained two separate modes. Additionally, only the sensors which had a cyclone to remove coarse dust were able to measure without fault for a longer duration (several weeks, until the campaign ended). Despite the less-than-perfect measurement results, air quality monitoring in an underground mine needs to include a method for UFP (as established with the size distribution measurements), and the diffusion charging based sensors are a decent option.

Paper III presented particle size distributions in two traffic influenced environments and showed how the measurement metric plays an important role in understanding air quality. The different LDSA distribution modes indicated that the most important lung-depositing particles are from different aerosol sources.

Whereas the particle number and mass size distributions had roughly the expected particles modes, the particle LDSA size distribution revealed a major difference between the two environments. This finding has significance for the future of air quality monitoring and the design of instruments for different environments.

Papers I-III revealed many challenges that aerosol instrumentation must overcome. Aerosol populations vary in concentration and in the particle mode sizes, both spatially and temporally. A single instrument is unlikely able to be suitable for every situation. Traffic environments typically have particles in one to three modes, as discussed in section 2.1, and found experimentally to be true for the environments in Paper II and Paper III. While number concentration emphasizes the nucleation mode particles, and mass concentration emphasizes the accumulation mode or coarse mode particles, surface area concentration gives a good middle ground. Additionally, surface area is a health relevant metric which can be monitored efficiently with electrical sensors.

Paper IV introduced the newly developed ICP-sensor for measuring the naturally occurring particle charge concentration. The sensor has high detection efficiency, over 90 % for the targeted range, and a limit of detection corresponding to 1500 100 nm particles/cm^3 at ambient charge distributions (three times the standard deviation of the noise level measured at 1 Hz). The signal is well-correlated with particle surface area in ambient air ($R^2=0.800$) and the sensor handles high concentrations without trouble, at least for some weeks. The roadside testing showed it to have good potential for monitoring purposes in highly polluted traffic environments. Interestingly, the ICP-sensor response was very well correlated with diffusion charged particles. Compared to diffusion-charging sensors, it has the benefit of not needing the corona charger: one less part which may break and lower power-usage. On the downside, it cannot measure low concentrations accurately, although different choices for the geometry, flowrate and collection voltage allow for endless possibilities to target specific particle size ranges or concentrations.

To reiterate, the two most important findings of this thesis are the vast difference in size between lung-depositing particles in the studied cities and the potential of monitoring particles based on their inherent charge, especially in areas with heavy pollution from traffic. These two findings are related in that inherent charge correlated very well with surface area, therefore targeting the metric that best differentiates the particle size distribution of these two locations. These findings also point a clear direction for next steps: expand the measurements to new cities and areas with different emission sources to further establish the potential and limitations

of measurement based on the inherent particle charge. Depending on the findings, new sensor versions can be built to better suit different surroundings.

REFERENCES

Aarnio, P., Yli-Tuomi, T., Kousa, A., Mäkelä, T., Hirsikko, A., Hämeri, K., Räisänen, M., Hillamo, R., Koskentalo, T., & Jantunen, M. (2005). The concentrations and composition of and exposure to fine particles (PM2.5) in the Helsinki subway system. *Atmospheric Environment*, *39*(28), 5059–5066. https://doi.org/10.1016/j.atmosenv.2005.05.012

Abbot, C. G., & Fowle, F. E. (1913). Volcanoes and climate. *Smithsonian Miscellaneous Collections*, *60*(29).

Aguilera, I., Dratva, J., Caviezel, S., Burdet, L., De Groot, E., Ducret-Stich, R. E., Eeftens, M., Keidel, D., Meier, R., Perez, L., Rothe, T., Schaffner, E., Schmit-Trucksäss, A., Tsai, M. Y., Schindler, C., Künzli, N., & Probst-Hensch, N. (2016). Particulate matter and subclinical atherosclerosis: Associations between different particle sizes and sources with carotid intima-media thickness in the SAPALDIA study. *Environmental Health Perspectives*, *124*(11), 1700–1706. https://doi.org/10.1289/EHP161

Aitken, J. (1881). Dust, Fogs, and Clouds. *Nature*, *23*(591), 384–385. https://doi.org/10.1038/023384a0

Aitken, J. (1895). On some Observations made without a Dust Counter on the Hazing Effect of Atmospheric Dust. *Proceedings of the Royal Society of Edinburgh*, *20*, 76–93. https://doi.org/10.1017/s0370164600048422

Aldrich, L. B. (1927). The influence of the atmospheric constituents upon climate. *Transactions, American Geophysical Union*, *8*(1), 19. https://doi.org/10.1029/TR008i001p00019

Aplin, K. L. (2005). Aspirated capacitor measurements of air conductivity and ion mobility spectra. *Review of Scientific Instruments*, *76*(10), 104501. https://doi.org/10.1063/1.2069744

Aurela, M., Mylläri, F., Konist, A., Saarikoski, S., Olin, M., Simonen, P., Bloss, M., Nešumajev, D., Salo, L., Maasikmets, M., Sipilä, M., Maso, M. D., Keskinen, J., Timonen, H., & Rönkkö, T. (2021). Chemical and physical characterization of oil shale combustion emissions in Estonia. *Atmospheric Environment: X*, *12*, 100139. https://doi.org/10.1016/j.aeaoa.2021.100139

Baltensperger, U., Gäggeler, H. W., Jost, D. T., Emmenegger, M., & Nägeli, W. (1991). Continuous background aerosol monitoring with the epiphaniometer. *Atmospheric Environment. Part A. General Topics*, *25*(3), 629–634. https://doi.org/10.1016/0960-1686(91)90060-K

Biskos, G., Reavell, K., & Collings, N. (2005). Unipolar diffusion charging of aerosol particles in the transition regime. *Journal of Aerosol Science*, *36*(2), 247–265. https://doi.org/10.1016/j.jaerosci.2004.09.002

Brook, R. D., Rajagopalan, S., Pope, C. A. 3rd, Brook, J. R., Bhatnagar, A., Diez-Roux, A. V., Holguin, F., Hong, Y., Luepker, R. V., Mittleman, M. A., Peters, A., Siscovick, D., Smith, S. C. J., Whitsel, L., & Kaufman, J. D. (2010). Particulate matter air pollution and cardiovascular disease: An update to the scientific statement from the American

Heart Association. *Circulation*, *121*(21), 2331–2378. https://doi.org/10.1161/CIR.0b013e3181dbece1

Chen, T.-L., Lai, C.-H., Chen, Y.-C., Ho, Y.-H., Chen, A. Y., & Hsiao, T.-C. (2023). Source-oriented risk and lung-deposited surface area (LDSA) of ultrafine particles in a Southeast Asia urban area. *Science of The Total Environment*, *870*, 161733. https://doi.org/10.1016/j.scitotenv.2023.161733

Debia, M., Couture, C., Njanga, P.-E., Neesham-Grenon, E., Lachapelle, G., Coulombe, H., Hallé, S., & Aubin, S. (2017). Diesel engine exhaust exposures in two underground mines. *International Journal of Mining Science and Technology*, *27*(4), 641–645. https://doi.org/10.1016/j.ijmst.2017.05.011

Dhaniyala, S., Fierz, M., Keskinen, J., & Marjamäki, M. (2011). Instruments Based on Electrical Detection of Aerosols. In *Aerosol Measurement: Principles, Techniques, and Applications: Third Edition* (pp. 393–416). John Wiley & Sons, Inc. https://doi.org/10.1002/9781118001684.ch18

Emmerson, K., & Keywood, M. (2021). Air quality: Climate change. In *Australia State of the environment 2021*. Australian Government Department of Agriculture, Water and the Environment. https://doi.org/10.26194/k7x7-0j76

Enroth, J., Saarikoski, S., Niemi, J., Kousa, A., Ježek, I., Močnik, G., Carbone, S., Kuuluvainen, H., Rönkkö, T., Hillamo, R., & Pirjola, L. (2016). Chemical and physical characterization of traffic particles in four different highway environments in the Helsinki metropolitan area. *Atmospheric Chemistry and Physics*, *16*(9), 5497–5512. https://doi.org/10.5194/acp-16-5497-2016

European Environment Agency (EEA). (2021). *Airbase*. European Commission. https://www.eea.europa.eu/data-and-maps/data/aqereporting-9

Fierz, M., Meier, D., Steigmeier, P., & Burtscher, H. (2014). Aerosol Measurement by Induced Currents. *Aerosol Science and Technology*, *48*(4), 350–357. https://doi.org/10.1080/02786826.2013.875981

Fissan, H., Neumann, S., Trampe, A., Pui, D. Y. H., & Shin, W. G. (2007). Rationale and principle of an instrument measuring lung deposited nanoparticle surface area. *Journal of Nanoparticle Research*, *9*(1), 53–59. https://doi.org/10.1007/s11051-006-9156-8

Flagan, R. C. (1998). History of Electrical Aerosol Measurements. *Aerosol Science and Technology*, *28*(4), 301–380. https://doi.org/10.1080/02786829808965530

Flagan, R. C. (2011). Electrical Mobility Methods for Submicrometer Particle Characterization. In P. Kulkarni (Ed.), *Aerosol Measurement: Principles, Techniques, and Applications* (3rd ed.). John Wiley & Sons, Incorporated.

Fleagle, R. G., & Businger, J. A. (1980). *An Introduction to Atmospheric Physics: Vol. 2d ed* (Issue v. 25). Academic Press; eBook Academic Collection (EBSCOhost).

Forsyth, B., Liu, B. Y. H., & Romay, F. J. (1998). Particle Charge Distribution Measurement for Commonly Generated Laboratory Aerosols. *Aerosol Science and Technology*, *28*(6), 489–501. https://doi.org/10.1080/02786829808965540

Fuchs, N. A. (1963). On the stationary charge distribution on aerosol particles in a bipolar ionic atmosphere. *Geofisica Pura e Applicata*, *56*(1), 185–193. https://doi.org/10.1007/BF01993343

Fussell, J. C., Franklin, M., Green, D. C., Gustafsson, M., Harrison, R. M., Hicks, W., Kelly, F. J., Kishta, F., Miller, M. R., Mudway, I. S., Oroumiyeh, F., Selley, L., Wang, M., & Zhu, Y. (2022). A Review of Road Traffic-Derived Non-Exhaust Particles: Emissions, Physicochemical Characteristics, Health Risks, and Mitigation Measures.

Environmental Science & Technology, *56*(11), 6813–6835. https://doi.org/10.1021/acs.est.2c01072

Gerdien, H. (1905). Demonstration eines Apparates zur absoluten Messung der elektrischen Leitfahigkeit der Luft. *Phys. Z.*, *6*, 800–801.

Gettelman, A., Lin, L., Medeiros, B., & Olson, J. (2016). Climate Feedback Variance and the Interaction of Aerosol Forcing and Feedbacks. *Journal of Climate*, *29*(18), 6659–6675. https://doi.org/10.1175/JCLI-D-16-0151.1

Gormley, P. G., & Kennedy, M. (1948). Diffusion from a Stream Flowing through a Cylindrical Tube. *Proceedings of the Royal Irish Academy. Section A: Mathematical and Physical Sciences*, *52*, 163–169.

Grau III, R. H., Mucho, T. P., Robertson, S. B., Smith, A. C., & Garcia, F. (2002). Practical techniques to improve the air quality in underground stone mines. *Proc. 9th North Am. US Mine Vent. Symp*, 123–129.

Gunn, R., & Woessner, R. H. (1956). Measurements of the systematic electrification of aerosols. *Journal of Colloid Science*, *11*(3), 254–259. https://doi.org/10.1016/0095-8522(56)90050-2

Gustafsson, Ö., Kruså, M., Zencak, Z., Sheesley, R. J., & Granat, L. (2009). *Brown Clouds over South Asia: Biomass or Brown Clouds over South Asia : 84*(February 2016), 495–498. https://doi.org/10.1126/science.1164857

Hama, S. M. L., Ma, N., Cordell, R. L., Kos, G. P. A., Wiedensohler, A., & Monks, P. S. (2017). Lung deposited surface area in Leicester urban background site/UK: Sources and contribution of new particle formation. *Atmospheric Environment*, *151*, 94–107. https://doi.org/10.1016/j.atmosenv.2016.12.002

Health Effects Institute. (2020). *State of Global Air 2020* (p. 28). Health Effects Institute. https://www.stateofglobalair.org/resources

Heikkilä, J., Virtanen, A., Rönkkö, T., Keskinen, J., Aakko-Saksa, P., & Murtonen, T. (2009). Nanoparticle Emissions from a Heavy-Duty Engine Running on Alternative Diesel Fuels. *Environmental Science and Technology*, *43*(24), 9501–9506. https://doi.org/10.1021/es9013807

Hewitt, G. W. (1957). The charging of small particles for electrostatic precipitation. *Transactions of the American Institute of Electrical Engineers, Part I: Communication and Electronics*, *76*(3), 300–306. https://doi.org/10.1109/TCE.1957.6372672

Hinds, W. C. (1999). *Aerosol technology: Properties, Behavior, and Measurement of Airborne Particles*. Wiley.

Hirsikko, A., Nieminen, T., Gagné, S., Lehtipalo, K., Manninen, H. E., Ehn, M., Hõrrak, U., Kerminen, V.-M., Laakso, L., McMurry, P. H., Mirme, A., Mirme, S., Petäjä, T., Tammet, H., Vakkari, V., Vana, M., & Kulmala, M. (2011). Atmospheric ions and nucleation: A review of observations. *Atmospheric Chemistry and Physics*, *11*(2), 767–798. https://doi.org/10.5194/acp-11-767-2011

Hoover, K., & Hanson, L. A. (2021). Wildfire Statistics. *Congressional Research Service*, 2.

Hopke, P. K., Dai, Q., Li, L., & Feng, Y. (2020). Global review of recent source apportionments for airborne particulate matter. *Science of The Total Environment*, *740*, 140091. https://doi.org/10.1016/j.scitotenv.2020.140091

Hoppel, W. A., & Frick, G. M. (1986). Ion—Aerosol Attachment Coefficients and the Steady-State Charge Distribution on Aerosols in a Bipolar Ion Environment. *Aerosol Science and Technology*, *5*(1), 1–21. https://doi.org/10.1080/02786828608959073

Hõrrak, U., Aalto, P. P., Salm, J., Komsaare, K., Tammet, H., Mäkelä, J. M., Laakso, L., & Kulmala, M. (2008). Variation and balance of positive air ion concentrations in a boreal forest. *Atmospheric Chemistry and Physics*, *8*(3), 655–675. https://doi.org/10.5194/acp-8-655-2008

Hudda, N., Simon, M. C., Zamore, W., & Durant, J. L. (2018). Aviation-Related Impacts on Ultrafine Particle Number Concentrations Outside and Inside Residences near an Airport. *Environmental Science & Technology*, *52*(4), 1765–1772. https://doi.org/10.1021/acs.est.7b05593

Humphreys, W. J. (1920). *Physics of the air*. Pub. for the Franklin institute of the state of Pennsylvania by J. B. Lippincott company.

Huynh, T., Ramachandran, G., Quick, H., Hwang, J., Raynor, P. C., Alexander, B. H., & Mandel, J. H. (2018). Real-time fine aerosol exposures in taconite mining operations. *BioRxiv*, 263442. https://doi.org/10.1101/263442

Hyytinen, E.-R., Tiina, S., Vainiotalo, S., Rantonen, J., & Linnainmaa, M. (2016). *Justification memo for inhalable and respirable dust target level. Text in Finnish*. Finnish Institute of Occupational Health.

ICRP. (1994). Human respiratory tract model for radiological protection. A report of a Task Group of the International Commission on Radiological Protection. *Annals of the ICRP*, *24*(1–3), 1–482.

Ingo, G. M., Riccucci, C., Pisani, G., Pascucci, M., D'Ercole, D., Guerriero, E., Boccaccini, F., Falso, G., Zambonini, G., Paolini, V., & Di Carlo, G. (2022). The vehicle braking systems as main source of inhalable airborne magnetite particles in trafficked areas. *Environment International*, *158*, 106991. https://doi.org/10.1016/j.envint.2021.106991

Jacob, D. J., & Winner, D. A. (2009). Effect of climate change on air quality. *Atmospheric Environment*, *43*(1), 51–63. https://doi.org/10.1016/j.atmosenv.2008.09.051

Järvinen, A., Aitomaa, M., Rostedt, A., Keskinen, J., & Yli-Ojanperä, J. (2014). Calibration of the new electrical low pressure impactor (ELPI+). *Journal of Aerosol Science*, *69*, 150–159. https://doi.org/10.1016/J.JAEROSCI.2013.12.006

Jayaratne, E. R., Ling, X., & Morawska, L. (2014). Observation of ions and particles near busy roads using a neutral cluster and air ion spectrometer (NAIS). *Atmospheric Environment*, *84*, 198–203. https://doi.org/10.1016/j.atmosenv.2013.11.045

Jayaratne, E. R., Ling, X., & Morawska, L. (2015). Comparison of charged nanoparticle concentrations near busy roads and overhead high-voltage power lines. *Science of The Total Environment*, *526*, 14–18. https://doi.org/10.1016/j.scitotenv.2015.04.074

J-Fatokun, F. O., Morawska, L., Jamriska, M., & Jayaratne, E. R. (2008). Application of aerosol electrometer for ambient particle charge measurements. *Atmospheric Environment*, *42*(38), 8827–8830. https://doi.org/10.1016/j.atmosenv.2008.08.025

Jokinen, V. (1995). *Aerosolinhiukkasten ja ilman ionien mittaus differentiaalisella liikkuvuusanalysaatorilla* (V. Jokinen, Ed.). Aerosolitutkimusseura.

Jung, H., & Kittelson, D. B. (2005a). Characterization of Aerosol Surface Instruments in Transition Regime. *Aerosol Science and Technology*, *39*(9), 902–911. https://doi.org/10.1080/02786820500295701

Jung, H., & Kittelson, D. B. (2005b). Measurement of Electrical Charge on Diesel Particles. *Aerosol Science and Technology*, *39*(12), 1129–1135. https://doi.org/10.1080/02786820500430357

Karjalainen, P., Pirjola, L., Heikkilä, J., Lähde, T., Tzamkiozis, T., Ntziachristos, L., Keskinen, J., & Rönkkö, T. (2014). Exhaust particles of modern gasoline vehicles: A

laboratory and an on-road study. *Atmospheric Environment*, *97*, 262–270. https://doi.org/10.1016/j.atmosenv.2014.08.025

Keller, A., Fierz, M., Siegmann, K., Siegmann, H. C., & Filippov, A. (2001). Surface science with nanosized particles in a carrier gas. *Journal of Vacuum Science & Technology A: Vacuum, Surfaces, and Films*, *19*(1), 1. https://doi.org/10.1116/1.1339832

Keskinen, J., Pietarinen, K., & Lehtimäki, M. (1992). Electrical Low Pressure Impactor. *Journal of Aerosol Science*, *23*(4), 353–360.

Kittelson, D. B. (1998). Engines and nanoparticles: A review. *Journal of Aerosol Science*, *29*(5–6), 575–588. https://doi.org/10.1016/S0021-8502(97)10037-4

Knutson, E. O., & Whitby, K. T. (1975). Aerosol classification by electric mobility: Apparatus, theory, and applications. *Journal of Aerosol Science*, *6*(6), 443–451. https://doi.org/10.1016/0021-8502(75)90060-9

Kovochich, M., Parker, J. A., Oh, S. C., Lee, J. P., Wagner, S., Reemtsma, T., & Unice, K. M. (2021). Characterization of Individual Tire and Road Wear Particles in Environmental Road Dust, Tunnel Dust, and Sediment. *Environmental Science & Technology Letters*, *8*(12), 1057–1064. https://doi.org/10.1021/acs.estlett.1c00811

Krecl, P., Ström, J., & Johansson, C. (2008). Diurnal variation of atmospheric aerosol during the wood combustion season in Northern Sweden. *Atmospheric Environment*, *42*(18), 4113–4125. https://doi.org/10.1016/j.atmosenv.2008.01.026

Krecl, P., Targino, A. C., Lara, C., Oukawa, G. Y., Soares, J., & Mollinedo, E. M. (2023). Detecting local and regional air pollution from biomass burning at a suburban site. *Atmospheric Environment*, *297*, 119591. https://doi.org/10.1016/j.atmosenv.2023.119591

Kukutschová, J., Moravec, P., Tomášek, V., Matějka, V., Smolík, J., Schwarz, J., Seidlerová, J., Šafářová, K., & Filip, P. (2011). On airborne nano/micro-sized wear particles released from low-metallic automotive brakes. *Environmental Pollution*, *159*(4), 998–1006. https://doi.org/10.1016/j.envpol.2010.11.036

Kulkarni, P., Baron, P. A., & Willeke, K. (2011). *Aerosol Measurement: Principles, Techniques, and Applications*. John Wiley & Sons, Incorporated. http://ebookcentral.proquest.com/lib/tampere/detail.action?docID=693191

Kulmala, M., Vehkamäki, H., Petäjä, T., Dal Maso, M., Lauri, A., Kerminen, V.-M., Birmili, W., & McMurry, P. H. (2004). Formation and growth rates of ultrafine atmospheric particles: A review of observations. *Journal of Aerosol Science*, *35*(2), 143–176. https://doi.org/10.1016/j.jaerosci.2003.10.003

Kumar, P., Morawska, L., Birmili, W., Paasonen, P., Hu, M., Kulmala, M., Harrison, R. M., Norford, L., & Britter, R. (2014). Ultrafine particles in cities. *Environment International*, *66*, 1–10. https://doi.org/10.1016/j.envint2014.01.013

Kuuluvainen, H., Kannosto, J., Virtanen, A., Másigná, J. M., Kulmala, M., Aalto, P., & Keskinen, J. (2010). Technical Note: Measuring condensation sink and ion sink of atmospheric aerosols with the electrical low pressure impactor (ELPI). *Atmospheric Chemistry and Physics*, *10*(3), 1361–1368. https://doi.org/10.5194/acp-10-1361-2010

Laakso, L., Hirsikko, A., Grönholm, T., Kulmala, M., Luts, A., & Parts, T.-E. (2007). Waterfalls as sources of small charged aerosol particles. *Atmospheric Chemistry and Physics*, *7*(9), 2271–2275. https://doi.org/10.5194/acp-7-2271-2007

Lähde, T., Rönkkö, T., Virtanen, A., Schuck, T. J., Pirjola, L., Hämeri, K., Kulmala, M., Arnold, F., Rothe, D., Keskinen, J., Lähde, T., Rönkkö, T., Virtanen, A., Schuck, T. J., Pirjola, L., Hämeri, K., Kulmala, M., Arnold, F., Rothe, D., & Keskinen, J. (2009). Heavy duty diesel engine exhaust aerosol particle and ion measurements.

Environmental Science & Technology, *43*(1), 163–168. https://doi.org/10.1021/es801690h

Langevin, P. (1872–1946). (1950). *Sur les ions de l'atmosphère, C. R. Acad. Sci., 1905, 140, 232*. CNRS. http://rcin.org.pl/Content/194833/PDF/WA35_226694_8818_Art11.pdf

Lelieveld, J., Evans, J. S., Fnais, M., Giannadaki, D., & Pozzer, A. (2015). The contribution of outdoor air pollution sources to premature mortality on a global scale. *Nature*, *525*(7569), 367–371. https://doi.org/10.1038/nature15371

Lelieveld, J., Klingmüller, K., Pozzer, A., Pöschl, U., Fnais, M., Daiber, A., & Münzel, T. (2019). Cardiovascular disease burden from ambient air pollution in Europe reassessed using novel hazard ratio functions. *European Heart Journal*, *40*(20), 1590–1596. https://doi.org/10.1093/eurheartj/ehz135

Lepistö, T., Kuuluvainen, H., Juuti, P., Järvinen, A., Arffman, A., & Rönkkö, T. (2020). Measurement of the human respiratory tract deposited surface area of particles with an electrical low pressure impactor. *Aerosol Science and Technology*, *0*(0), 1–21. https://doi.org/10.1080/02786826.2020.1745141

Lepistö, T., Kuuluvainen, H., Lintusaari, H., Kuittinen, N., Salo, L., Helin, A., Niemi, J. V., Manninen, H. E., Timonen, H., Jalava, P., Saarikoski, S., & Rönkkö, T. (2022). Connection between lung deposited surface area (LDSA) and black carbon (BC) concentrations in road traffic and harbour environments. *Atmospheric Environment*, *272*, 118931. https://doi.org/10.1016/j.atmosenv.2021.118931

Leskinen, J., Tissari, J., Uski, O., Virén, A., Torvela, T., Kaivosoja, T., Lamberg, H., Nuutinen, I., Kettunen, T., Joutsensaari, J., Jalava, P. I., Sippula, O., Hirvonen, M. R., & Jokiniemi, J. (2014). Fine particle emissions in three different combustion conditions of a wood chip-fired appliance—Particulate physico-chemical properties and induced cell death. *Atmospheric Environment*, *86*, 129–139. https://doi.org/10.1016/j.atmosenv.2013.12.012

Li, J., Carlson, B. E., Yung, Y. L., Lv, D., Hansen, J., Penner, J. E., Liao, H., Ramaswamy, V., Kahn, R. A., Zhang, P., Dubovik, O., Ding, A., Lacis, A. A., Zhang, L., & Dong, Y. (2022). Scattering and absorbing aerosols in the climate system. *Nature Reviews Earth & Environment*, *3*(6), Article 6. https://doi.org/10.1038/s43017-022-00296-7

Li, X., Jin, L., & Kan, H. (2019). Air pollution: A global problem needs local fixes. *Nature*, *570*(7762), 437–439. https://doi.org/10.1038/d41586-019-01960-7

Li, Y., Chen, X., & Jiang, J. (2022). Measuring size distributions of atmospheric aerosols using natural air ions. *Aerosol Science and Technology*, *56*(7), 655–664. https://doi.org/10.1080/02786826.2022.2060795

Ling, X., Jayaratne, R., & Morawska, L. (2010). Air ion concentrations in various urban outdoor environments. *Atmospheric Environment*, *44*(18), 2186–2193. https://doi.org/10.1016/j.atmosenv.2010.03.026

Liu, B. Y. H., & Pui, D. Y. H. (1974a). A submicron aerosol standard and the primary, absolute calibration of the condensation nuclei counter. *Journal of Colloid and Interface Science*, *47*(1), 155–171.

Liu, B. Y. H., & Pui, D. Y. H. (1974b). Equilibrium bipolar charge distribution of aerosols. *Journal of Colloid And Interface Science*, *49*(2), 305–312. https://doi.org/10.1016/0021-9797(74)90366-X

Maricq, M. M. (2006). On the electrical charge of motor vehicle exhaust particles. *Journal of Aerosol Science*, *37*(7), 858–874. https://doi.org/10.1016/j.jaerosci.2005.08.003

Martikainen, S., Salo, L., Kuuluvainen, H., Teinilä, K., Hooda, R. K., Datta, A., Sharma, V. P., Rahman, H., Subudhi, S., Kumar, P., Karjalainen, P., Keskinen, J., Timonen, H.,

Hyvärinen, A., & Rönkkö, T. (2023). Reducing particle emissions of heavy-duty diesel vehicles in India: Combined effects of diesel, biodiesel and lubricating oil. *Atmospheric Environment: X, 17,* 100202. https://doi.org/10.1016/j.aeaoa.2023.100202

McClelland, J. A. (1898). II. On the conductivity of the hot gases from flames. *The London, Edinburgh, and Dublin Philosophical Magazine and Journal of Science, 46*(278), 29–42.

McDonald, J. D., Zielinska, B., Sagebiel, J. C., McDaniel, M. R., & Mousset-Jones, P. (2003). Source Apportionment of Airborne Fine Particulate Matter in an Underground Mine. *Journal of the Air \& Waste Management Association, 53*(4), 386–395. https://doi.org/10.1080/10473289.2003.10466178

Mylläri, F., Asmi, E., Anttila, T., Saukko, E., Vakkari, V., Pirjola, L., Hillamo, R., Laurila, T., Häyrinen, A., Rautiainen, J., Lihavainen, H., O'Connor, E., Niemelä, V., Keskinen, J., Dal Maso, M., & Rönkkö, T. (2016). New particle formation in the fresh flue-gas plume from a coal-fired power plant: Effect of flue-gas cleaning. *Atmospheric Chemistry and Physics, 16*(11), 7485–7496. https://doi.org/10.5194/acp-16-7485-2016

Myung, C. L., & Park, S. (2012). Exhaust nanoparticle emissions from internal combustion engines: A review. *International Journal of Automotive Technology, 13*(1), 9–22. https://doi.org/10.1007/s12239-012-0002-y

Noll, J. D., Bugarski, A. D., Patts, L. D., Mischler, S. E., & McWilliams, L. (2007). Relationship between Elemental Carbon, Total Carbon, and Diesel Particulate Matter in Several Underground Metal/Non-metal Mines. *Environmental Science & Technology, 41*(3), 710–716. https://doi.org/10.1021/es061556a

Nosko, O., Vanhanen, J., & Olofsson, U. (2017). Emission of 1.3–10 nm airborne particles from brake materials. *Aerosol Science and Technology, 51*(1), 91–96. https://doi.org/10.1080/02786826.2016.1255713

Oberdörster, G. (1996). Significance of particle parameters in the evaluation of exposure-dose response relationships of inhaled particles. *Particulate Science and Technology, 14*(2), 135–151. https://doi.org/10.1080/02726359608906690

Pandis, S. N., Baltensperger, U., Wolfenbarger, J. K., & Seinfeld, J. H. (1991). Inversion of aerosol data from the epiphaniometer. *Journal of Aerosol Science, 22*(4), 417–428. https://doi.org/10.1016/0021-8502(91)90002-Y

Patel, S., Leavey, A., Sheshadri, A., Kumar, P., Kandikuppa, S., Tarsi, J., Mukhopadhyay, K., Johnson, P., Balakrishnan, K., Schechtman, K. B., Castro, M., Yadama, G., & Biswas, P. (2018). Associations between household air pollution and reduced lung function in women and children in rural southern India. *Journal of Applied Toxicology, 38*(11), 1405–1415. https://doi.org/10.1002/jat.3659

Paulot, F., Paynter, D., Winton, M., Ginoux, P., Zhao, M., & Horowitz, L. W. (2020). Revisiting the Impact of Sea Salt on Climate Sensitivity. *Geophysical Research Letters, 47*(3), e2019GL085601. https://doi.org/10.1029/2019GL085601

Pirjola, L., Niemi, J. V., Saarikoski, S., Aurela, M., Enroth, J., Carbone, S., Saarnio, K., Kuuluvainen, H., Kousa, A., Rönkkö, T., & Hillamo, R. (2017). Physical and chemical characterization of urban winter-time aerosols by mobile measurements in Helsinki, Finland. *Atmospheric Environment, 158,* 60–75. https://doi.org/10.1016/j.atmosenv.2017.03.028

Pirjola, L., Pajunoja, A., Walden, J., Jalkanen, J. P., R??nkk??, T., Kousa, A., & Koskentalo, T. (2014). Mobile measurements of ship emissions in two harbour areas in Finland. *Atmospheric Measurement Techniques, 7*(1), 149–161. https://doi.org/10.5194/amt-7-149-2014

Platt, S. M., El Haddad, I., Pieber, S. M., Zardini, A. A., Suarez-Bertoa, R., Clairotte, M., Daellenbach, K. R., Huang, R. J., Slowik, J. G., Hellebust, S., Temime-Roussel, B., Marchand, N., De Gouw, J., Jimenez, J. L., Hayes, P. L., Robinson, A. L., Baltensperger, U., Astorga, C., & Prévôt, A. S. H. (2017). Gasoline cars produce more carbonaceous particulate matter than modern filter-equipped diesel cars. *Scientific Reports*, *7*(1), 1–9. https://doi.org/10.1038/s41598-017-03714-9

Polidori, A., Hu, S., Biswas, S., Delfino, R. J., & Sioutas, C. (2008). Real-time characterization of particle-bound polycyclic aromatic hydrocarbons in ambient aerosols and from motor-vehicle exhaust. *Atmospheric Chemistry and Physics*, *8*(5), 1277–1291. https://doi.org/10.5194/acp-8-1277-2008

Pope, C. A. (1989). Respiratory disease associated with community air pollution and a steel mill, Utah Valley. *American Journal of Public Health*, *79*(5), 623–628. https://doi.org/10.2105/AJPH.79.5.623

Pronk, A., Coble, J., & Stewart, P. A. (2009). Occupational exposure to diesel engine exhaust: A literature review. *Journal of Exposure Science & Environmental Epidemiology*, *19*(5), 443–457. https://doi.org/10.1038/jes.2009.21

Qian, Y., Li, Z., Yu, L., Wang, X., & Lu, X. (2019). Review of the state-of-the-art of particulate matter emissions from modern gasoline fueled engines. *Applied Energy*, *238*, 1269–1298. https://doi.org/10.1016/j.apenergy.2019.01.179

Reche, C., Viana, M., Brines, M., Perez, N., Beddows, D., Alastuey, A., & Querol, X. (2015). Determinants of aerosol lung-deposited surface area variation in an urban environment. *The Science of the Total Environment*, *517*, 38–47. https://doi.org/10.1016/j.scitotenv.2015.02.049

Ritchie, H., & Roser, M. (2022, January). *Outdoor Air Pollution*. Our World in Data. https://ourworldindata.org/outdoor-air-pollution

Rivas, I., Beddows, D. C. S., Amato, F., Green, D. C., Järvi, L., Hueglin, C., Reche, C., Timonen, H., Fuller, G. W., Niemi, J. V., Pérez, N., Aurela, M., Hopke, P. K., Alastuey, A., Kulmala, M., Harrison, R. M., Querol, X., & Kelly, F. J. (2020). Source apportionment of particle number size distribution in urban background and traffic stations in four European cities. *Environment International*, *135*, 105345. https://doi.org/10.1016/j.envint.2019.105345

Rohmann, H. (1923). Methode zur Messung der Grösse von Schwebeteilchen. *Zeitschrift für Physik*, *17*(1), 253–265. https://doi.org/10.1007/BF01328683

Rönkkö, T., Kuuluvainen, H., Karjalainen, P., Keskinen, J., Hillamo, R., Niemi, J. V., Pirjola, L., Timonen, H. J., Saarikoski, S., Saukko, E., Järvinen, A., Silvennoinen, H., Rostedt, A., Olin, M., Yli-Ojanperä, J., Nousiainen, P., Kousa, A., & Dal Maso, M. (2017). Traffic is a major source of atmospheric nanocluster aerosol. *Proceedings of the National Academy of Sciences*, *114*(29), 7549–7554. https://doi.org/10.1073/pnas.1700830114

Rostedt, A. (2018). *Diffusion Charging-Based Aerosol Instrumentation: Design, Response Characterisation and Performance* (Vol. 1527, Issue 2018) [Tampere University of Technology]. http://www.tut.fi/tutcris

Russell, W. T. (1926). The relative influence of fog and low temperature on the mortality from respiratory disease. *The Lancet*, *208*(5387), 1128–1130. https://doi.org/10.1016/S0140-6736(01)02367-4

Saarikoski, S., Salo, L., Bloss, M., Alanen, J., Teinilä, K., Reyes, F., Vázquez, Y., Keskinen, J., Oyola, P., Rönkkö, T., & Timonen, H. (2019). Sources and characteristics of particulate matter at five locations in an underground mine. *Aerosol and Air Quality Research*, *19*(12), 2613–2624. https://doi.org/10.4209/aaqr.2019.03.0118

Saarikoski, S., Teinilä, K., Timonen, H., Aurela, M., Laaksovirta, T., Reyes, F., Vásques, Y., Oyola, P., Artaxo, P., Pennanen, A. S., Junttila, S., Linnainmaa, M., Salonen, R. O., & Hillamo, R. (2018). Particulate matter characteristics, dynamics, and sources in an underground mine. *Aerosol Science and Technology*, *52*(1), 114–122. https://doi.org/10.1080/02786826.2017.1384788

Saffaripour, M., Chan, T. W., Liu, F., Thomson, K. A., Smallwood, G. J., Kubsh, J., & Brezny, R. (2015). Effect of Drive Cycle and Gasoline Particulate Filter on the Size and Morphology of Soot Particles Emitted from a Gasoline-Direct-Injection Vehicle. *Environmental Science and Technology*, *49*(19), 11950–11958. https://doi.org/10.1021/acs.est.5b02185

San-Miguel-Ayanz, J., Durrant, T., Boca, R., Maianti, P., Liberta', G., Artes Vivancos, T., Jacome Felix Oom, D., Branco, A., De Rigo, D., Ferrari, D., Pfeiffer, H., Grecchi, R., Nuijten, D., & Leray, T. (2020). *Forest Fires in Europe, Middle East and North Africa 2019*. Publications Office of the European Union. https://doi.org/10.2760/468688

Schmid, O., & Stoeger, T. (2016). Surface area is the biologically most effective dose metric for acute nanoparticle toxicity in the lung. *Journal of Aerosol Science*, *99*, 133–143. https://doi.org/10.1016/j.jaerosci.2015.12.006

Sgro, L. A., D'Anna, A., & Minutolo, P. (2011). Charge fraction distribution of nucleation mode particles: New insight on the particle formation mechanism. *Combustion and Flame*, *158*(7), 1418–1425. https://doi.org/10.1016/j.combustflame.2010.11.010

Sgro, L. A., Sementa, P., Vaglieco, B. M., Rusciano, G., D'Anna, A., & Minutolo, P. (2012). Investigating the origin of nuclei particles in GDI engine exhausts. *Combustion and Flame*, *159*(4), 1687–1692. https://doi.org/10.1016/j.combustflame.2011.12.013

Shah, R. U., Padilla, L. E., Peters, D. R., Dupuy-Todd, M., Fonseca, E. R., Ma, G. Q., Popoola, O. A. M., Jones, R. L., Mills, J., Martin, N. A., & Alvarez, R. A. (2023). Identifying Patterns and Sources of Fine and Ultrafine Particulate Matter in London Using Mobile Measurements of Lung-Deposited Surface Area. *Environmental Science & Technology*, *57*(1), 96–108. https://doi.org/10.1021/acs.est.2c08096

Shen, G., Preston, W., Ebersviller, S. M., Williams, C., Faircloth, J. W., Jetter, J. J., & Hays, M. D. (2017). Polycyclic Aromatic Hydrocarbons in Fine Particulate Matter Emitted from Burning Kerosene, Liquid Petroleum Gas, and Wood Fuels in Household Cookstoves. *Energy & Fuels*, *31*(3), 3081–3090. https://doi.org/10.1021/acs.energyfuels.6b02641

Siegmann, K., & Siegmann, H. C. (2000, June 19). Fast and Reliable "in situ" Evaluation of Particles and their Surfaces with Special Reference to Diesel Exhaust. *SAE Technical Paper Series*. https://doi.org/10.4271/2000-01-1995

Strasser, G., Hiebaum, S., & Neuberger, M. (2018). Commuter exposure to fine and ultrafine particulate matter in Vienna. *Wiener Klinische Wochenschrift*, *130*(1–2), 62–69. https://doi.org/10.1007/s00508-017-1274-z

Tammet, H. (1970). The aspiration method for the determination of atmospheric-ion spectra. In *Scientific Notes of Tartu State University: Vol. II* (Issue 195). Israel Program for Scientific Translations Ltd.

Tammet, H., Hõrrak, U., Laakso, L., & Kulmala, M. (2006). Factors of air ion balance in a coniferous forest according to measurements in Hyytiälä, Finland. *Atmospheric Chemistry and Physics*, *6*(11), 3377–3390. https://doi.org/10.5194/acp-6-3377-2006

Taxell, P., Hyytinen, E.-R., Ahonen, I., & Santonen, T. (2015). *Justification memo for diesel exhaust aerosol target level. Text in Finnish*. Finnish Institute of Occupational Health.

The measurement of atmospheric dust. (1925). *The Lancet*, *206*(5327), 712–713. https://doi.org/10.1016/S0140-6736(00)45587-X

Tran, C. L., Buchanan, D., Cullen, R. T., Searl, A., Jones, A. D., & Donaldson, K. (2000). Inhalation of poorly soluble particles. II. Influence of Particle Surface Area on Inflammation and Clearance. *Inhalation Toxicology*, *12*(12), 1113–1126. https://doi.org/10.1080/08958370050166796

United Nations Environment Programme. (2022). Spreading like Wildfire – The Rising Threat of Extraordinary Landscape Fires. In *A UNEP Rapid Response Assessment*.

Wiedensohler, A. (1988). An approximation of the bipolar charge distribution for particles in the submicron size range. *Journal of Aerosol Science*, *19*(3), 387–389. https://doi.org/10.1016/0021-8502(88)90278-9

Wilson, W. E., Stanek, J., Han, H.-S. (Ryan), Johnson, T., Sakurai, H., Pui, D. Y. H., and, J. T., Chen, D.-R., & Duthie, S. (2007). Use of the Electrical Aerosol Detector as an Indicator of the Surface Area of Fine Particles Deposited in the Lung. *Journal of the Air & Waste Management Association*, *57*(2), 211–220. https://doi.org/10.1080/10473289.2007.10465321

World Health Organization. (2021). *WHO global air quality guidelines: Particulate matter (PM2.5 and PM10), ozone, nitrogen dioxide, sulfur dioxide and carbon monoxide.* (p. 273). World Health Organization. https://apps.who.int/iris/handle/10665/345329

World Health Organization. Occupational and Environmental Health Team. (2006). *WHO Air quality guidelines for particulate matter, ozone, nitrogen dioxide and sulfur dioxide: Global update 2005: Summary of risk assessment* (p. 20). World Health Organization. https://apps.who.int/iris/handle/10665/69477

Wu, T., & Boor, B. E. (2021). Urban aerosol size distributions: A global perspective. *Atmospheric Chemistry and Physics*, *21*(11), 8883–8914. https://doi.org/10.5194/acp-21-8883-2021

Wu, Z., Hu, M., Lin, P., Liu, S., Wehner, B., & Wiedensohler, A. (2008). Particle number size distribution in the urban atmosphere of Beijing, China. *Atmospheric Environment*, *42*(34), 7967–7980. https://doi.org/10.1016/j.atmosenv.2008.06.022

Yli-Ojanperä, J., Mäkelä, J. M., Marjamäki, M., Rostedt, A., & Keskinen, J. (2010). Towards traceable particle number concentration standard: Single charged aerosol reference (SCAR). *Journal of Aerosol Science*, *41*(8), 719–728. https://doi.org/10.1016/j.jaerosci.2010.04.012

Yu, F., Lanni, T., & Frank, B. P. (2004). Measurements of ion concentration in gasoline and diesel engine exhaust. *Atmospheric Environment*, *38*(10), 1417–1423. https://doi.org/10.1016/j.atmosenv.2003.12.007

PAPERS

PAPER I

Emission measurements with gravimetric impactors and electrical
devices: An aerosol instrument comparison

Salo, L., Mylläri, F., Maasikmets, M., Niemelä, V., Konist, A., Vainumäe,
K., Kupri, H. L., Titova, R., Simonen, P., Aurela, M., Bloss, M., Keskinen,
J., Timonen, H., & Rönkkö, T.

Emission measurements with gravimetric impactors and electrical devices: An aerosol instrument comparison

Laura Salo, Fanni Mylläri, Marek Maasikmets, Ville Niemelä, Alar Konist, Keio Vainumäe, Hanna-Lii Kupri, Riina Titova, Pauli Simonen, Minna Aurela, Matthew Bloss, Jorma Keskinen, Hilkka Timonen & Topi Rönkkö

Check for updates

Emission measurements with gravimetric impactors and electrical devices: An aerosol instrument comparison

Laura Salo[a] (iD), Fanni Mylläri[a], Marek Maasikmets[b] (iD), Ville Niemelä[c], Alar Konist[d] (iD), Keio Vainumäe[b], Hanna-Lii Kupri[b], Riina Titova[b], Pauli Simonen[a] (iD), Minna Aurela[e], Matthew Bloss[e] (iD), Jorma Keskinen[a], Hilkka Timonen[e] (iD), and Topi Rönkkö[a]

[a]Aerosol Physics, Faculty of Engineering and Natural Sciences, Tampere University, Tampere, Finland; [b]Air Quality Management Department, Estonian Environmental Research Centre, Tallinn, Estonia; [c]Dekati Ltd, Kangasala, Finland; [d]Department of Energy Technology, Tallinn University of Technology, Tallinn, Estonia; [e]Atmospheric Composition Research, Finnish Meteorological Institute, Helsinki, Finland

ABSTRACT

Particulate matter in the atmosphere is known to affect Earth's climate and to be harmful to human health. Accurately measuring particles from emission sources is important, as the results are used to inform policies and climate models. This study compares the results of two ELPI + devices, two PM10 cascade impactors and an eFilter, in combustion emission measurements. The comparison of the instruments in a realistic setting shows what types of challenges arise from measuring an emission aerosol with unknown particle morphologies and densities, different particle concentrations and high temperature. Our results show that the PM10 cascade impactors have very good intercorrelation when the collected mass is greater than 150 μg, but below that, the uncertainty of the results increases with decreasing mass. The raw signals of two ELPI + devices were nearly identical in most samples, as well as the particle number concentrations and size distributions calculated from raw signals; however, transforming the current distributions into mass distributions showed variation in the mass concentration of particles larger than 1 μm. The real-time time signal measured by eFilter was similar to the total current measured by ELPI+. The eFilter and PM10 cascade impactors showed similar particle mass concentrations, whereas ELPI + showed clearly higher ones in most cases. We concluded that the difference is at least partially due to volatile components being measured by ELPI+, but not by the mass collection measurements.

1. Introduction

Anthropogenic aerosols are of great concern, as it is well-established that they are harmful to human health (e.g. Lelieveld et al. 2015) and have climate effects (e.g. Andreae, Jones, and Cox 2005; Lee, Reddington, and Carslaw 2016).Combustion emissions are a major source of atmospheric particle pollution. To understand their full effect on health and climate, researchers create dispersion and climate models to predict effects. These models require accurate measurements directly from the emission source as input. Otherwise, inaccuracies in measurements are passed onto the models, and the inaccurate models are used to inform decision making and environmental policies. One established way to gain information on the instrument performance is to compare results from instruments in concurrent measurements.

In atmospheric aerosol measurements, instrument comparisons are commonplace. For example, Hitzenberger et al. (2004) compared more than 50 mass measurement instruments in their atmospheric aerosol study, including Electrical Low Pressure Impactor (ELPI) and several cascade impactors. In combustion emission measurements, results for each studied characteristic (particle number concentration, mass concentration, size distribution, etc.) are often reported based on the measurement data from a single instrument. Instruments are of course calibrated before use, but laboratory calibration is conducted with known particle material, concentration and size distribution, under controlled environmental conditions. Considering the harsh conditions of emission measurements—high temperatures, varying pressure, high particle concentrations—and the rapidly changing source, it would be surprising not to encounter

---

Table 1. Information on the three instrument types used in this study.

Instruments used in this study	Flow rate (L/min)	Particle sizes measured	Data outputs	Other information
ELPI+ (x2)	10	6 nm–10 μm	Stage-specific electrical current	Current size distribution may be processed into number and mass distributions. Cutoff sizes for impactor stages (μm): [10 5.3 3.6 2.5 1.6 0.94 0.60 0.38 0.25 0.15 0.094 0.054 0.030 0.016 0.006]
PM10 gravimetric cascade impactor (x2)	10	0 nm–10 μm	Sampling time averaged mass concentration of three particle size ranges: 0–1 μm, 1–2.5 μm, 2.5–10 μm	There are three cut points (impactors) at particle diameters 10 μm, 2.5 μm, and 1 μm. The remaining particles are collected with a filter.
eFilter (x1)	20 (mass collection) and 0.5 (electrical measurement)	0 nm <	Sampling time averaged total mass concentration and related real-time electrical current	Combining the data outputs gives an estimation of the time-resolved mass concentration.

any discrepancies between instruments. In addition to the conditions within the tubing, the surroundings create challenges as well: vibrations from moving components, high or low temperatures and tight spaces. Small differences in operation methods by different users may also have noticeable effects on the results.

Instrument comparisons between different instances of combustion emission measurements are difficult, as sampling methods are also known to affect results (Burtscher 2005; Lipsky and Robinson 2006; Rönkkö et al. 2006). Despite the general lack of comparison studies, some instrument pairs have been studied: ELPI and Scanning Mobility Particle Sizer (SMPS) in particle size distribution measurements (Amaral et al. 2015; Maricq, Podsiadlik, and Chase 2000; Marjamäki et al. 2000), SMPS and Engine Exhaust Particle Sizer (EEPS) in particle size distribution measurements (Xue et al. 2015) and ELPI and gravimetric impactor particle mass concentration in the submicron size-range (Maricq, Xu, and Chase 2006). As far as we could tell, only one previous study compared identical instruments (condensation particle counters) in the same combustion emission measurement (Petzold et al. 2011).

In addition to accuracy, other instrument properties to consider when choosing instruments for a measurement setup are price, time resolution, size, measurement output, and how much maintenance is required. Aerosol measurement techniques can be divided into two main groups: offline and online, with the former generally being the more inexpensive method upfront (Dhaniyala et al. 2011). Collecting particles with an impactor or filter are types of offline measurements. Although the instruments are inexpensive, the collected substrates require handling, consuming work hours. Online instruments are generally more expensive, but offer numerous benefits: high time-resolution, instantaneous results and fewer work

hours. When it comes to measurement output, mass concentration is commonly used, as particle air quality standards are defined by mass concentration ("Air Quality Standards" 2017). Particle number is also commonly measured, as small particles are not well represented by mass, and particle number emissions are limited for vehicles. When possible, it is better to measure both in order to get a full picture of the emissions.

In this study, we present a comparison of five aerosol measurement instruments: two PM10 gravimetric cascade impactors (Dekati Ltd., Kangasala, Finland), two ELPI+'s (Dekati Ltd.) and one eFilter (Dekati Ltd.). The instruments were used to measure flue gas from oil shale and wood combustion. Data from each instrument was then used to calculate the mass concentration of particles in the flue gases. Additionally, the electrical currents measured by eFilter and ELPI + were compared. The two measured emission types, oil shale and wood, contained highly different concentrations of particles, giving a good range of data. The purpose of our study is to report on the correlation of results from essentially identical instruments operated by different research groups, to discover limitations of the selected instruments by comparing results, and to discuss the reliable utilization of these instruments for emission measurements. We also hope to encourage a culture of instrument comparison studies in combustion emission measurements.

2. Materials and methods

2.1. Instrument descriptions

The three instrument types used in this study are summarized in Table 1. ELPI + is an online device, whereas the PM10 cascade impactor is offline. The eFilter is a hybrid, measuring electrical current while
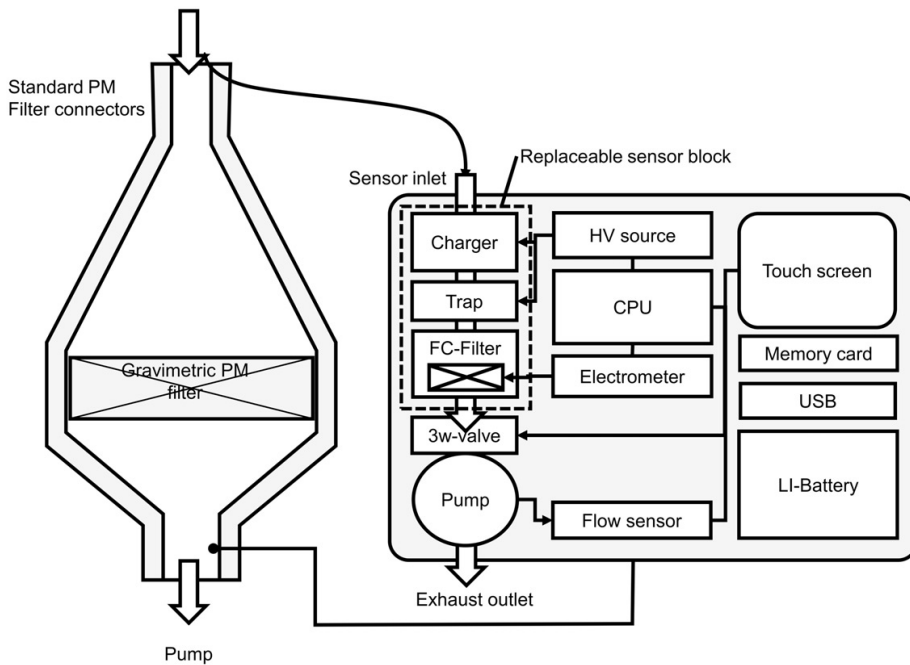
Figure 1. Graphical representation of the eFilter operation principle, image provided by Dekati®.

simultaneously collecting particulate mass onto a filter, which needs to be weighed. In addition to the studied instruments, an SMPS was in use during the measurements, but the data is only included in the supplementary material, as it was not part of the initial study design.

PM10 gravimetric cascade impactors (Dekati Ltd.) are used to measure the mass concentration of particles smaller than 10 μm in aerodynamic diameter. Incoming particles are deposited on collection plates by impaction. The PM10 impactors in this study also have an impactor cutoff at 2.5 μm, and another at 1 μm. A filter collects any remaining particles (less than 1 μm in aerodynamic diameter). Thus, they can also be used to determine $PM_{2.5}$ and PM_1. These impactors are commonly used in atmospheric measurements as well as measurements from an emission source. They fulfill the requirements for ISO23210, which sets the standard for particle mass concentration measurements from stationary emission sources.

ELPI+, as well as its predecessor ELPI (Dekati Ltd) (Keskinen, Pietarinen, and Lehtimäki 1992), is widely used for both atmospheric and emission measurements (Brachert et al. 2014; Duan et al. 2012; Liu et al. 2011; Maricq, Xu, and Chase 2006; Pirjola et al. 2017). The ELPI + includes an impactor with 14 stages, each connected to an electrometer. The

particles entering the device are electrically charged and then classified by aerodynamic diameter in the cascade impactor. The charged and impacted particles impart an electrical current, which is then recorded. The current from each stage can be converted into a particle number concentration, and together the fourteen stages give the number size distribution. The particle number distribution can also be converted to other distributions, such as particle surface area, volume and mass. The ELPI+ (and ELPI) time resolution is 1 s, making it useful for measuring transient particle size distributions. The particle size range measureable by ELPI + is approximately 6 nm to 10 μm. Calibration coefficients and stage-specific cutoff sizes for the ELPI + are reported in Järvinen et al. (2014).

The eFilter (Dekati Ltd.), marketed since 2016, combines electrical measurement and gravimetric mass collection of particles. The benefit of this novel two-pronged approach is that it allows the user to see the changes in the particle concentration during the gravimetric particle collection. The instrument components and operation principle can be seen in Figure 1. The instrument has a large primary flowrate of 20–100 lpm through a 47 mm collection filter and a secondary flowrate of 0.5 lpm for the electrical measurement (through the replaceable sensor block). The secondary flow is generated with an internal pump,

Table 2. Information on the measured combustion cases, the sampling times for PM10 cascade impactors and the dilution ratios for ELPI + and eFilter. The cascade impactors measured the flue gas undiluted.

	Fuel	Details	Sampling time (min)	Dilution ratio (ELPI + and eFilter)
1	Oil-shale		75	84
2	Oil-shale		94	9.6
3	Oil-shale		90	9.6
4	Oil-shale		70	9.6
5	Oil-shale		96	10
6	Oil-shale		30	10
7	Wood	Ignition	20	80
8	Wood	Burning	5	80
9	Wood	Burning	10	80
10	Wood	Burning	10	86
11	Wood + waste	Ignition	10	86
12	Wood + waste	Burning	10	86
13	Wood + waste	Burning	10	86
14	Wood + waste	Burning	10	86
15	Wood + soot remover	Ignition	7	177
16	Wood + soot remover	Burning	10	177
17	Wood + soot remover	Burning	10	177
18	Wood + soot remover	Burning	10	177

and it does not affect the gravimetric collection. The electrical portion of the instrument first charges incoming particles with a corona charger and then collects the particles onto a fiberglass filter inside a Faraday-cup connected to an electrometer. Electrical measurement is automatically switched on when the instrument detects the primary flow. This is useful, as the filter collection time then corresponds to the electrical measurement. The data output of the instrument is the current measured from the diffusion charged particles. If necessary, the electrical portion may also be used separately, i.e., independently of the filter collection of particles. In this study, quartz filters were used for the gravimetric collection. They were weighed as described in Section 2.2. The filter collection could also be used to perform chemical analysis of the sample.

2.2. Measurements

Table 2 displays the different measurement cases. The first six measurements were for oil shale combustion, and final twelve for wood combustion, with three different subcases: wood, wood and waste, and wood and a concentrated soot remover (Hansa^{TM}, UAB Triju artele, Kaišiadorys, Lithuania). For the wood combustion, one measurement was taken during each ignition phase and three during the normal burning phase. Oil shale tests were conducted at a 60 kWth Circulating Fluidized Bed (CFB) combustion test facility in Tallinn University of Technology, described in detail in Konist et al. (2018). In this facility, the fluidized bed is produced from mineral matter of the oil

shale; the amount of mineral matter can be 43–53% of the original mass of the fuel (Konist et al. 2016). The CFB facility was operated with its normal circulation and temperature profile. Wood combustion tests were carried out in the Estonian Environmental Research Centre (EERC) stove laboratory, using a 3500 kg brick made masonry heater, which is built according to the standard "EN 15544 One off Kachelgrundöfen/Putzgrundöfen (tiled/mortared stoves) – Dimensioning". Logwood from three species, spruce (*Picea abies*), alder (*Alnus incana*) and pine (*Pinus silvestris*), was used. In each case, the wood was cut into pieces of 0.4–0.5 m length and split into halves or quarters. The wood was stored in a conventional way in an outdoor woodshed and was brought to stove laboratory at least 1 day prior to combustion experiment. Fuel was ignited from the top, in order to ensure good startup for the wood ignition. The wood moisture content ranged between 14% and 18% on wet basis. Each log batch was weighed, the heating value was measured and the relative humidity of each log was measured separately.

One research group operated one ELPI + and one PM10 cascade impactor, while the other two identical devices were operated by the other group. This article will refer to these research groups as group A and group B. The measurement setups are shown in Figure 2a (cascade impactors) and Figure 2b (ELPI + and eFilter). The two PM10 cascade impactors sampled for the exact same time periods in order to allow comparison. The other instruments sampled for longer periods. For the purposes of this article, only the data for the times matching the cascade impactor samples was compared.

The PM10 cascade impactors each had their own sampling tubes of the same length, diameter, and bends, as well as identical cyclones to remove large particles. The inlets were oriented parallel to the surrounding flow. The only notable difference between the oil shale and wood combustion experiments was in the heating of the cyclone and PM10 cascade impactor, as it was about 80–100 °C in the oil shale cases and 120–150 °C in the wood cases. The nominal volumetric flowrate through the PM10 impactor needs to be 10 lpm for the cutoffs of 10 μm, 2.5 μm, and 1.0 μm. For PM10 A the flow was controlled with a mass flow controller (Alicat, Alicat Scientific, USA), set to 10 SLPM. The PM10 B flow rate was controlled using Aquaria CF-20 Alfa Basic (AQUARIA Srl, Lacchiarella (MI), Italy) pump, where flow rate is measured with the high precision flow-meters and the flow rate was set to 10 SLPM. Because the cascade
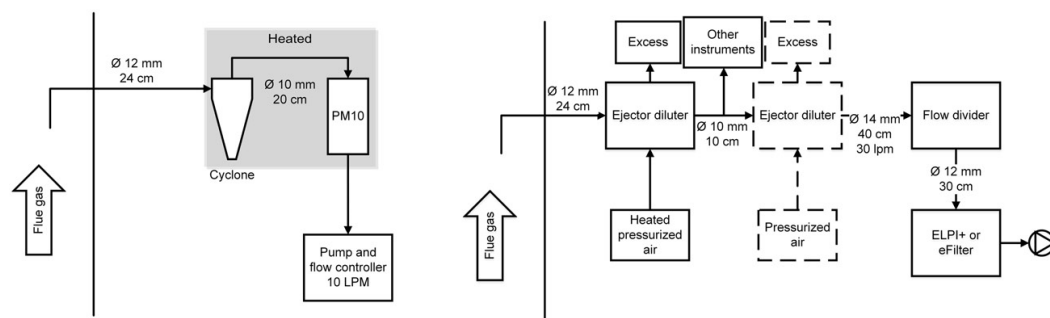
Figure 2. Measurement setups for (a) the PM10 cascade impactors and (b) ELPI + and eFilter. The second ejector diluter, drawn in dashed lines, was used in the first oil shale measurement and all of the wood measurements. The PM10 cascade impactors, along with the cyclones were heated to approximately 90 °C and 135 °C in the oil shale and wood cases, respectively.

impactors were heated, the true cutoff particle diameters varied slightly, at most 6% from the given values, calculated according to Hering (1995). The difference was not taken into account in the results. In preparation for sampling, the PM10 cascade impactors and cyclone were allowed to heat up for about 20 min before each run. If they were still warm from the previous sampling run, this time was shorter. The cascade impactor plates were covered with greased foils, which were changed for each sample, and the used foils were stored for weighing. The PM10 cascade impactor filter, which collects the smallest particles, was similarly changed and stored for weighing between each measurement. The PM10 impactors were clean before beginning the experiments and were cleaned in an ultrasonic bath after the first sampling from wood combustion, as they were visibly soot-covered.

Both ELPI + instruments measured after dilution of the flue gas, at the same distance from the source. The flue gas was diluted with an ejector diluter (Dekati Ltd.), in which heated (70 °C) and pressurized air was used for dilution. The setups for wood and oil shale experiments were almost identical, but in the wood combustion case, an additional ejector diluter was used. The flow rate in ELPI + is 10 lpm, and it is controlled by a critical orifice within the instrument. Before measuring, the ELPI + collection plates were covered with greased foils. The foils were changed daily to avoid measurement error due to particles bouncing. ELPI + devices were switched on about an hour in advance, to allow their electrometers to settle before actual measurement. Instruments' outlet pressures were checked to be 40 mbar and adjusted accordingly. The instruments were zeroed by sampling room air through a HEPA-filter, and administering the zeroing routine from the software menu. After

zeroing, the HEPA-filter was left in place for 5–10 min to check that the zero levels did not change. The corona needle of the ELPI + A was cleaned twice during the measurement campaign.

The eFilter measured from the same location as the ELPI + instruments and used the same dilution system. The flowrate to the gravimetric filter was 20 lpm—the total sampled volume was measured using a pump with integrated flow measurement. The flowrate through the electrical measurement portion of the eFilter was 0.5 lpm, taken from the main flow, as seen in Figure 1. The eFilter was switched on at least 30 min before the measurement in order to stabilize the electronics temperatures. Sampling was started and stopped manually by switching on and off the gravimetric sample pump. This started also the electrical measurement and data logging. Electrical data was saved to a memory card for further data processing. After measurement, the sample filter was removed for gravimetric analysis. The weighing procedure was the same as for the PM10 cascade impactors.

The ELPI + and PM10 impactor foils were greased with Dekati® Collection Substrate Spray to improve particle attachment. The PM10 filters and impactor foils were weighed before and after sampling. The filters were heated to 200 °C for 2 h, before sampling, and to 160 °C for 1 h after sampling, to remove moisture. After sampling and before weighing, the foils were allowed to cool inside a desiccator for at least 1 h and the filters for 2 h, as temperature can affect the weighing. The weighing room conditions were controlled and set to 50% humidity and a temperature of 22 °C. The foils and filters were weighed with a Kern 770 balance (10 μg precision).

A blockage occurred in the second ejector diluter during sample 11, which affected the ELPI + and
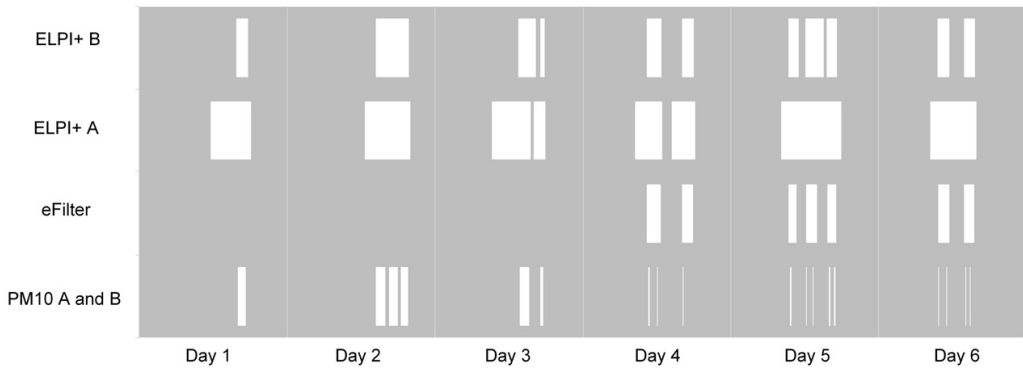
Figure 3. The white boxes show the times when the specified instrument (y-axis) has been actively measuring. For eFilter and PM10 A and B, this means the duration of mass collection. The black rectangle shows the times when the ejector diluter was blocked, and affected eFilter and ELPI + measurements.

eFilter results. For the eFilter, this means that also the particle mass concentration for sample 12 must be excluded, as it was collected with the same filter as sample 11. Figure 3 shows the times when each instrument was sampling the aerosol.

2.3. Data processing

2.3.1. pm10
The PM10 size fractioned results were obtained from the difference in collection foil and filter masses before and after sampling. Each particle mass concentration was calculated by dividing the collected particulate mass by the volume of aerosol sampled. The sampled volume was calculated by multiplying the sample flow rate by the sampling time.

2.3.2. elpi+
The ELPI + results were obtained using the datasheet provided by Dekati Ltd., and entering the required beginning and ending times for each measurement. We used $1 \, g/cm^3$ as the particle density setting and 1 as the dilution ratio (corrected later to reflect the true dilution ratio). the data sheet first applies a simple non-iterative calculation algorithm (Moisio 1999) to correct the current values for the secondary collection of sub-cut diameter particles (Virtanen et al. 2001). Then the number concentration is calculated from

$$N = \frac{I}{eQPn} \left[\frac{1}{cm^3} \right] \qquad (1)$$

where is the current measured from an impactor stage, is the elementary charge (1.602e − 19 C), is the flowrate. The term is a particle diameter dependent product of particle penetration through the charger and the average number of elementary charges per particle. The number size distribution is the combined number concentration for each stage, plotted against the geometric mean diameter of the corresponding stage. From the number size distribution, the mass is calculated by multiplying by volume and density. The values for as well as the correction values to account for secondary collection, by diffusion can be found in Järvinen et al (2014).

2.3.3. eFilter
The eFilter results for the electric current were the reading given by the instrument. The eFilter mass collection times were not the same as the PM10 cascade impactors, as can be seen from Figure 3. The eFilter was used to collect mass for the whole duration of a combustion event, from ignition to burning out. The eFilter particle mass concentration was calculated for the same duration as the PM10 sampling period, in order to compare results. The ability to determine mass from any period within one measurement, related to just one filter sample, is a key feature of the eFilter. Figure 3 displays the eFilter collection times along with the PM10 sample times. First, the average particle mass concentration was obtained by dividing the measured particle mass with the total sampled volume (Equation 2). Dividing the mass concentration by the average current gives a conversion factor (Equation 3). To convert the average current during any time period to to the corresponding particle mass concentration, the current is multiplied by the conversion factor (Equation 4). The conversion factor is not a calibrated constant, but a value which must be determined on-site for the studied particle population. The conversion factors used in this study are listed in Table S4.
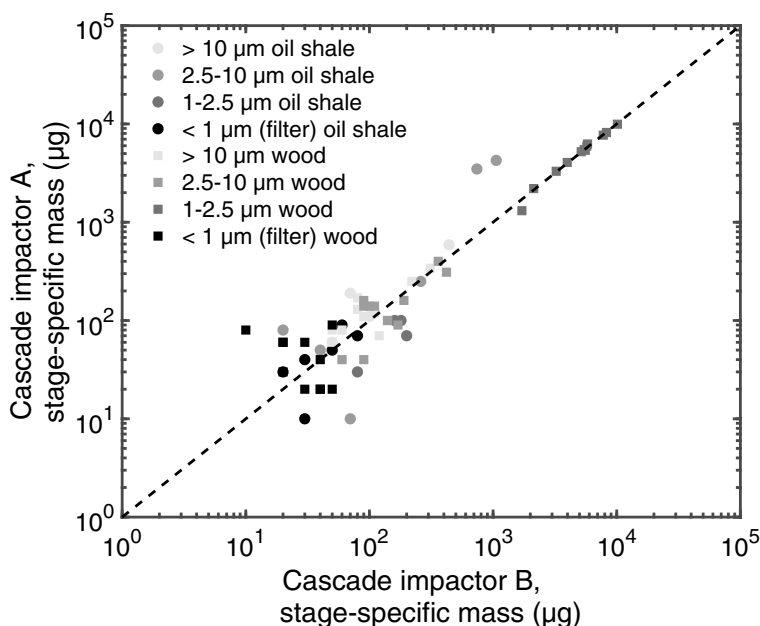
Figure 4. Total particulate mass for each sample: correlation between impactors PM10 A and PM10 B. Samples from oil shale measurements are represented with circles and wood with squares. Each color represents a different size fraction, and the dashed line is the one-to-one curve. Some of the results are missing from this plot, as they had a negative mass and the axes are logarithmically scaled.

The underlying approximation here is that there is a direct correlation between the particle mass concentration and measured current. From one mass collection, it is possible to determine one coefficient of correlation. Best results are obtained if the particle size distribution width (geometric standard deviation), modal diameter and dilution ratio is constant throughout the collection period.

In order to compare all instruments to each other, the results from the ELPI+ instruments and eFilter were multiplied by the dilution ratio (shown in Table 2). The dilution ratio was determined by measuring the carbon dioxide concentration (SICK Maihak, SIDOR, China) before and after the dilution of the combustion aerosol samples. There was no coarse particle pre-separator on the eFilter line, but the (double) ejector diluter effectively acts as one, having a low penetration of particles larger than $3 \mu m$ (Koch et al. 1988). Therefore, the contribution of particles larger than $10 \mu m$ was expected to be negligible.

3. Results

3.1. Comparison of similar instruments

Figure 4 shows a stage-by-stage comparison for the particulate masses measured from the two PM10 cascade impactors. The numerical values can be found in Table S1. The correlation for the total collected PM_{10} mass for the two impactors is $y = 0.97x + 1.68$, $R^2 = 0.986$. The highest stage (particles above $10 \mu m$) also depends on the performance of the cyclone preceding the impactor. The correlation for this stage was $R^2 = 0.756$, with PM10 B generally having a larger mass. The offset between the two instruments is small ($1.68 \mu g$) considering the total range of measurements. The visibly symmetrical distribution around the one-to-one curve indicates that the deviations of the instruments are caused by random errors; there is little to no systematic deviation due to user influence or instrument properties. Some of the results for impactor stages were showed negative mass, and are excluded from Figure 4 (but included in the correlation values). Figure S7 in the supplementary material shows the relative difference in the measured mass between the two PM10 cascade impactors, plotted on a linear scale.

There are two outliers in the $2.5–10 \mu m$ size range for oil shale samples. The particulate mass collected was much larger for PM10 B than for PM10 A—this is most likely due to the inlet nozzle of PM10 A being misaligned. There were also a few human errors during the process of taking out the foils and weighing them. The filter stage stuck to its container very easily,
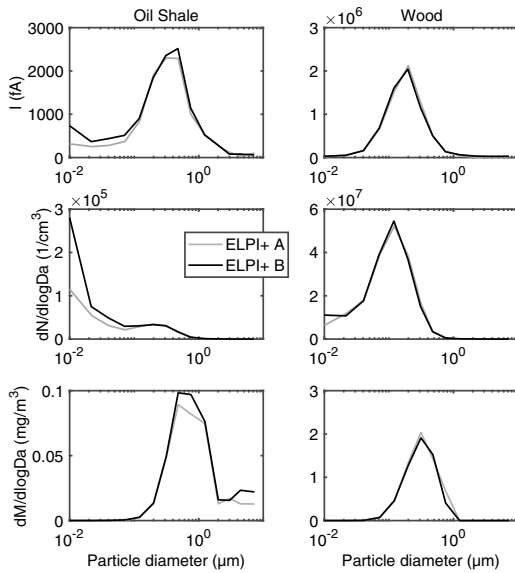
Figure 5. Comparison of the electric current, particle number concentration and particle mass concentration size distributions as measured by ELPI + A and ELPI + B. The left column is the average of the oil shale emission measurement samples (excluding sample six) and the right column is the average of the wood emission measurement samples. The separate distributions for each sample can be found in Figures S1–S3.

and often had to be carefully scraped off. The weighing room was also quite windy due to the air exchanger, which caused challenges when handling the foils and filters. Despite these challenges, the overall results for the PM10 cascade impactor comparison were very good: $R^2 = 0.986$.

Figure 5 shows averaged flue gas particle size distributions measured with ELPI+, for electric current (diffusion corrected), particle number and particulate mass. The oil shale and wood combustion cases have been separated, as the particle concentrations were vastly different. The current distributions are nearly identical, whereas there are slight differences in number distributions in the small particle range and notable differences in the mass concentration of large particles. In each distribution plot, the particle mode is at the same particle size.

In both combustion cases, ELPI + B reports a higher number concentration of the smallest measured particles. This is true for each separate measurement as well, as can be seen from the raw current results in Figure S1. For the mass concentrations, there is a difference in the largest particle sizes. Again, the ELPI + B consistently reported a larger mass in the larger particle sizes. ELPI + B experienced an error during the measurement of sample 6, and the sample

has been excluded from these results. The number and mass distributions are plotted separately in supplementary Figures S2 and S3.

The R^2 value was over 0.98 for current measured from stages 3 to 8. For the small particle stages the correlation was slightly worse, $R^2 = 0.71$ (filter stage) and $R^2 = 0.90$ for stage 2. The large particle stages had the lowest correlation values, of only $R^2 = 0.09$ for stage 12 and 0.38–0.97 for the others. The reason stage 12 had such poor correlation is that it received almost no current.

To compare the total particle mass concentration reported by each ELPI + to the other instruments, any mass measured from a stage which received less than 2.5% of the total current (after correcting the current for secondary collection effects) was ignored. Although the measured mass in these higher stages can be large, it results from a very small current. Over all 18 measurement cases, stages 10–14 contributed an average of 6.2% of the total current to ELPI + A and 7.3% of the total current to ELPI + B. For the wood cases (7–18), this percentage drops even further, to 1.0% and 2.7% (ELPI + A and ELPI + B). The error margins in the higher stages are quite large due to secondary collection of small particles, which the correction may not adequately account for. For stage 10, the correction (applied by the ELPI + datasheet) was approximately 40% of the measured current, and it is even larger for the higher stages.

3.2. Comparison of electrical measurements

Figure 6 displays the average of the total electric current during each sample as measured by ELPI + A, ELPI + B and eFilter. For ELPI+, the reported current is the sum of all the stages (averaged over the sampling period). The eFilter current is the average of the current over the sampling period. The correlation between the ELPI + instruments is $y = 1.00x + 409$, $R^2 = 0.999$; there is a very small difference in the reported total current, with ELPI + B consistently giving a slightly larger value. The eFilter current is very close to the ELPI + current if adjusted for the different flowrate, correlation curve being $y = 0.053x - 128.4$, $R^2 = 0.875$, compared to ELPI + A. Figure S4 shows the time series data of the electrical current for each measurement sample.

3.3. Comparison of mass measurements

Figure 7 shows the particle mass concentration calculated from PM10 cascade impactor and eFilter
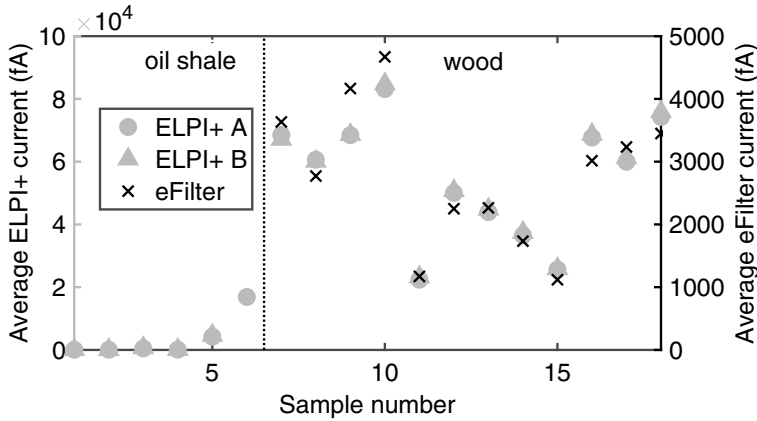
Figure 6. Average measured electric current for ELPI + A, ELPI + B and eFilter at each sample point. These values have not been dilution corrected, as the dilution was the same for all three instruments. Sample 6 has been excluded for ELPI + B due to an error during the measurement.
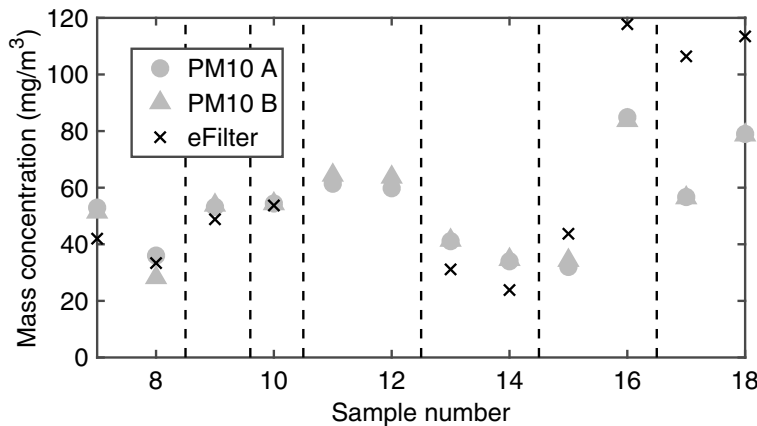

Figure 7. The flue gas particle mass concentration measured for each sample by the PM10 cascade impactors and eFilter. The vertical lines show when the eFilter collection filter was changed. Points 11 and 12 are excluded from the eFilter results, as the ejector diluter was partially blocked.

measurements for the wood combustion cases. The oil shale cases have been left out, as the eFilter was not used in these measurements and the results for the PM10 impactors are shown in Figure 8. Only the particle mass concentration up to 10 μm particles is included for the PM10 impactors, in order to leave out any cyclone effects. The eFilter results compare well (less than 21% difference, R^2 = 0.78 and 0.77, respectively for comparison to PM10 A and B) with the PM10 results for the four pure wood combustion cases (7–10), the results are lower (−24% to −31%) for the wood and waste combustion cases (13 and 14), and higher (+39% to +89%) for the wood and soot remover cases (15–18). The vertical lines show when the filter in the eFilter was exchanged. For example,

the particle mass concentration for sample periods 7 and 8 are reported from just one weighed filter, combined with the electric current data. Samples 15 and 16 show that in the eFilter, even relatively small changes in particle mass concentrations can be detected, even when the filter is not changed between the measurements.

Figure 8 shows the particle mass concentration from each of the studied instruments for each sampling period. The particle mass concentration measured by ELPI+ (A and B) only includes stages which contributed at least 2.5% of the total electrical current, as discussed previously (Section 3.1). In the oil shale combustion cases (samples 1–6); the average results from ELPI + were 26% of the PM10 cascade impactor
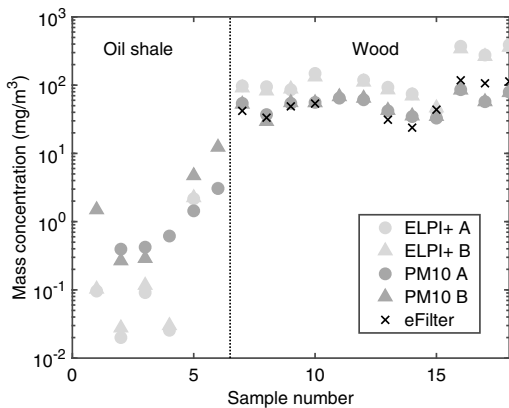
Figure 8. The flue gas particle mass concentration measured by each studied instrument for the 18 sample cases. The dotted vertical line separates oil shale and wood combustion samples. Sample 6 for ELPI + B has been excluded due to an instrument error, other missing points are due to sampling errors (ELPI + A and B, eFilter), or negative mass (PM10 A and B).

masses. For the wood combustion cases (7–18) the average ELPI + result is 272% compared to PM10, with the ELPI + instruments reporting values that are 1.4–6.3 times larger than the PM10 reported values. The eFilter results are closer to PM10 values than ELPI+. The results between similar instruments are very consistent. The PM10 impactors vary somewhat in the oil shale case, where particle mass concentrations are small, but ELPI+'s are nearly identical throughout all samples (R^2 = 0.995).

4. Discussion

Using the PM10 cascade impactors in emission measurements gave nearly identical results. As was seen in Figure 4, the largest deviations were generally in the smallest collected particulate masses, due to the precision of the scale used to weigh the samples. To avoid small masses, low particle concentrations (such as in the oil shale cases, <0.1 mg/m³) need long collection times. This leads to a loss in time resolution, and may even be impossible in cases where the particle production does not last long enough, or the particle source strength varies in time. The correlation for collected mass above 150 μg had much less variance (), compared to smaller particulate masses (). The correlation is even better overall (R^2 = 0.997), if the points where the inlet may have been misaligned are excluded, showing the importance of the sampling nozzle orientation. Additionally, without a comparison instrument, this error would have gone unnoticed. This highlights

the importance of parallel measurements with similar instruments, each with their own inlet.

The electrical current distributions measured by the two ELPI + devices were well correlated for both combustion types, as seen in Figure 5. The correlation was especially good in the wood case. The particle number concentration distributions varied slightly, with ELPI + B consistently showing a slightly larger value in the smaller particle size range, and similarly the mass distribution in the larger particle stages. The small discrepancies between ELPI + A and B in the large and small size ranges indicate a small difference between the instruments, or in the measurement methods employed by research groups A and B; however, the R^2 was greater than 0.98 for current from most stages and R^2 = 0.995 for the resulting total mass, meaning that overall the results compared well.

Figure 6 displays the average current measured during each sample by ELPI + A, ELPI + B and eFilter. There was almost no difference between the time-averaged total currents of the two ELPI + instruments (R^2 = 0.999). The eFilter charging efficiency seems to be similar to the ELPI+, as the measured current was very similar after correcting for the different flow rates between the two instruments (R^2 = 0.875 and 0.900, respectively for comparison to ELPI + A and B). The particle charge applied by the ELPI + charger has been previously measured to be dependent on for particles smaller than 1 μm (Järvinen et al. 2014). Changes in the eFilter current as compared to ELPI + seem to be caused by a poorly zeroed electrometer. This can be seen from Figure S4, where the eFilter to ELPI + measured current ratio changes during the sampling period in samples 9, 10, and 18. Electrometer drift can be minimized by allowing the instrument more time to warm up, and by checking that the zero level does not change while measuring clean air. As the electrometer drift can play a role in calculating the results, it would be beneficial to record the data also from the zeroing time period. Unfortunately, the zeroing measurements were not recorded for later investigation. There are no previous studies regarding the eFilter, and only one device was available for this study, so we cannot comment on how typical the results are.

As seen in Figure 8, particle mass concentrations calculated from ELPI + are smaller than the PM10 cascade impactor results for oil shale, but 1.3–4.8 times larger when compared to the PM10 results in the wood combustion cases, even when higher stages are excluded, as described in Section 3.1. The ELPI + sample was diluted with one ejector diluter in

the oil shale case and with a double ejector in the wood case. These results could have indicated that the difference might be caused by effects from dilution; however, the eFilter results for particle mass concentration had a reasonably good correlation with the PM10 impactor results ($R^2 = 0.78$), even though it measured the same diluted flue gas as the ELPI+ instruments. As both ELPI+ instruments showed similarly high particle mass concentrations, it is evident that the instruments were working as intended. The deviation of the mass concentration results compared to the results from other instruments was highest in the final three measurement cases, in which wood was burned along with the soot remover. However, also the eFilter showed higher particle mass concentrations than the cascade impactors in these three cases, suggesting dilution might have played a partial role. Figure S5 shows ELPI+ particle number distributions compared to SMPS distributions. The SMPS results are only indicative, as one measurement cycle is 3 min, which was far too long for these measurements. However, the shapes of the particle number distributions (from ELPI+ and SMPS) were similar, and the largest differences were observed in the small particle size range, which does not contribute significantly to the PM.

Previous studies have also indicated higher particle mass concentration results with ELPI+ and its predecessor ELPI, when compared to filter collection. Maricq, Xu, and Chase (2006) found that ELPI overestimated mass and reported several concerns regarding ELPI mass measurements from diesel emissions. Two of these concerns are applicable to the results presented in this article. First, the particle loading effect, which can change the impactor jet geometry due to the accumulation of particles in the jets. Second, Maricq et al. discuss the role of density, and show how a non-constant density can be used to obtain better results. In this study, the particle loading effect was minimized by wiping the jet plates with a cloth and chancing the foils after each measurement day. The mass calculation from ELPI+ results would have been improved by taking into account the nonconstant density of the particles. In our study, adjustments for density were not made during data processing, as the size-specific density could not be reliably calculated from the available data. Using the SMPS and ELPI+ data together, we calculated the densities for the wood combustion measurements to be between 0.7 and 3.8 g/cm^3 (Table S3). Leskinen et al. report a range of 0.25–2 g/cm^3 for particles from wood combustion emissions, depending on particle size and the burning phase the particles were emitted from (2014). In addition, it should be noted that other

studies have found that the assumed (constant) density of particles had a minor effect on the overall particle mass concentration reported by ELPI (Charvet et al. 2015; Moisio 1999).

Hitzenberger et al. (2004) measured PM$_{2.5}$ in ambient air and noticed that ELPI gave a mass concentration 1.92 times higher than the average of other measurement methods. They speculated that the cause was moisture in ambient air, as the aerosol was not dried before measuring with ELPI. As we used ELPI+ current data to calculate particulate mass, and did not weigh the collected particulate mass from the impactor stages, the sample conditioning can affect the ELPI+ results. In our measurements, the raw flue gas was highly diluted (dilution ratio over 80 in the wood combustion cases), thus it is unlikely that the humidity of the flue gas played any role in the ELPI+ results. Hitzenberger et al. also speculate that the online measurement by ELPI included semi-volatile compounds, whereas semi-volatile compounds evaporate from filter samples before weighing. Thus, the mass of the nonvolatile PM can be lower than the calculated PM from ELPI+ data. The volatility of particles was not measured in our study, and their role remains an uncertainty. In future measurements, we would recommend removing the volatile particle fraction by using a thermodenuder or a hot double ejector diluter system, if the aim of the study is related to nonvolatile/solid particle characterization.

A wood combustion literature review by Obaidullah et al. (2012) gives the typical range of particle number concentrations as particles/cm^3. The particle number concentrations calculated from ELPI+ in our study were well within this range, with an average of particles/cm^3. PM10 concentrations are also reported by Obaidullah et al., ranging from 13 to 67, measured from filter samples. In our study, the PM10 cascade impactor and eFilter results are of similar magnitude, while the ELPI+ results are considerably larger, even when discounting higher stages. Oil shale combustion emissions have been studied for pulverized fuel boilers (Aunela-Tapola, Frandsen, and Häsänen 1998; Häsänen et al. 1997). In their study, the average emission factor for pulverized oil shale combustion was 1100 mg/MJ. Since then, many pulverized fuel power plants have been upgraded and CFB boilers have been built in new power plants (Parve et al. 2011).

In addition to the operation principles, the instruments have some physical differences as well. The ELPI+ is the most sophisticated of the three instruments, but it is also the largest. The PM10 cascade impactors and the eFilter are closer in size, but the

eFilter offers the advantage of real-time data (as does the ELPI+). This is useful for following trends in combustion, and it can help with detecting problems related to the boiler operation or instrument operation. On the other hand, the PM10 is very robust and can withstand high temperatures, allowing particle collection without dilution. Each of the three instruments requires a separate pump for operation. The eFilter flowrate does not need to be exact, as long as it is approximately constant. The PM10 impactor and ELPI + require a specific flowrate to ensure the impaction of the particles to the correct collection plates. The ELPI + sample flowrate can easily be adjusted with a valve within the instrument, whereas the PM10 impactor requires an additional flow controller. While conducting the measurements, the PM10 impactor requires the most attention from the user. Preparation of the foils is similar between ELPI + and PM10 impactors, but the PM10 foils need baking and weighing before assembling the impactor. After the measurement, the process of taking out the collection foils and weighing them needs to be done very carefully to avoid removing (or adding) mass. The ELPI + produces the highest amount of data, since it gives information about the particle current and number size distribution once every second. The ELPI + can be processed with the software provided with the instrument or with user's own software. Where the ELPI + data has detailed information about the particle number distribution, the eFilter only gives the current imparted by the particles in the sample flow. To use the eFilter efficiently, weighing the filter to gain information about the collected mass is necessary. The analysis of the results is always left to the user. The least laborious data processing is with the PM10 impactor.

To summarize the major points in this discussion, the particle number and mass concentration in the wood combustion cases was much larger than in the oil shale combustion cases. In all cases, electrical signals were very well correlated and mass concentrations were well correlated for the PM10 impactors and the eFilter, whereas the ELPI + mass concentrations were significantly larger for almost every case. Our hypothesis for this discrepancy is a) the effective density of the particles was not the assumed value of 1, and b) volatile particles were measured by ELPI+, but were not measured from the filter samples, as volatile compounds would have evaporated before the weighing. A better comparison between instruments could have been made by adding a thermodenuder before the ELPI + instruments and by measuring the effective density by some other means. The eFilter average current correlated well with the ELPI + current in these measurements. When the current signals for the two different instruments were adjusted by the respective flow rates, they matched almost exactly, showing that the eFilter charger efficiency is similar to that of the ELPI+. Comparing the eFilter mass concentration to the PM10 mass concentration showed that the measurement method introduced in the eFilter is valid.

5. Conclusions

Our study shows that the PM10 gravimetric cascade impactor and ELPI + are highly comparable, in that the two different instruments produce the same results, even when operated by different research groups. ELPI + or eFilter is a good alternative to offline measurement methods, when measuring a transient source, as they give data with a 1-s time resolution. To measure particle mass concentration from an emission source, eFilter or a PM10 impactor is generally a better choice, whereas ELPI + is well suited for particle number concentration and size distribution measurements.

The eFilter was shown to have the advantage of real-time current measurement which is comparable to ELPI+, combined with mass concentration results that are comparable to the results from PM10 cascade impactors. In addition, the eFilter requires less attendance (than the PM10 impactor) by the operator during the measurements, as the online current measurement can be used to calculate the approximate particulate mass concentration for any time period. For these reasons, it is a convenient new instrument for emission measurements.

ORCID

Laura Salo 🔟 http://orcid.org/0000-0002-8388-1610
Marek Maasikmets 🔟 http://orcid.org/0000-0002-2381-0968
Alar Konist 🔟 https://orcid.org/0000-0001-5492-248X
Pauli Simonen 🔟 http://orcid.org/0000-0002-4267-6098
Matthew Bloss 🔟 http://orcid.org/0000-0003-1614-4415
Hilkka Timonen 🔟 http://orcid.org/0000-0002-7987-7985

References

"Air Quality Standards." 2017 European Commission. 2017. Accessed September 6, 2018. http://ec.europa.eu/environment/air/quality/standards.htm.

Amaral, S., J. de Carvalho, M. Costa, and C. Pinheiro. 2015. An overview of particulate matter measurement instruments. *Atmosphere* 6 (9):1327–1345. doi:10.3390/atmos6091327.

Andreae, M. O., C. D. Jones, and P. M. Cox. 2005. Strong present-day aerosol cooling implies a hot future. *Nature* 435 (7046):1187–1190. doi:10.1038/nature03671.

Aunela-Tapola, L. A., F. J. Frandsen, and E. K. Häsänen. 1998. Trace metal emissions from the estonian oil shale fired power plant. *Fuel Processing Technol.* 57 (1):1–24. doi:10.1016/S0378-3820(98)00069-1.

Brachert, L., J. Mertens, P. Khakharia, and K. Schaber. 2014. The challenge of measuring sulfuric acid aerosols: Number concentration and size evaluation using a condensation particle counter (CPC) and an electrical low pressure impactor (ELPI+). *J. Aerosol Sci.* 67:21–27. doi:10.1016/j.jaerosci.2013.09.006.

Burtscher, H. 2005. Physical characterization of particulate emissions from diesel engines: A review. *Aerosol Sci.* 36 (7):896–932.

Charvet, A., S. Bau, D. Bémer, and D. Thomas. 2015. On the importance of density in ELPI data Post-Treatment. *Aerosol Sci. Technol.* 49 (12):1263–1270. doi:10.1080/02786826.2015.1117568.

Dhaniyala, S., M. Fierz, J. Keskinen, and M. Marjamäki. 2011. Instruments based on electrical detection of aerosols. In *Aerosol Measurement: Principles, Techniques, and Applications*, ed. Pramod Kulkarni, Paul A. Baron and Klaus Willeke, 393–416. 3rd ed. New York: John Wiley & Sons, Inc. doi:10.1002/9781118001684.ch18.

Duan, J., J. Tan, S. Wang, J. Hao, and F. Chai. 2012. Size distributions and sources of elements in particulate matter at curbside, Urban and rural sites in beijing. *J. Environ. Sci.* 24 (1):87–94. doi:10.1016/S1001-0742(11)60731-6.

Häsänen, E., L. Aunela-Tapola, V. Kinnunen, K. Larjava, A. Mehtonen, T. Salmikangas, J. Leskelä, and J. Loosaar. 1997. Emission factors and annual emissions of bulk and trace elements from oil shale fueled power plants. *Sci. Total Environ.* 198 (1):1–12. doi:10.1016/S0048-9697(97)05432-6.

Hering, S. V. 1995. "Impactors, cyclones, and other inertial and gravitational collectors." In *Air sampling instruments for evaluation of atmospheric contaminants*, ed. B. S. Cohen and S. V. Hering, 279–321, 8th ed. Ohio: ACGIH.

Hitzenberger, R. M., A. Berner, Z. Galambos, W. Maenhaut, J. Cafmeyer, J. Schwarz, and K. Müller. 2004. Intercomparison of methods to measure the mass concentration of the atmospheric aerosol during INTERCOMP2000 - Influence of instrumentation and size cuts. *Atmos. Environ.* 38 (38):6467–6476. doi:10.1016/j.atmosenv.2004.08.025.

Järvinen, A., M. Aitomaa, A. Rostedt, J. Keskinen, and J. Yli-Ojanperä. 2014. Calibration of the new electrical low pressure impactor (ELPI+). *J. Aerosol. Sci.* 69 (March):150–159. doi:10.1016/J.JAEROSCI.2013.12.006.

Keskinen, J., K. Pietarinen, and M. Lehtimäki. 1992. Electrical low pressure impactor. *J. Aerosol Sci.* 23 (4):353–360.

Koch, W., H. Lödding, W. Mölter, and F. Munzinger. 1988. Verdünnungssystem für die messung hochkonzentrierter aerosole mit optischen partikelzählern. *Staub. Reinhaltung Der Luft* 48 (9):341–344.

Konist, A., O. Järvik, T. Pihu, and D. Neshumayev. 2018. Combustion as a possible solution pyrolytic wastewater utilization. *Chem. Eng. Trans.* 70:859–864. doi:10.3303/CET1870144.

Konist, A., B. Maaten, L. Loo, D. Neshumayev, and T. Pihu. 2016. Mineral sequestration of Co_2 by carbonation of Ca-Rich oil shale ash in natural conditions. *Oil Shale* 33 (3):248–259. doi:10.3176/oil.2016.3.04.

Lee, L. A., C. L. Reddington, and K. S. Carslaw. 2016. On the relationship between aerosol model uncertainty and radiative forcing uncertainty. *Proc. Nat. Acad. Sci.* 113 (21):5820–5827. doi:10.1073/pnas.1507050113.

Lelieveld, J., J. S. Evans, M. Fnais, D. Giannadaki, and A. Pozzer. 2015. The contribution of outdoor air pollution sources to premature mortality on a global scale. *Nature* 525 (7569):367–371. doi:10.1038/nature15371.

Leskinen, J., M. Ihalainen, T. Torvela, M. Kortelainen, H. Lamberg, P. Tiitta, and G. Jakobi. 2014. Effective density and morphology of particles emitted from small-scale combustion of various wood fuels. *Environ. Sci. Technol.* 48 (22):13298–13306. doi:10.1021/es502214a.

Lipsky, E. M., and A. L. Robinson. 2006. Effects of dilution on fine particle mass and partitioning of semivolatile organics in diesel exhaust and wood smoke. *Environ. Sci. Technol.* 40 (1):155–162. doi:10.1021/es050319p.

Liu, Z., Y. Ge, K. C. Johnson, A. N. Shah, J. Tan, C. Wang, and L. Yu. 2011. Real-World operation conditions and on-Road emissions of beijing diesel buses measured by using portable emission measurement system and electric Low-Pressure impactor. *Sci. Total Environ.* 409 (8):1476–1480. doi:10.1016/j.scitotenv.2010.12.042.

Maricq, M. M., D. H. Podsiadlik, and R. E. Chase. 2000. Size distributions of motor vehicle exhaust PM: A comparison between ELPI and SMPS measurements. *Aerosol Sci. Technol.* 33 (3):239–260. doi:10.1080/027868200416231.

Maricq, M. M., N. Xu, and R. E. Chase. 2006. Measuring particulate mass emissions with the electrical low pressure impactor. *Aerosol Sci. Technol.* 40 (1):68–79. doi:10.1080/02786820500466591.

Marjamäki, M.,. J. Keskinen, D.-R. Chen, and D. Y. H. Pui. 2000. Performance evaluation of the electrical Low-Pressure impactor. *J. Aerosol Sci.* 31 (2): 249–261. doi:10.1016/S0021-8502(99)00052-X.

Moisio, M. 1999. Real-time size distribution measurement of combustion aerosols. Tampere University of Technology.

Obaidullah, M., S. Bram, V. K. Verma, and J. De Ruyck. 2012. A review on particle emissions from small scale biomass combustion. *Int. J. Renew. Energy Res.* 2 (1):147–159. http://www.ijrer.net/index.php/ijrer/article/view/147.

Parve, T., J. Loosaar, M. Mahhov, and A. Konist. 2011. Emission of fine particulates from oil shale fired large boilers. *Oil Shale* 28 (1S):152–161. doi:10.3176/oil.2011.1S.07.

Petzold, A., R. Marsh, M. Johnson, M. Miller, Y. Sevcenco, D. Delhaye, A. Ibrahim., et al. 2011. Evaluation of methods for measuring particulate matter emissions from gas turbines. *Environ. Sci. Technol.* 45 (8):3562–3568. doi:10.1021/es103969v.

Pirjola, L., T. Rönkkö, E. Saukko, H. Parviainen, A. Malinen, J. Alanen, and H. Saveljeff. 2017. Exhaust emissions of Non-Road mobile machine: Real-World and laboratory studies with diesel and HVO fuels. *Fuel* 202: 154–164. doi:10.1016/j.fuel.2017.04.029.

Rönkkö, T., A. Virtanen, K. Vaaraslahti, J. Keskinen, L. Pirjola, and M. Lappi. 2006. Effect of dilution conditions and driving parameters on nucleation mode particles in diesel exhaust: Laboratory and on-Road study. *Atmos. Environ.* 40 (16):2893–2901. doi:10.1016/j.atmosenv.2006.01.002.

Virtanen, A., M. Marjamäki, J. Ristimäki, and J. Keskinen. 2001. Fine particle losses in electrical low-pressure impactor. *J. Aerosol Sci.* 32 (3):389–401. doi:10.1016/S0021-8502(00)00087-2.

Xue, J., Y. Li, X. Wang, T. D. Durbin, K. C. Johnson, G. Karavalakis, A. Asa-Awuku, M. Villela, D. Quiros, S. Hu, T. Huai, A. Ayala, and H. S. Jung. 2015. Comparison of vehicle exhaust particle size distributions measured by SMPS and EEPS during steady-state conditions. *Aerosol Sci. Technol.* 49 (10):984–996. doi:10.1080/02786826.2015.1088146.

PAPER II

Concentrations and Size Distributions of Particle Lung-deposited Surface Area (LDSA) in an Underground Mine

Salo, L., Rönkkö, T., Saarikoski, S., Teinilä, K., Kuula, J., Alanen, J., Arffman, A., Timonen, H., & Keskinen, J.

Aerosol and Air Quality Research
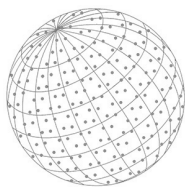
Concentrations and Size Distributions of Particle Lung-deposited Surface Area (LDSA) in an Underground Mine

Laura Salo[1][*], Topi Rönkkö[1], Sanna Saarikoski[2], Kimmo Teinilä[2], Joel Kuula[2], Jenni Alanen[1], Anssi Arffman[1][†], Hilkka Timonen[2], Jorma Keskinen[1]

[1] Aerosol Physics Laboratory, Physics Unit, Tampere University, Tampere 33720, Finland
[2] Atmospheric Composition Research, Finnish Meteorological Institute, Helsinki 00560, Finland

ABSTRACT

Ultrafine particles produced by diesel-powered vehicles in underground mines are largely unaccounted for in mass-based air quality metrics. The Lung Deposited Surface Area concentration (LDSA) is an alternative to describe the harmfulness of particles. We aim to study concentrations and size distributions of LDSA at various locations in an underground mine as well as to evaluate the applicability of sensor-type measurement of LDSA. This study was conducted in an underground mine in Kemi, Finland, in 2017. Our main instrument was an electrical low-pressure impactor (ELPI+) inside a mobile laboratory. Additionally, five diffusion-charging based sensors were tested. The environment was challenging for the sensors as the particle size distribution was often outside the optimum range (20–300 nm) and dust accumulated inside the instruments. Despite this, the correlations with the ELPI+ were decent (R^2 from 0.53 to 0.59). With the ELPI+ we determined that the maintenance area had the lowest mean LDSA concentration (79 ± 38 μm^2 cm^{-3}) of the measured locations. At the other locations, concentrations ranged from 137 to 405 μm^2 cm^{-3}. The mode particle size for the LDSA distribution was around 100 nm at most locations, with the blasting site as a notable exception (mode size closer to 700 nm). Diffusion-charging based sensors—perhaps aided by optical sensors—are potential solutions for long-term monitoring of LDSA if dust accumulation is taken care of. Our research indicates worker exposure could be reduced with the implementation of a sensor network to show which locations need either protective gear or increased ventilation.

Keywords: Occupational exposure, Electrical particle sensor, Fine aerosol, Ultrafine aerosol

1 INTRODUCTION

Particulate matter (PM) in the air is known to be harmful for human health (Lelieveld *et al.*, 2015; Burnett *et al.*, 2018), mostly due to the ability of particles to penetrate and deposit into the human lungs (Pope, 2000; Pope and Dockery, 2006). This lung-deposition, as well as the deposition of particles in other parts of the human respiratory tract, is strongly dependent on the size distribution of particles. Especially ultrafine particles (particle diameter smaller than 100 nm) and to some extent larger fine particles (particle diameter smaller than 2.5 µm) can reach the most vulnerable alveolar areas of human lungs and deposit there (Oberdörster, 2001). These particles can consist of compounds that are toxic for the human body or they can carry the toxic components on their surfaces (Goulaouic *et al.*, 2008). In addition to acute symptoms, the particulate matter of inhaled air has been observed to cause cardiovascular diseases, lung cancer and brain diseases (Grahame *et al.*, 2014).

Historically, mine work has been a notably hazardous occupation, but even modern-day mines often struggle with air quality concerns. Underground mines are especially challenging environments, and efficient mechanical ventilation is necessary for keeping the air clear of polluting gases and

particles. The particulate matter originates from different sources: exhaust of mine vehicles, surfaces of mine galleries, and from the different processes related to mining work (Saarikoski *et al.*, 2019; Afshar-Mohajer *et al.*, 2020). The particles from different sources have varying chemical and physical characteristics and the total mixture and concentration of particles can therefore vary significantly, both temporally and spatially (Saarikoski *et al.*, 2019), making monitoring and air quality control a challenge. Ventilation of an underground mine is an energy-intensive process, so to limit costs it is preferential to use increased ventilation only at times and places where workers are at risk of exposure. To protect against particle inhalation, workers may also use personal protection (masks), or stay inside vehicles equipped with HEPA-filters (High-efficiency particulate air filter).

In outdoor air, coarse (PM_{10}, sub 10 µm) and fine ($PM_{2.5}$, sub 2.5 µm) particles are closely monitored and efforts are put into keeping mass concentrations low. The World Health Organization gives guidelines for yearly averages of $PM_{2.5}$ (10 µg m^{-3}) and PM_{10} (20 µg m^{-3}). Occupational exposure limits are much higher and vary from country to country. Some countries set limits on inhalable dust (PM_{100}), while others limit respirable dust ($\sim PM_4$) or thoracic dust (another name for PM_{10}). The Finnish Institute of Occupational Health (FIOH) recommends limits of 2000 µg m^{-3} for inhalable dust and 500 µg m^{-3} for respirable dust (Hyytinen *et al.*, 2016). In addition, diesel particulate matter (DPM) is often monitored, usually measured indirectly through a surrogate, such as elemental carbon (Noll *et al.*, 2007; Pronk *et al.*, 2009). For DPM limits, FIOH uses Switzerland's officials' suggested value of 100 µg m^{-3} for elemental carbon (Taxell *et al.*, 2015). Most recent aerosol studies related to underground mining focus on DPM, as there is evidence of health effects related to it (Chang and Xu, 2017; Barrett *et al.*, 2019). The problem with these existing mass-based exposure limits is that they do not adequately account for ultrafine particles (sub 100 nm), which are able to penetrate deep into human airways and deposit into lung alveoli (Braakhuis *et al.*, 2014). This is especially worrisome, since the majority of particle emissions (measured by number) from diesel engines fall into the ultrafine category (Karjalainen *et al.*, 2019; Pirjola *et al.*, 2019).

One metric better suited for ultrafine particle measurement is the Lung Deposited Surface Area (LDSA) concentration of particles. It has been introduced to describe the harmfulness of particulate pollutants of inhaled air. LDSA combines the idea that toxic compounds lie especially on the surfaces of particles, with deposition efficiency of particles into the alveolar area of the human respiratory system. The LDSA of 20–300 nm particles can be easily monitored by sensor type devices (Kuuluvainen *et al.*, 2018; Kuula *et al.*, 2019) which has increased its use in air quality monitoring applications, especially related to urban ambient air. The sensors are small, stand-alone units, allowing them to be used in sensor networks for overall air quality monitoring or for personal exposure monitoring. The first instrument designed for LDSA measurement was presented by Fissan *et al.* (2007), and since then many more designs have become available. In the original LDSA instrument, the user could choose to measure the deposition in a certain lung-region, but recent research has focused on the alveolar region, as it has been assumed to have the highest health-impact.

LDSA concentrations, size distribution and height profiles have been measured in ambient conditions in different urban environments (Kuuluvainen *et al.*, 2016; Kuula *et al.*, 2020; Tran *et al.*, 2020). In urban ambient air studies, the LDSA concentrations have been observed to be linked with emissions from combustion sources, such as engines and residential wood burning. Studies conducted in working environments and indoor conditions have measured LDSA e.g., to characterize LDSA exposure in printing centers (Setyawati *et al.*, 2020) or to study influence of air cleaner devices to LDSA in offices (Küpper *et al.*, 2019). In ambient air the LDSA concentrations typically vary from ~10–50 µm^2 cm^{-3} measured at clean background areas (Kuula *et al.*, 2020), to values up to ~100–150 µm^2 cm^{-3} typically observed near PM sources such as roads (Leavey *et al.*, 2017; Cheristanidis *et al.*, 2020). LDSA concentrations related to mining operations have recently been studied using real time instruments in the context of open taconite mining operations. Huynh *et al.* (2018) studied ambient fine particle concentration in six taconite mines, using several particle concentration metrics, including LDSA. In their study, LDSA concentrations ranged from 50 to 300 µm^2 cm^{-3} depending on the processing area. Afshar-Mohajer *et al.* (2020) studied the variability of aerosol concentrations in different processing areas of a taconite mine using different metrics, including LDSA, which ranged from 85 to 200 µm^2 cm^{-3}. Within these studies, the highest readings were found in the pelletizing area. To the best of our knowledge, LDSA concentrations of underground mines have not been reported before.

In this study, we measured total LDSA along with the LDSA size distribution of particles up to 10 µm. The measurements were conducted in an underground mine in Kemi, Finland, in 2017. The aim of this article is to report the concentrations of LDSA in various locations in the mine and evaluate the applicability of LDSA as a measurement metric and the applicability of sensor-type measurements of LDSA in a mine environment.

2 METHODS

The total LDSA and LDSA particle size distributions were measured in an underground chrome mine located in Kemi, Finland, and operated by Outokumpu. The mine has been in operation since 1968, and the underground operations began in 2003. In 2016, the mine employed approximately 200 people through Outokumpu and an additional 300 people through permanent contractors, and in total, 3 million tons of rock was mined within the year (https://www.kaivosvastuu.fi/yrity skortti/outokumpu-chrome-oy/). The measurement campaign took place from March 21st to March 30th in 2017. Two sensors were left to monitor the mine air for an additional 12 days, until April 11th.

Five measurement sites were chosen for this study, each to represent an aerosol source or a location of personnel exposure (or both). Three sites—the dumping area, crushing station and maintenance area—each had workers operating in the area, although in the dumping area most workers were inside vehicles. The maintenance area also had vehicle traffic, and many people were also walking in the area, as offices and the cafeteria were located on this level. The two remaining sites were the blasting area and conveyor belt. The blasting area did not have workers during the blasting for safety reasons, but trucks arrived shortly afterwards to transport rocks. The conveyor belt location did not have much human activity during our measurements, although the belt itself was in operation. We expected vehicle emissions to be present in all locations, but especially in the dumping area and in the blasting area (after the blasting, which were scheduled to be at 14:00 and 22:00), where heavy-duty traffic was frequent. The maintenance area was frequented by passenger vehicles, taking people to the offices and cafeteria, so some traffic exhaust was expected to originate from there as well. We expected to see coarser particles at the crushing station as well as the blast site. The measurement locations along with the mobile laboratory setup are described in more detail by Saarikoski *et al.* (2019), where other aspects (particle mass, number, and chemical composition) of this measurement campaign are reported.

Measurements were conducted primarily using ELPI+ (Electrical Low-Pressure Impactor, Dekati Ltd.) but, in addition, the applicability and performance of five smaller, sensor-type instruments was tested in the mine environment.

ELPI+ is a 14-stage low-pressure cascade impactor. Unlike in traditional impactors, the particles are measured electrically in real time (Keskinen *et al.*, 1992). For the particles to be detected, they are first charged with positive ions from a diffusion charger. The raw data from the instrument is the current measured from each of the 14 stages. The lowest stage is a filter, which collects essentially all particles, but due to weakened charging of very small particles, the lowest detectable size is 6 nm. Before the highest stage, there is an impactor to remove particles over 10 µm in aerodynamic size. When handling the data, the currents were first corrected using zero measurement data (current measured when a HEPA filter was placed at the inlet) and then adjusted to account for secondary collection by diffusion (Järvinen *et al.*, 2014). The LDSA distribution was then calculated from the current distribution, using the method described by Lepistö *et al.* (2020). Total LDSA was calculated for different size ranges, based on the impactor cut-off sizes. In this article we have rounded the actual cut-off sizes to nearest round values, true cut-offs can be found in Table S1.

The chemical composition of submicron (< 1 µm) particles was determined by a Soot Particle Aerosol Mass Spectrometer (Aerodyne Research Inc.). The SP-AMS was equipped with both laser and tungsten vaporizers, and therefore, it was able to measure both non-refractory material (organics, sulfate, nitrate, ammonium and chloride), and refractory material (i.e., the refractory BC and metals) in particles. The details of the SP-AMS analysis can be found in Saarikoski *et al.* (2019). Additionally, the black carbon concentrations were measured with a dualspot Aethalometer (AE33; Magee Scientific).

The five electrical particle sensors included in this study were two Partectors (Naneos), one DiSCmini (Testo) and two AQ Indoors (Pegasor). The sensors employ a diffusion charger to charge incoming particles and the electrical current generated by the particles is measured. The raw current is transformed into LDSA using an internal calibration factor. The calibration factor relies on the linear relationship between diffusion charging and LDSA, but this linear relationship is only true for a rather small size range of approximately 20–300 nm. If a sensor is calibrated with 100 nm particles, as is the case with the Partector, then the LDSA of 300 nm particles will be over-estimated, while the LDSA of 50 nm particles is under-estimated (Fierz *et al.*, 2014). The three different sensor types employed in this study all measure alveolar deposition.

While each of the sensors uses the same basic principle for LDSA measurement, there are some notable differences in the measurement techniques. The Partector uses pulsed charging, and it measures the induced current created by the changing charge (Fierz *et al.*, 2014). The benefit of this method is that the particles do not need to be collected. The DiSCmini has two-stage collection, which allows for it to estimate the mean size of the particle population. The first stage is a diffusion collector, collecting only the smallest particles, and the second stage is a filter, collecting what is left over after the first stage. The AQ Indoor employs a particle trap with a cycling voltage to remove some of the particle population, also allowing for an estimation of the particle size. The larger the voltage, the larger the particles which can be removed. To ensure coarse particles and dirt do not get inside the sensors, the Partector uses a wire mesh at the inlet, the DiSCmini has an impactor which can be inserted at the inlet, and AQ Indoor has a cyclone.

The ELPI+ was located inside a mobile measurement laboratory along with various other air quality instruments. The sensors were located initially in the Maintenance area of the mine and connected to each other with Tygon tubing, to make sure they sampled the same air for the duration of a sensor comparison. Later, the AQ Indoor sensors were moved to different locations in the mine (AQ Indoor A to the dumping area and AQ Indoor B to the crushing station), for the sensor network type measurement. The Partector and DiSCmini instruments began reporting faults after just a few days of measurements, due to over-loading, and were not employed further.

3 RESULTS

Fig. 1 shows the time series of total LDSA concentration, based on the measurements using ELPI+. Color bars in the figure indicate measurement locations and time periods analyzed, these are the same times and locations as in the study by Saarikoski *et al.* (2019). In general, Fig. 1 shows that the LDSA concentration had a large spatial and temporal variation in the air of studied underground mine. This variation can be seen both between the locations and within one location as a function of time. For instance, in the blasting area, the total LDSA concentration varied from values lower than 100 μm^2 cm^{-3} to values larger than 700 μm^2 cm^{-3}, and similar variation can be seen in crushing station. In the maintenance area the LDSA concentration remained relatively low,
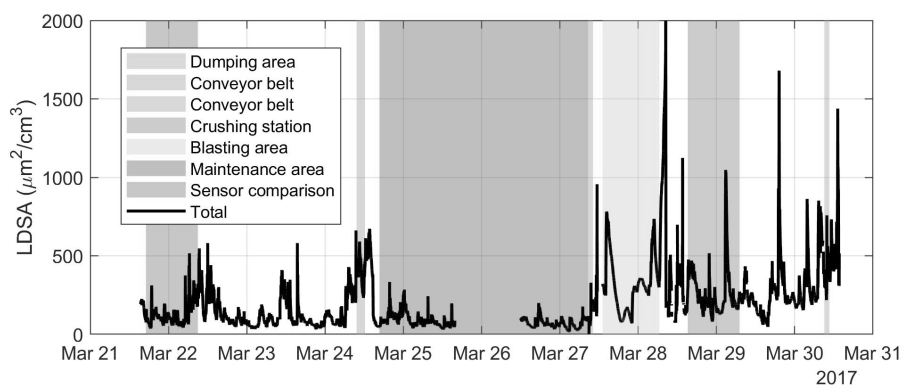

Fig. 1. Timeseries of total LDSA concentration measured with ELPI+, and measurement locations shown with color bars.

mostly under 200 μm² cm⁻³. In general, rapid changes in LDSA concentrations indicate that local sources affect the concentrations. However, measurements conducted simultaneously in two different locations (dumping area and crushing site, Fig. S1) indicate that emissions also spread between locations. Sensors were also used to measure LDSA inside the canteen and offices located at the maintenance level, separated by doors. Both locations showed essentially zero LDSA concentrations.

Fig. 2 shows the time series of particle LDSA size distributions for each measurement location. The figure shows that particle sizes from 10 nm to 6 μm contribute to the LDSA in an underground mine. However, the relative contribution of different size ranges varies among locations. The highest contributions from largest particles, i.e., from particles larger than 200 nm in diameter, were observed in the blasting area and were directly linked with blasting events. However, occasional short periods of high LDSA from large particles were also observed at the crushing station and in the maintenance area, where the sensor comparison was made. While at the crushing station the high LDSA concentration was likely from a local source, in the maintenance area it was most likely caused by blasting originated large particles transported from a distant blasting event.

Fig. 3 shows the time-averaged particle LDSA size distributions. In the figure, each line corresponds to one of the color plots in Fig. 2. Most locations had the largest particle mode around 50–200 nm, the Blasting area being the main exception, with a mode size around 500 nm. Several locations had two particle modes. Looking back at Fig. 2, at the blasting area and the crushing station these
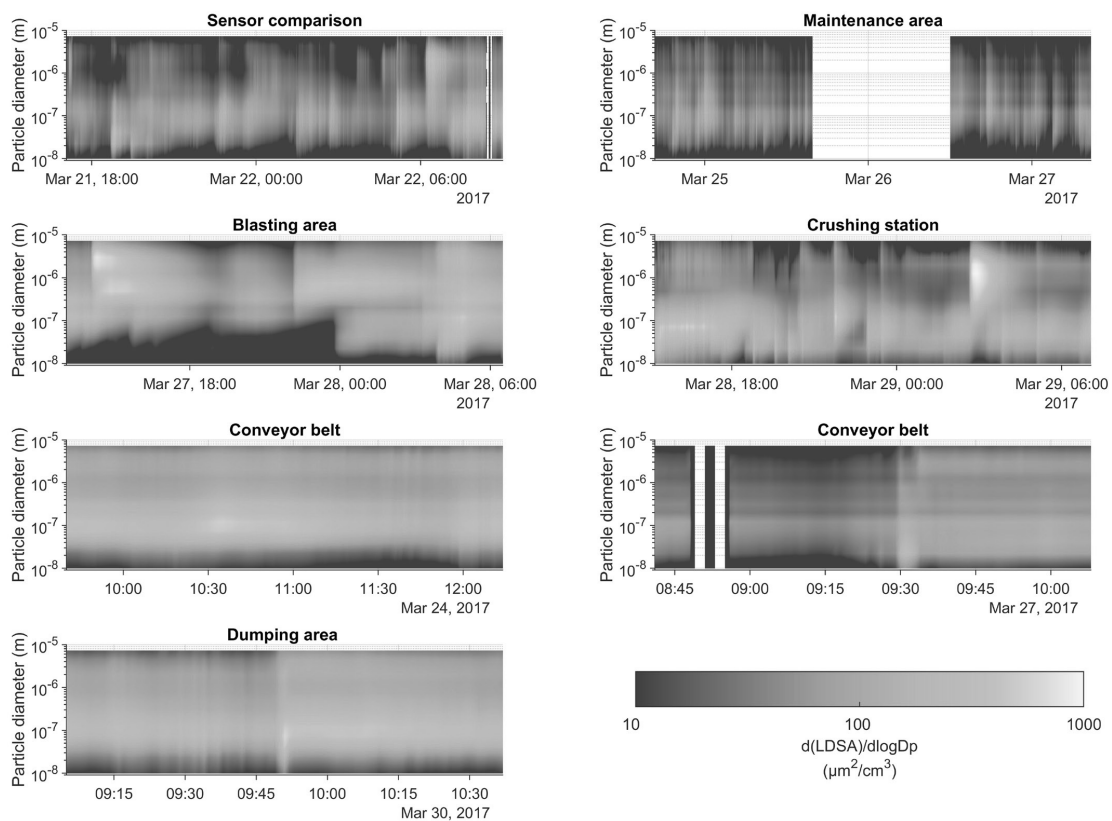

Fig. 2. Location-specific LDSA distribution timeseries measured with ELPI+. The sensor comparison was conducted in the Maintenance area. Note that the Conveyor belt and Dumping area measurements were much shorter than others, due to difficulties with the power supply.
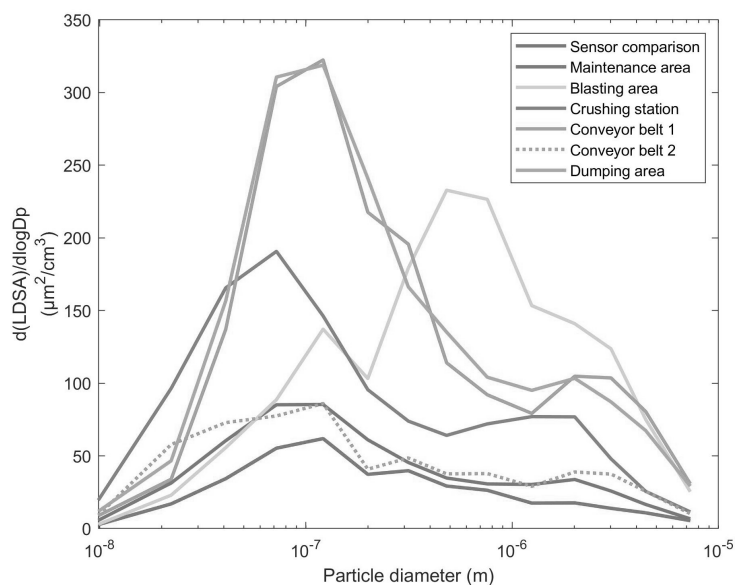
Fig. 3. Mean LDSA size distribution from each location.

different modes occur independently, meaning they must be from different sources. In contrast, at the dumping area and conveyor belt, both modes appear at the same time. The particles are either from the same source, or from different sources which have activity at the same time. From Fig. 3 it may seem as though the conveyor belt and dumping area had less activity (plots are smooth); however, the smooth appearance is due to the shorter time periods measured. The dumping area was also measured with a sensor for a longer duration (Fig. S1), which shows dramatic changes in the total LDSA.

Fig. S2 shows the chemical composition of particles by mass fraction, plotted against particle size. As the data is by mass, it is difficult to directly compare with the LDSA size distributions in Figs. 2 and 3. However, the particles consisted mostly of organics, with black carbon (soot) being the second most common substance. The blasting area had a large amount of sulphate as well. It should be noted that the SP-AMS only detects particles up to 1 μm in diameter, and it requires that the detected particles either vaporize at 600°C or absorb light at a wavelength of 1064 nm, which is why it did not detect mineral dust. In-depth discussion on the aerosol chemical composition can be found in Saarikoski *et al.* (2019).

Table 1 contains a summary of the numerical results for LDSA for each measurement location (columns) and separated into particle size ranges (rows). The size ranges have been selected to relate to the conventions in mass concentration measurement (PM_{10}, $PM_{2.5}$, PM_1, $PM_{0.1}$); additionally, diffusion-charging based sensors are often calibrated for sizes between 30–300 nm. The table shows that a large portion of particles (34–70%) is measured incorrectly with these sensors, due to the particles being larger than the size range that the sensors are calibrated for. On the other hand, less than 13% of LDSA is contributed from particles over 2.5 μm.

Fig. 4 shows a time series (top panel) of the sensor comparison performed at the beginning of the measurement campaign (see Fig. 1). Five different diffusion-charging sensors were used, and the 5-minute averaged values were compared to ELPI+. The lower plot shows the correlation between ELPI+ and each sensor, along with fitted lines. The best correlations were with AQ Indoor (A and B, $R^2 = 0.59$). Some of the discrepancy between ELPI+ and the sensors is probably due to the slightly different measurement locations (the ELPI+ measurement point was approximately 5 meters away from the sensors). The largest discrepancy between sensors and ELPI+ was at the end of the sensor comparison, where all sensors overestimated the LDSA concentration. The overestimation did not persist after the sensors were moved to new locations (Fig. S4, Fig. S5).

Correlations between each of the similar sensor pairs (Partector A & B, AQ Indoor A & B) are in Fig. S6. The AQ Indoor sensors were remarkably well-correlated, with a correlation factor of R^2 = 1.00.

Table 1. Mean and standard deviation of LDSA ($\mu m^2\ cm^{-3}$) for each measurement location (measured with ELPI+) divided into particle size bins. The percentage represents the fraction of LDSA attributable to particles smaller than the specified size.

|	LDSA mean ± standard deviation ($\mu m^2\ cm^{-3}$)						
	Sensor comparison	Maintenance area	Blasting area	Crushing station	Conveyor belt 1	Conveyor belt 2	Dumping area
Total (Sub 10 µm)	120 ± 66 100%	79 ± 38 100%	323 ± 175 100%	270 ± 157 100%	389 ± 89 100%	137 ± 68 100%	405 ± 107 100%
Sub 2.5 µm	112 ± 59 94%	74 ± 36 94%	282 ± 139 87%	246 ± 138 91%	349 ± 84 90%	124 ± 62 91%	370 ± 93 91%
Sub 1 µm	99 ± 49 83%	67 ± 33 84%	220 ± 107 68%	214 ± 93 80%	312 ± 80 80%	110 ± 55 80%	329 ± 85 81%
Sub 300 nm	79 ± 42 66%	49 ± 25 62%	97 ± 77 30%	175 ± 74 65%	237 ± 64 61%	86 ± 46 63%	253 ± 71 62%
Sub 100 nm	47 ± 30 39%	28 ± 14 35%	44 ± 46 14%	122 ± 56 45%	120 ± 33 31%	58 ± 37 42%	132 ± 43 32%
Sub 30 nm	11 ± 10 9%	6 ± 4 7%	8 ± 11 2%	35 ± 14 13%	13 ± 4 3%	20 ± 19 15%	18 ± 9 4%
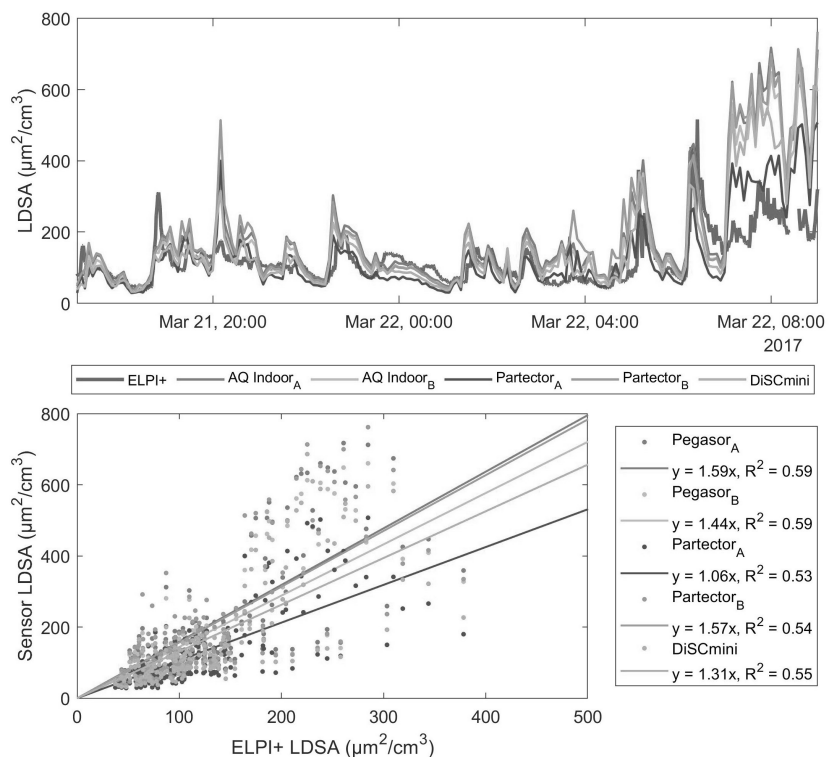
Fig. 4. Time series of electrical sensors and ELPI+ measuring LDSA concentration and related correlation plot. The sensors were all located on a table in the mine, whereas ELPI+ was measuring about 5 m away, inside the mobile laboratory.

During the measurements, the Partectors and DiSCmini reported faults and had to be cleaned several times. The DiSCmini impactor collected dust quite quickly and needed frequent cleaning (once per day). The AQ Indoor sensors were not cleaned during the entire measurement period, and they did not report faults. These sensors have a rather large cyclone at the entrance of the instrument, which seems to have helped keep the insides clean.

4 DISCUSSION

We successfully measured the LDSA distribution of several locations in the underground mine. In most locations, the majority of the total LDSA concentration was contributed by sub 300 nm particles; however, a significant portion (34%–70%) of LDSA was in larger particle sizes.

Despite the large size range of particles in the mine, electrical sensors were able to measure total LDSA with a good correlation to ELPI+ (R^2 = 0.53–0.59). Somewhat surprisingly, discrepancies between sensors and ELPI+ measurements in the sensor comparison were unrelated to the presence of large particles, and perhaps slightly effected by sub 30 nm particles. The relationship was investigated by plotting the percentage difference of each sensor vs. ELPI+ on the y-axis, and the portion of particles over 300 nm on the x-axis (Fig. S3(a)), and similarly for particles smaller than 30 nm (Fig. S3(b)). A slight correlation was observed only in the latter case. A previous laboratory study showed that sub 20 nm particles are overestimated by LDSA sensors, while particles over 400 nm are underestimated (Todea *et al.*, 2015), which is also explained by the relationship of the diffusion charger *Pn*-curve (particle penetration efficiency multiplied by the number of unit charges) compared to the deposition probability function (Fierz *et al.*, 2014). We did find some evidence of LDSA from large particles being underestimated by the AQ Indoor sensor from a measurement at the crushing station (Fig. S4, not included in the main measurements covered in this article). The main problem, however, was overloading of the sensors caused by coarse dust—an inlet cyclone removing coarse particles is a necessity for long-term measurement. An optical particle sensor would be a useful addition for locations with coarse particles, as they are better suited for particle diameters over 300 nm.

Another recent study (Barrett *et al.*, 2019) also examined particle sensors for underground mine applications; however, they focused on measuring the mass concentration of elemental or black carbon. They found good potential in a prototype black carbon sensor, which had good correlation with the reference method during field testing (R^2 = 0.85). Barrett *et al.* (2019) used 30-minute averages for the comparison (compared to 5 minutes in our study—30 minute averaging would likely improve the correlation coefficient for the LDSA sensors). Particle loading was a problem in Barrett's study as well (Barrett *et al.*, 2019).

Longer measurements with the two AQ Indoor sensors indicated that particle populations in the mine mix and spread quickly, at least in these two locations (Fig. S1). This means that to improve air quality at a specific location requires changes in ventilation, in addition to controlling the location-specific sources. Based on total LDSA time series data, the air exchange rate at the dumping area was approximately 15 (1/h) (Fig. S7(a)) and 22 (1/h) in the crushing station (Fig. S7(b)).

Comparing the mean LDSA size distributions, the lowest concentrations in all sizes were seen in the maintenance area. Compared to the taconite mine study which also reported LDSA concentrations (Huynh *et al.*, 2018), our results were in a similar range, although slightly higher (mean LDSA in our study: 79–405 $\mu m^2\, cm^{-3}$, Huynh *et al.* (2018): 54–303 $\mu m^2\, cm^{-3}$, excluding office and laboratory spaces, which were very clean, < 10 $\mu m^2\, cm^{-3}$). However, it should be noted that this previous study only included particles up to 1 μm in diameter, which, if the distributions were similar to ours, leaves out 20%–30% of total LDSA. The LDSA values measured both in our study and in the previous taconite mine study are very high when comparing to the ambient background levels (e.g., 10-50 $\mu m^2\, cm^{-3}$ measured in Helsinki (Kuula *et al.*, 2019)). Although the concentrations are high in comparison to ambient levels, they are comparable to several other working environments. For instance, personal exposure measurements by Setyawati *et al.* (2020) at a printing center revealed a maximum exposure of 220 $\mu m^2\, cm^{-3}$. The worker with highest exposure levels had an overall mean exposure of 106 $\mu m^2\, cm^{-3}$. In another exposure study, airport taxiway personnel were found to operate in mean LDSA concentrations of 59 to 174 $\mu m^2\, cm^{-3}$ (Marcias *et al.*, 2019).

Our study was not a personal exposure study and cannot be directly compared to these values; however, the potential for similar or even higher exposure exists.

The previous paper covering other measurements from this same campaign shows average PM_{10} was highest at the blasting area (355 μg m^{-3}) and lowest in the maintenance area (49 μg m^{-3}) (Saarikoski *et al.*, 2019). While the LDSA is also higher in the blasting area than in the maintenance area, the average LDSA to mass ratios for these locations are 0.9 and 1.6 (units μm^2 cm^{-3} μg^{-1} m^3), respectively. This indicates that one unit of particle mass in the blasting area is likely to be less toxic than one unit of mass in the maintenance area, based on the lung-deposition. Basing guidelines or regulation purely on mass concentration misses this effect.

5 CONCLUSION

This study shows that there are large variations in the LDSA concentrations and LDSA size distributions of an underground mine. This should be considered in future air quality guidelines and monitoring in occupational surroundings, which are currently trailing behind the science of aerosol health effects. Furthermore, this study shows that diffusion charging based particle sensors are a viable method for long-term monitoring of LDSA in underground mines if dust accumulation is taken care of, perhaps aided by optical sensors or other solutions for a larger particle size range coverage. Finally, occupational exposure limits need to be extended to smaller particles, and LDSA is a good choice for the measurement metric, as it is easily measurable and intrinsically health relevant.

ACKNOWLEDGMENTS

SUPPLEMENTARY MATERIAL

Supplementary material for this article can be found in the online version at https://doi.org/10.4209/aaqr.200660

REFERENCES

Afshar-Mohajer, N., Foos, R., Volckens, J., Ramachandran, G. (2020). Variability of aerosol mass and number concentrations during taconite mining operations. J. Occup. Environ. Hyg. 17, 1–14. https://doi.org/10.1080/15459624.2019.1688823

Barrett, C., Sarver, E., Cauda, E., Noll, J., Vanderslice, S., Volkwein, J. (2019). Comparison of several DPM field monitors for use in underground mining applications. Aerosol Air Qual. Res. 19, 2367–2380. https://doi.org/10.4209/aaqr.2019.06.0319

Braakhuis, H.M., Park, M.V.D.Z., Gosens, I., De Jong, W.H., Cassee, F.R. (2014). Physicochemical characteristics of nanomaterials that affect pulmonary inflammation. Part. Fibre Toxicol. 11, 18. https://doi.org/10.1186/1743-8977-11-18

Burnett, R., Chen, H., Szyszkowicz, M., Fann, N., Hubbell, B., Pope, C.A. 3rd, Apte, J.S., Brauer, M., Cohen, A., Weichenthal, S., Coggins, J., Di, Q., Brunekreef, B., Frostad, J., Lim, S.S., Kan, H., Walker, K.D., Thurston, G.D., Hayes, R.B., Lim, C.C., *et al.* (2018). Global estimates of mortality associated with longterm exposure to outdoor fine particulate matter. Proc. Natl. Acad. Sci. U.S.A. 115, 9592–9597. https://doi.org/10.1073/pnas.1803222115

Chang, P., Xu, G. (2017). A review of the health effects and exposure-responsible relationship of diesel particulate matter for underground mines. Int. J. Min. Sci. Technol. 27, 831–838. https://doi.org/10.1016/j.ijmst.2017.07.020

Cheristanidis, S., Grivas, G., Chaloulakou, A. (2020). Determination of total and lung-deposited particle surface area concentrations, in central Athens, Greece. Environ. Monit. Assess. 192, 627. https://doi.org/10.1007/s10661-020-08569-8

Fierz, M., Meier, D., Steigmeier, P., Burtscher, H. (2014). Aerosol Measurement by Induced Currents. Aerosol Sci. Technol. 48, 350–357. https://doi.org/10.1080/02786826.2013.875981

Fissan, H., Neumann, S., Trampe, A., Pui, D.Y.H., Shin, W.G. (2007). Rationale and principle of an instrument measuring lung deposited nanoparticle surface area. J. Nanoparticle Res. 9, 53–59. https://doi.org/10.1007/s11051-006-9156-8

Goulaouic, S., Foucaud, L., Bennasroune, A., Laval-Gilly, P., Falla, J. (2008). Effect of polycyclic aromatic hydrocarbons and carbon black particles on pro-inflammatory cytokine secretion: Impact of PAH coating onto particles. J. Immunotoxicol. 5, 337–345. https://doi.org/10.1080/15476910802371016

Grahame, T.J., Klemm, R., Schlesinger, R.B. (2014). Public health and components of particulate matter: The changing assessment of black carbon. J. Air Waste Manage. Assoc. 64, 620–660. https://doi.org/10.1080/10962247.2014.912692

Huynh, T., Ramachandran, G., Quick, H., Hwang, J., Raynor, P.C., Alexander, B.H., Mandel, J.H. (2018). Ambient fine aerosol concentrations in multiple metrics in taconite mining operations. Ann. Work Exposures Health 63, 77–90. https://doi.org/10.1093/annweh/wxy086

Hyytinen, E.R., Tiina, S., Vainiotalo, S., Rantonen, J., Linnainmaa, M. (2016). Justification memo for inhalable and respirable dust target level. Text in Finnish. Finnish Institute of Occupational Health.

Järvinen, A., Aitomaa, M., Rostedt, A., Keskinen, J., Yli-Ojanperä, J. (2014). Calibration of the new electrical low pressure impactor (ELPI+). J. Aerosol Sci. 69, 150–159. https://doi.org/10.1016/j.jaerosci.2013.12.006

Karjalainen, P., Rönkkö, T., Simonen, P., Ntziachristos, L., Juuti, P., Timonen, H., Teinilä, K., Saarikoski, S., Saveljeff, H., Lauren, M., Happonen, M., Matilainen, P., Maunula, T., Nuottimäki, J., Keskinen, J. (2019). Strategies to diminish the emissions of particles and secondary aerosol formation from diesel engines. Environ. Sci. Technol. 53, 10408–10416. https://doi.org/10.1021/acs.est.9b04073

Keskinen, J., Pietarinen, K., Lehtimäki, M. (1992). Electrical low pressure impactor. J. Aerosol Sci. 23, 353–360. https://doi.org/10.1016/0021-8502(92)90004-F

Küpper, M., Asbach, C., Schneiderwind, U., Finger, H., Spiegelhoff, D., Schumacher, S. (2019). Testing of an indoor air cleaner for particulate pollutants under realistic conditions in an office room. Aerosol Air Qual. Res. 19, 1655–1665. https://doi.org/10.4209/aaqr.2019.01.0029

Kuula, J., Kuuluvainen, H., Rönkkö, T., Niemi, J. V., Saukko, E., Portin, H., Aurela, M., Saarikoski, S., Rostedt, A., Hillamo, R., Timonen, H. (2019). Applicability of optical and diffusion charging-based particulate matter sensors to urban air quality measurements. Aerosol Air Qual. Res. 19, 1024–1039. https://doi.org/10.4209/aaqr.2018.04.0143

Kuula, J., Kuuluvainen, H., Niemi, J.V., Saukko, E., Portin, H., Kousa, A., Aurela, M., Rönkkö, T., Timonen, H. (2020). Long-term sensor measurements of lung deposited surface area of particulate matter emitted from local vehicular and residential wood combustion sources. Aerosol Sci. Technol. 54, 190–202. https://doi.org/10.1080/02786826.2019.1668909

Kuuluvainen, H., Rönkkö, T., Järvinen, A., Saari, S., Karjalainen, P., Lähde, T., Pirjola, L., Niemi, J. V., Hillamo, R., Keskinen, J. (2016). Lung deposited surface area size distributions of particulate matter in different urban areas. Atmos. Environ. 136, 105–113. https://doi.org/10.1016/j.atmosenv.2016.04.019

Kuuluvainen, H., Poikkimäki, M., Järvinen, A., Kuula, J., Irjala, M., Dal Maso, M., Keskinen, J., Timonen, H., Niemi, J. V., Rönkkö, T. (2018). Vertical profiles of lung deposited surface area concentration of particulate matter measured with a drone in a street canyon. Environ. Pollut. 241, 96–105. https://doi.org/10.1016/j.envpol.2018.04.100

Leavey, A., Reed, N., Patel, S., Bradley, K., Kulkarni, P., Biswas, P. (2017). Comparing on-road real-time simultaneous in-cabin and outdoor particulate and gaseous concentrations for a range of ventilation scenarios. Atmos. Environ. 166, 130–141. https://doi.org/10.1016/j.atmosenv.2017.07.016

Lelieveld, J., Evans, J.S., Fnais, M., Giannadaki, D., Pozzer, A. (2015). The contribution of outdoor air pollution sources to premature mortality on a global scale. Nature 525, 367–371. https://doi.org/10.1038/nature15371

Lepistö, T., Kuuluvainen, H., Juuti, P., Järvinen, A., Arffman, A., Rönkkö, T. (2020). Measurement of the human respiratory tract deposited surface area of particles with an electrical low pressure impactor. Aerosol Sci. Technol. 54, 958–971. https://doi.org/10.1080/02786826.2020.1745141

Marcias, G., Casula, M., Uras, M., Falqui, A., Miozzi, E., Sogne, E., Pili, S., Pilia, I., Fabbri, D., Meloni, F., Pau, M., Sanna, A., Fostinelli, J., Massacci, G., d'Aloja, E., Filon, F., Campagna, M., Lecca, L. (2019). Occupational fine/ultrafine particles and noise exposure in aircraft personnel operating in airport taxiway. Environments 6, 35. https://doi.org/10.3390/environments6030035

Noll, J.D., Bugarski, A.D., Patts, L.D., Mischler, S.E., McWilliams, L. (2007). Relationship between elemental carbon, total carbon, and diesel particulate matter in several underground metal/non-metal mines. Environ. Sci. Technol. 41, 710–716. https://doi.org/10.1021/es061556a

Oberdörster, G. (2001). Pulmonary effects of inhaled ultrafine particles. Int. Arch. Occup. Environ. Health 74, 1–8. https://doi.org/10.1007/s004200000185

Pirjola, L., Kuuluvainen, H., Timonen, H., Saarikoski, S., Teinilä, K., Salo, L., Datta, A., Simonen, P., Karjalainen, P., Kulmala, K., Rönkkö, T. (2019). Potential of renewable fuel to reduce diesel exhaust particle emissions. Appl. Energy 254, 113636. https://doi.org/10.1016/j.apenergy.2019.113636

Pope, C.A. 3rd (2000). Epidemiology of fine particulate air pollution and human health: Biologic mechanisms and who's at risk? Environ. Health Perspect. 108, 713–723. https://doi.org/10.1289/ehp.108-1637679

Pope, C.A. 3rd, Dockery, D.W. (2006). Health effects of fine particulate air pollution: Lines that connect. J. Air Waste Manage. Assoc. 56, 709–742. https://doi.org/10.1080/10473289.2006.10464485

Pronk, A., Coble, J., Stewart, P.A. (2009). Occupational exposure to diesel engine exhaust: A literature review. J. Exposure Sci. Environ. Epidemiol. 19, 443–457. https://doi.org/10.1038/jes.2009.21

Saarikoski, S., Salo, L., Bloss, M., Alanen, J., Teinilä, K., Reyes, F., Vázquez, Y., Keskinen, J., Oyola, P., Rönkkö, T., Timonen, H. (2019). Sources and characteristics of particulate matter at five locations in an underground mine. Aerosol Air Qual. Res. 19, 2613–2624. https://doi.org/10.4209/aaqr.2019.03.0118

Setyawati, M.I., Singh, D., Krishnan, S.P.R., Huang, X., Wang, M., Jia, S., Goh, B.H.R., Ho, C.G., Yusoff, R., Kathawala, M.H., Poh, T.Y., Ali, N.A.B.M., Chotirmall, S.H., Aitken, R.J., Riediker, M., Christiani, D.C., Fang, M., Bello, D., Demokritou, P., Ng, K.W. (2020). Occupational inhalation exposures to nanoparticles at six singapore printing centers. Environ. Sci. Technol. 54, 2389–2400. https://doi.org/10.1021/acs.est.9b06984

Taxell, P., Hyytinen, E.-R., Ahonen, I., Santonen, T. (2015). Justification memo for diesel exhaust aerosol target level. Text in Finnish. Finnish Institute of Occupational Health.

Todea, A.M., Beckmann, S., Kaminski, H., Asbach, C. (2015). Accuracy of electrical aerosol sensors measuring lung deposited surface area concentrations. J. Aerosol Sci. 89, 96–109. https://doi.org/10.1016/j.jaerosci.2015.07.003

Tran, P.T.M., Ngoh, J.R., Balasubramanian, R. (2020). Assessment of the integrated personal exposure to particulate emissions in urban micro-environments: A pilot study. Aerosol Air Qual. Res. 20, 341–357. https://doi.org/10.4209/aaqr.2019.04.0201
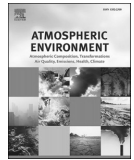
PAPER III

The characteristics and size of lung-depositing particles vary significantly between high and low pollution traffic environments

Salo, L., Hyvärinen, A., Jalava, P., Teinilä, K., Hooda, R. K., Datta, A., Saarikoski, S., Lintusaari, H., Lepistö, T., Martikainen, S., Rostedt, A., Sharma, V. P., Rahman, M. H., Subudhi, S., Asmi, E., Niemi, J. V., Lihavainen, H., Lal, B., Keskinen, J., Kuuluvainen, H., Timonen, H., Rönkkö, T.

The characteristics and size of lung-depositing particles vary significantly between high and low pollution traffic environments

Laura Salo [a,*], Antti Hyvärinen [b], Pasi Jalava [c], Kimmo Teinilä [b], Rakesh K. Hooda [b], Arindam Datta [b], Sanna Saarikoski [b], Henna Lintusaari [a], Teemu Lepistö [a], Sampsa Martikainen [a], Antti Rostedt [a], Ved Prakash Sharma [d], Md. Hafizur Rahman [d], Sanjukta Subudhi [e], Eija Asmi [b], Jarkko V. Niemi [f], Heikki Lihavainen [b,g], Banwari Lal [d], Jorma Keskinen [a], Heino Kuuluvainen [a], Hilkka Timonen [b], Topi Rönkkö [a]

[a] *Aerosol Physics Laboratory, Physics Unit, Tampere University, Tampere, FI-33720, Finland*
[b] *Atmospheric Composition Research, Finnish Meteorological Institute, P.O. Box 503, FI-00101, Helsinki, Finland*
[c] *Inhalation Toxicology Laboratory, Department of Environmental and Biological Sciences, University of Eastern Finland, P.O. Box 1627, FI-70211, Kuopio, Finland*
[d] *Earth Sciences and Climate Change Division, The Energy and Resources Institute, New Delhi, 110003, India*
[e] *Advanced Biofuels Program, The Energy and Resources Institute, New Delhi, 110003, India*
[f] *Helsinki Region Environmental Services Authority, Helsinki, P.O. Box 100, FI-00066, Finland*
[g] *Svalbard Integrated Arctic Earth Observing System, P.O. Box 156, 9171, Longyearbyen, Norway*

HIGHLIGHTS

- LDSA particle size distributions compared between Delhi-NCR and Helsinki.
- Particles contributing to LDSA were up to five times larger in Delhi-NCR.
- Size differences indicate different sources and different chemical composition.
- Results may explain reported discrepancies in $PM_{2.5}$ toxicity between the cities.

ABSTRACT

Currently, only the mass of sub 2.5 μm and sub 10 μm particles ($PM_{2.5}$, PM_{10}) in ambient air is regulated and monitored closely, but the same increase in $PM_{2.5}$ can cause different degrees of health effects in different cities (sometimes more harmful effects per unit mass in less polluted cities) (Li et al., 2019). In addition to mass concentration, other measurement metrics are needed to connect particle pollution data and health effects. In our measurements made in traffic-influenced environments in Helsinki, Finland (a relatively clean city), and Delhi-National Capital Region (Delhi-NCR), India (a polluted area), we noted a large difference in the median particle size for lung-deposited surface area (LDSA). In Helsinki, the median size was 80 nm, corresponding to soot particles emitted from diesel engines. However, the median size increased to 190 nm during a long-range transport event of air mass. In Delhi-NCR, surprisingly, the median size was even larger, 410 nm. These larger particles were likely to originate from regional sources rather than local traffic. The LDSA to $PM_{2.5}$ ratio for particles in Helsinki was 2–4 times the amount in Delhi-NCR, potentially linked with the higher toxicity of a unit of particulate mass in Helsinki.

1. Introduction

Particulate matter in urban air is one of the leading causes of premature death. Recent studies provide numbers between 3.3 and 4.2 million excess deaths annually due to ambient air pollution (Lelieveld et al., 2015; Cohen et al., 2017). The relationship between $PM_{2.5}$ and

health effects has been thoroughly verified in epidemiological studies around the world (e.g. US (Samet et al., 2000), China (Lu et al., 2015; Song et al., 2017), Europe (Pelucchi et al., 2009; Lelieveld et al., 2019) and India (Balakrishnan et al., 2019)). While most studies and current regulations are based on particulate mass concentrations, the relationship between particle mass concentration and health effects differs from city to city (Li et al., 2019; Ritchie, 2019). For example, the per unit mass death rate caused by outdoor air pollution is 40% higher in Finland than in India (Ritchie, 2019). To address this issue, researchers have proposed the adoption of additional metrics like particle number concentration (e. g. (de Jesus et al., 2019)), surface area concentration (e.g. (Oberdörster, 1996; Schmid and Stoeger, 2016)), oxidative potential (OP) (Daellenbach et al., 2020) and chemical composition (e.g. (Li et al., 2019)). These metrics require new measurement techniques, as well as applying those techniques in real environments before conclusions can be made on their explanatory power.

The surface area of micro-scale particles has been foreseen as one of the main determinants of harmfulness in toxicological studies (Schmid and Stoeger, 2016; Oberdörster et al., 2005; Stoeger et al., 2006) and in lung functions (Moshammer and Neuberger, 2003). The increase in surface area of particles, compared to mass, causes more reactivity between the inhaled materials and the biological systems, leading to toxic effects (Bakand and Hayes, 2016), as well as inflammatory reactions (Keller et al., 2014). It should be noted, however, that these studies have been conducted with insoluble particles, and the results are likely to differ for soluble particles. However, not only is the surface of the particle the reaction site; toxic vapors released from emission sources can condense on surfaces, increasing the harmfulness of particles and even turning otherwise innocuous particles into harmful ones. Soluble as well as insoluble particles can act as condensation nuclei, so from this perspective the surface area of soluble particles can also be relevant when considering potential health effects of ambient aerosols.

The lung-deposited surface area (LDSA) of particles is a metric related to the abovementioned harmfulness of particulate surface area, defined as the concentration of particle surface area multiplied by a deposition function (usually alveolar deposition), which is dependent on the particle size. LDSA concentration has been shown to be a health-relevant metric in some health assessments (Patel et al., 2018; Aguilera et al., 2016). So far, only a few epidemiological studies have been published on LDSA and health effects (Patel et al., 2018; Aguilera et al., 2016; Pañella et al., 2017; Mostafavi et al., 2019; Tran et al., 2020; Habre et al., 2018). These studies have reported LDSA as a sensitive marker for lung function (Patel et al., 2018; Habre et al., 2018), atherosclerosis (Aguilera et al., 2016), cardiovascular mortality (Hennig et al., 2018), and asthma (Pañella et al., 2017; Mostafavi et al., 2019; Habre et al., 2018) as well as a good indicator of personal exposure in different environments (Tran et al., 2020). In a review of mouse and rat exposure studies, the delivered dose of particle surface area was the most relevant metric for acute lung toxicity, when comparing non-soluble spherical nanoparticles of different compositions (Schmid and Stoeger, 2016). In principle, LDSA could be used to estimate the adverse health effects of particles in ambient air, however, information on the LDSA of particles in different environments is currently very limited. This makes it impossible to fully understand the contribution of ambient particles' LDSA to diseases and premature deaths.

Atmospheric transformation processes have a significant role in the toxicity of particulate matter. The OP of particles is often used as a proxy for measuring the intrinsic toxicity of an aerosol in acellular assays. In general, smaller particles have more OP than larger particles, but OP also varies spatially (Saffari et al., 2014). A previous study reported that organic aerosol from biomass burning and cooking has a larger OP than urban background aerosol (Verma et al., 2015). It has also been shown that secondary organic aerosol (SOA) formed from gasoline engine exhaust has greater OP than primary engine emissions (Lovett et al., 2019). This suggests that the atmospheric conversion of vehicle exhaust emissions may increase OP. However, the mechanism of particulate

matter (PM) toxicity is not straightforward and various toxicity mechanisms have to be considered. While SOA causes adverse health effects through inflammation and oxidative stress, it is not effective in causing cell death. The health effects of SOA might be mediated through increased particle number concentration rather than mass (Gaschen et al., 2010). A study by Park et al. (2018) investigated fresh emissions from biomass and diesel exhaust, SOA, as well as sulfate and nitrate aerosols, and found the long-aged aerosols to be less toxic. This is also supported by a previous article studying the effects of long-range transport (LRT) episodes in Helsinki (Jalava et al., 2006). It was reported that the inflammatory and cytotoxic potential of the locally produced, fresh aerosol was higher than that of LRT aerosols, indicating that after several days in the atmosphere, the toxicity of PM decreases. Previous measurements of OP in Delhi showed that OP of $PM_{2.5}$ was mainly dependent on SOA (Puthussery et al., 2020); however, OP per unit of particulate mass was low, when compared to similar measurements in Illinois, USA, where both SOA and traffic contributed to the OP (Puthussery et al., 2018).

LDSA measurements inherently include deposition into lungs, which has not been considered in past toxicological studies. New toxicological methods, such as air-liquid interface exposure of cells, can detect the effects of the whole aerosol on cell cultures (Aufderheide and Mohr, 1999; Mülhopt et al., 2016; Ihalainen et al., 2019; Ihantola et al., 2020). In these methods, the aerosol sample is directed to cells and thereafter toxicological endpoints can be measured and correlated to aerosol properties, including surface area. However, this methodology needs to be further evaluated to build a direct link to adverse health effects.

Only a few previous studies report the total LDSA concentrations measured in cities. For example, during a long-term measurement in a street canyon in Helsinki, the total LDSA was found to be 22 $\mu m^2 cm^{-3}$ on average (Kuula et al., 2020). A study in Barcelona reported a mean of 37 $\mu m^2 cm^{-3}$, and determined that particles between 50 and 200 nm contributed the most (Reche et al., 2015). There is a single previous study which reports on LDSA size distributions in various locations in Helsinki, Finland (Kuuluvainen et al., 2016). The highest particle mode at traffic sites was at around 100 nm, corresponding to fresh vehicle emissions (Kittelson, 1998), while a residential suburban area had the highest mode at 200–300 nm.

In this study, we employed a recently developed method to measure LDSA as a function of particle size over a large size range of particles (Lepistö et al., 2020). Measurements were conducted at two contrasting measurement sites: Helsinki, Finland and Delhi-NCR, India. Both measurement sites were in the immediate vicinity of busy roads with similar traffic rates. Our main aim was to characterize the differences in LDSA size distributions between the relatively clean traffic environment (Helsinki) and the very polluted traffic environment (Delhi-NCR).

2. Material and methods

2.1. Measurement locations

This study consisted of two measurement campaigns that were both conducted in roadside environments, the first in Delhi-NCR, India, and the second in Helsinki, Finland. The exact locations of the measurement sites are shown in Fig. 1. In Helsinki, we were able to use an existing long-term measurement site, and in Delhi-NCR we used a mobile laboratory to house the instruments close to the road.

Helsinki is a coastal city in the Southern region of Finland, north of the Baltic sea with a population of 650 000 (Population, 2019). The air quality in Helsinki is relatively good on average (Pohjola et al., 2002; Virtanen et al., 2006; Pirjola et al., 2017). In 2019, the $PM_{2.5}$ concentration did not exceed WHO guidelines (yearly average below 10 $\mu g/m^3$) at any of 11 measurement locations (Korhonen et al., 2020). The Helsinki measurements were conducted at the HSY supersite (60°11′N, 24°57′E), operated by Helsinki Region Environmental Services Authority (HSY). The supersite was on the south-west side of the road, which
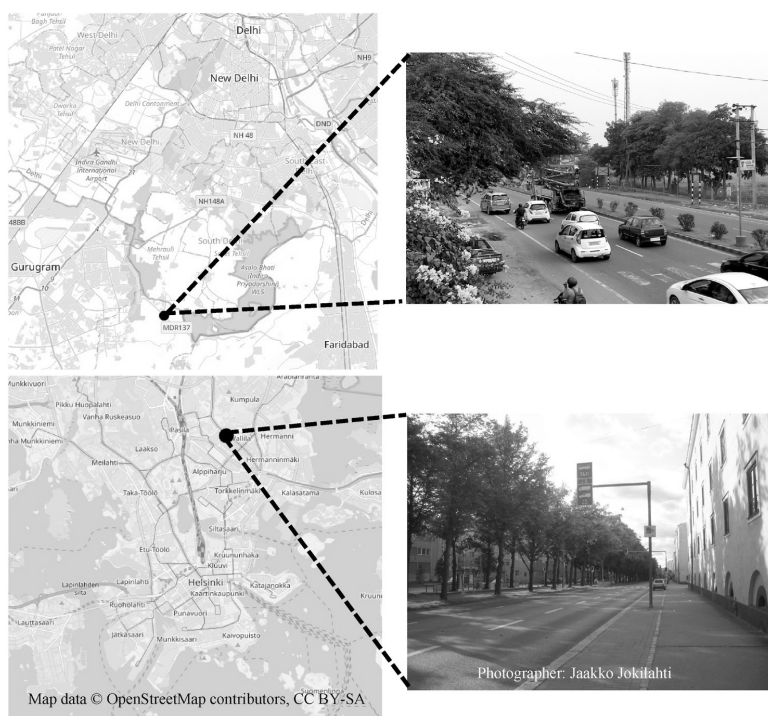
Fig. 1. Measurement locations marked with a black dot in Delhi-NCR (top) and Helsinki (bottom).

has three lanes going both ways, separated by trees, and a tram-railway in between. The surroundings are described in more detail in Kuulu-vainen et al. (2018). Our study was conducted during a rather warm period (temperatures between 10 and 20 °C) in the beginning of September 2019. During that time, the most significant local particle source was traffic of the closest road, with 1167 vehicles/hour, 10% of which were heavy-duty (information from City of Helsinki).

The measurement site in India was in Gwal Pahari, on the south border of Delhi-NCR (28°43′N, 77°15′E), along a busy road with two lanes in both directions. The measurements were conducted during November and December of 2018. The ambient temperature varied between 8 °C to 20 °C during the period. The area is located approximately 20 km southward from the center of Delhi, which is one of the largest cities in the world, with an estimated population of 29 million in 2018 (Delhi and India Population, 2019). It is in the Indo-Gangetic Plain in northern India. Many studies report on the air quality and meteorology in the area (Nair et al., 2007; Hyvärinen et al., 2010; Tiwari et al., 2013; Joshi et al., 2016). $PM_{2.5}$ pollution is usually high (Raatikainen et al., 2014), especially during the winter (for example, the average $PM_{2.5}$ measured in 2011 was over 300 µg/m^3 for December) (Tiwari et al., 2013). Deaths due to poor air quality in India have been increasing between 1998 and 2015, especially in North India (Jia et al., 2020). The diurnal variation during winter is affected by the planetary boundary layer, which heightens during the day, leading to the dilution of polluting components (Nair et al., 2007; Hyvärinen et al., 2010; Tiwari et al., 2013). To the north-east of the measurement site there was a golf course and a green area, and in the south-west direction a road connecting Gurugram and Faridabad. Across the road was a busy street. The average traffic rate was 843 vehicles/hour and 7.5% of those were heavy-duty. The traffic count was done in March 2019 (spring after the measurement campaign) by hand and was limited to daytime traffic.

In Helsinki, the campaign instruments were housed next to a permanent measurement site, inside a shipping container. The sampled air came from inlets through the container roof, at a height of about 2.5 m. In Delhi NCR, instruments were housed in a mobile measurement laboratory. Again, the inlet was through the roof of the van, at a height of approximately 2.5 m. Due to the highly polluted air in Delhi NCR, we used a $PM_{2.5}$ impactor inlet to remove coarse particles and avoid clogging instruments. In all the presented results, the size distribution data has been limited to 2.5 µm from both measurement sites.

2.2. Instrumentation

Measurements in both locations used the same instrumentation: an ELPI+ (Electrical Low Pressure Impactor (Keskinen et al., 1992; Marjamäki et al., 2000; Järvinen et al., 2014), Dekati) to measure particle size distributions, a Quadrupole-ACSM or ToF-ACSM (Time-of-Flight Aerosol Chemical Speciation Monitor (Fröhlich et al., 2013), Aerodyne Research Inc.) to measure particle chemistry and an aethalometer (Magee Scientific, type AE31) for particle light absorption and black carbon. Both sites also had instrumentation for measuring basic meteorological data (data presented in Fig. S1 and Fig. S2). For Helsinki we have also included data from a nearby weather station (Pasila, measurement from a rooftop at 53 m above ground), as wind direction and speed below building height are influenced by the canyon geometry and passing traffic. Detailed information on each instrument is included in the Supplementary material.

2.3. Calculating LDSA

LDSA is the particle surface area multiplied by a size-dependent deposition function describing the efficiency of deposition into the

alveolar region. Most often the deposition function used is based on data from an ICRP (International Commission on Radiological Protection) model (Human respiratory tract m, 1994) which has been formulated into an empirical equation by Hinds (1999). The current from particles in the size range 30 nm–300 nm charged by a diffusion charger have a roughly linear relationship with LDSA, and this relationship is used in some sensor-type aerosol measurement devices (Fierz et al., 2014). Because the ELPI+ separates particles into bins based on their aerodynamic size, it can be used to transform the current of diffusion-charged particles into LDSA for a much larger particle size range. Instead of using just one coefficient, a coefficient can be applied to each impactor stage separately. The coefficients used in this paper use the method reported by Lepistö et al. (2020). The stage-specific values for three different effective densities of particles are presented in Table 1. Unit density is used in this article, excluding one section where the dependency of LDSA distributions on effective density is examined.

For data analysis of Delhi-NCR measurements we chose the most reliable ELPI+ data from our measurements, the first 48 h after cleaning the instrument. Because the ELPI+ collects particles, the accumulation of particles can change the response functions. This can be seen in Fig. S3, which shows the full measurement data from Delhi-NCR. We used greased aluminum foils for particle collection and, to extend the measurement period between instrument maintenance, the sample was diluted with clean air using one-to-one dilution ratio. In future long-term measurements in polluted areas, sintered collection plates could make maintenance-free measurement periods longer.

3. Results and discussion

3.1. LDSA concentrations

Fig. 2 shows the time resolved particle LDSA size distributions from the measurement locations in Delhi-NCR and Helsinki. The variation in LDSA concentrations was significant in both locations; however, it should be noted that, overall, the average LDSA concentrations were more than ten times higher in Delhi-NCR ($329 \pm 127 \ \mu m^2/cm^3$) than in Helsinki ($27 \pm 15 \ \mu m^2/cm^3$) and much larger than LDSA concentrations observed in previous ambient studies (Cheristanidis et al., 2020).

Although the LDSA concentrations in Helsinki were relatively low, an increase in LDSA concentration and mean LDSA size (Fig. 2 and Fig. 3) was observed between September 9th to 11th. During this period, PM mass and sulfate concentrations (Fig. S4, Fig. S5, Fig. S6) were also higher than usual. This coincided with an LRT pollution episode in Helsinki, confirmed by $PM_{2.5}$ increases also observed in background stations. Based on air mass trajectories, the pollution during the LRT period originated from central Europe and Russia (Fig. S7). Several LRT episodes are observed in Helsinki every year and their contribution to particulate mass concentrations of ambient air can be substantial (Niemi et al., 2009). Compared to this study, earlier studies (Timonen et al., 2008; Teinilä et al., 2019) have reported relatively similar changes in PM mass, composition and size distribution during LRT episodes. In this study, the LRT episode affected the data interpretation and presentation so that we divided the measurement period in Helsinki to two parts, one describing the situation dominated by local sources (later referred to as Helsinki Local) and the other describing the situation when the air quality was significantly affected by LRT aerosol (later referred to as Helsinki LRT).

The mean, minimum, maximum, and standard deviation of hourly averaged values for $PM_{2.5}$, LDSA, and mass concentration measured in Delhi-NCR and Helsinki are presented in Table 2, together with black carbon (BC) concentrations. The total BC time series are presented in Fig. S8. For the measurements in Helsinki, values are presented separately for Helsinki Local and Helsinki LRT. Although both measurements were made in roadside environments with relatively similar traffic rates on the adjacent roads (1167 vehicles/hour in Helsinki and 843 vehicles/hour in Delhi-NCR), extremely large differences were seen in LDSA concentrations. While the mean LDSA concentration in Helsinki was 27 $\mu m^2/cm^3$ and 40 $\mu m^2/cm^3$ during Helsinki Local and Helsinki LRT, respectively, the mean LDSA concentration in Delhi-NCR was 329 $\mu m^2/cm^3$. Regarding the variation of the LDSA concentrations, even the minimum hourly averaged LDSA concentration in Delhi-NCR (114 $\mu m^2/cm^3$) was larger than the mean LDSA concentrations in Helsinki. These differences were linked to concentrations of $PM_{2.5}$ and BC, which were also significantly higher in Delhi-NCR.

In addition to total LDSA concentrations, Table 2 shows the mean LDSA concentrations separately for particle size ranges of 10–30 nm, 30–150 nm and 150 nm - 2.5 μm. In this paper we will also use the terms nucleation, soot and accumulation mode for these three size ranges, as those modes can be seen in the size distributions (Fig. 3). Based on the numbers in Table 2, there were large differences in how different particle size ranges contributed to total LDSA. In Delhi-NCR, 78% of the total LDSA concentrations was from the largest size range (150 nm - 2.5 μm), whereas in Helsinki LRT data the contributions of size ranges 30–150 nm and 150 nm - 2.5 μm were more equal (38% and 50% of the total LDSA concentration, respectively). Furthermore, in Helsinki Local the dominating size range was 30–150 nm with 59% contribution to the total LDSA of ambient particles. Importantly, the variation of contributions of different particle size ranges led to differences in the LDSA to $PM_{2.5}$ ratio, which varied from 1.2 $\mu m^2 m^3/cm^3 \mu g$ in Delhi-NCR to 2.1 in Helsinki LRT and 4.5 in Helsinki Local.

The diurnal variation of the LDSA was different in the studied locations (Fig. S9); while in Helsinki no clear trend was observable, in Delhi-NCR the lowest LDSA concentrations were repeatedly observed between 11 a.m. and 5 p.m. The same day-night variation has been observed in previous studies on particle mass concentrations during wintertime in Delhi-NCR and is likely a result of the aerosol diluting due to the planetary boundary layer heightening (Raatikainen et al., 2014; Hooda et al., 2016; Wang et al., 2020).

3.2. Comparison of particle number, mass and LDSA size distributions

Fig. 3 shows the average particle size distributions for particle number (left), lung-deposited surface area (middle) and particle mass (right) for Delhi-NCR, Helsinki Local and Helsinki LRT. In the Helsinki data, the LRT episode is separated as it clearly represents a different PM source, and the size distributions for the LRT episode are different from the local distribution for each metric, and especially for LDSA.

The observed particle number concentrations and size distributions for Helsinki and Delhi-NCR were relatively similar, with a maximum concentration in nucleation mode particles, and a smaller peak in soot mode particles. However, larger differences were observed for LDSA and mass size distributions. For Helsinki (local) the LDSA maximum was in the soot mode (median particle size 80 nm) and in Delhi-NCR in the accumulation mode (median particle size 410 nm). The maximum in PM
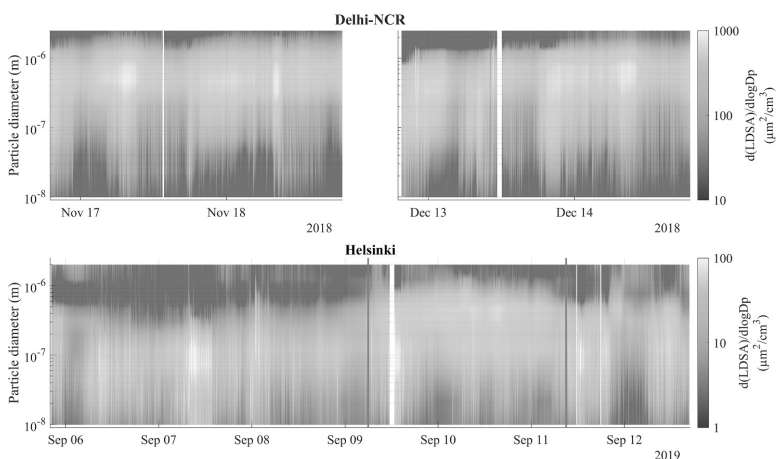
Table 1
Stage-specific coefficients used to calculate LDSA from current in the ELPI+ instrument.

		Stage												
		1	2	3	4	5	6	7	8	9	10	11	12	13	14
ρ (g/cm^3)	0.7	0.030	0.049	0.051	0.042	0.032	0.032	0.049	0.091	0.174	0.268	0.317	0.308	0.283	0.226
	1.0	0.020	0.042	0.052	0.048	0.037	0.031	0.041	0.077	0.150	0.245	0.290	0.282	0.240	0.192
	1.5	0.011	0.032	0.048	0.052	0.044	0.033	0.035	0.062	0.125	0.218	0.262	0.255	0.214	0.159

Fig. 2. LDSA size distributions for the measured time periods in Delhi-NCR and Helsinki, averaged minutely. Note the order of magnitude difference in the scales of the color bars. The Delhi-NCR time series here is relatively short but it is representative of the observed overall concentrations in Delhi-NCR during wintertime. Due to the gradual instrument overloading in the Delhi-NCR measurements, a full hourly averaged time series for LDSA is shown only in Fig. S3. The vertical red lines in the lower panel show the duration of the LRT episode.
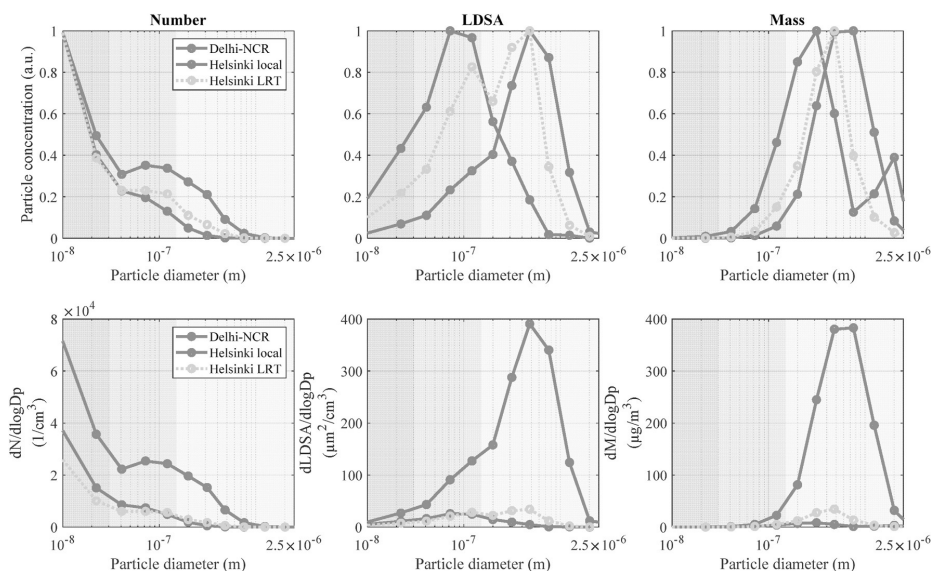
Fig. 3. Average particle size distributions for number, LDSA and mass concentrations. In the upper panel, the size distributions are normalized by dividing by the maximum value, and in the lower panel the absolute concentrations are shown. Each column represents a different moment of the distribution (number, LDSA and mass). The x-axis has been divided into three particle size bins, representing the nucleation, soot, and accumulation mode particles. For tracheobronchial and head airway deposition-weighted surface areas see Fig. S10.

Table 2
Mean, minimum, maximum, and standard deviation of hourly averaged values for PM2.5, LDSA, and BC measured in Delhi-NCR and Helsinki.

	Delhi-NCR				Helsinki Local				Helsinki LRT			
	Mean	Min	Max	Std	Mean	Min	Max	Std	Mean	Min	Max	Std
$PM_{2.5}$ (μg/m³)	268	81	607	114	6	1	18	3	19	7	30	6
LDSA (μm²/cm³)	329	114	737	137	27	9	82	15	40	17	146	20
LDSA 150 nm - 2.5 μm (μm²/cm³)	257	85	581	108	6	0	21	4	20	8	33	6
LDSA 30 nm–150 nm (μm²/cm³)	60	13	178	40	16	3	65	11	15	7	92	13
LDSA 10 nm–30 nm (μm²/cm³)	12	1	34	8	5	1	18	4	4	1	21	4
LDSA/PM2.5 (μm²m³/cm³μg)	1.2				4.5				2.1			
BC (μg/m³)	15.1	2.6	42.6	9.0	1.1	0.0	16.7	1.7	1.4	0.0	8.1	1.2

mass size distributions were in the accumulation mode both cases; however, the median particle size for Delhi-NCR was slightly larger (580 nm in Delhi-NCR compared to 280 nm in Helsinki). During the LRT episode, the LDSA size distribution in Helsinki became bimodal: in addition to the soot mode particles, an accumulation mode clearly appeared in the LDSA size distribution. This larger mode during the LRT episode was in a similar size range to the accumulation particle mode of the LDSA size distribution observed in Delhi-NCR. The particle size distributions for number, LDSA and mass in Helsinki are relatively similar to size distributions previously measured in Helsinki traffic environments (Kuuluvainen et al., 2016; Enroth et al., 2016). Indications of a bimodal LDSA size distribution during the LRT period have been seen in a previous study (Pirjola et al., 2017), but here the shape is very clear.

The side-by-side comparison of the different particle size distributions in Fig. 3 highlights the dependency of measurement results on the chosen metric. The number distribution emphasizes the small particles, and the mass distribution emphasizes the large particles. The LDSA distribution falls somewhere in between and shows the largest difference between the two measurement sites.

In the Delhi-NCR results, the LDSA concentration in the soot mode, representing local and fresh emissions of traffic (see e.g. (Rönkkö and Timonen, 2019)), was small in comparison to accumulation mode particle concentrations, which typically represents more aged particles, grown by condensation and coagulation, or originating from biomass combustion. In contrast, the accumulation mode particle concentration for LDSA was very small in Helsinki when the particles were from local sources; however, during the LRT event the soot mode and accumulation mode particle concentrations were approximately equal. Somewhat surprisingly, Delhi-NCR only had approximately twice the number concentration of sub 30 nm particles compared to Helsinki, partially due to the prevalence of condensation sinks in ambient air (i.e. vapors condense onto previous particles, rather than going through nucleation) and the similar amount of vehicles, which are a major source of nano-sized particles (Rönkkö et al., 2017). These smallest particles from nearby sources were therefore not the key factor for differences in the pollution levels of the studied environments during our measurement period.

Fig. 4 shows the LDSA versus mass concentration for particles in the above-mentioned three particle size groups (10–30 nm, 30–150 nm, and 150 nm - 2.5 µm), along with best-fit lines. In Delhi-NCR, the total LDSA and mass concentrations of particles are highly correlated ($R^2 = 0.81$) with close to a 1-to-1 ratio; thus, using either metric would yield the same result, i.e., a doubling of particle mass also doubles the LDSA concentration. In Helsinki local, there was almost no correlation between the $PM_{2.5}$ and total LDSA concentration—an increase in particle mass concentration can have almost no effect on total LDSA or vice versa.

As seen in Fig. 4, the slopes of correlation plots differ significantly between the measurement sites and between the chosen particle size ranges. In general, in Helsinki the increase of $PM_{2.5}$ causes a much larger relative increase of total LDSA than in Delhi-NCR; the slopes of the correlation plots between the total LDSA and $PM_{2.5}$ were 1.2 in Delhi-NCR, 2.0 in Helsinki LRT, and 3.4 in Helsinki Local. These values clearly demonstrate the differences between the studied environments, and they can explain why the ambient $PM_{2.5}$ has been observed to be more dangerous for human health in Helsinki than in Delhi (Ritchie, 2019). Furthermore, this result demonstrates that the monitoring of ambient particle LDSA and especially the particle LDSA size distributions could significantly improve the explanatory power of air quality monitoring regarding the harmful effects of particulate pollution on human health. For instance, the effect of LRT events on health in Helsinki may therefore be *less* severe than one might expect by simply observing an increase in particle mass concentration.

In addition to concentrations and lung-deposition efficiencies of the particles, the health impacts of the particles likely depend on the physical and chemical characteristics of the particles. These characteristics can vary significantly as a function of particle size and depend on the prevailing particle sources, and they likely affect the toxicity and e.g. the above-mentioned oxidative potential of the particles. Fig. 5 summarizes how the results of this study relate to particle composition and sources in an urban traffic environment. In the Figure, the LDSA and mass size distribution modes measured in our study are represented by the horizontal bars at the bottom part of the figure, showing that the soot mode size range dominate the LDSA in Helsinki but the accumulation mode size range dominates the LDSA in Delhi-NCR and, in addition, that
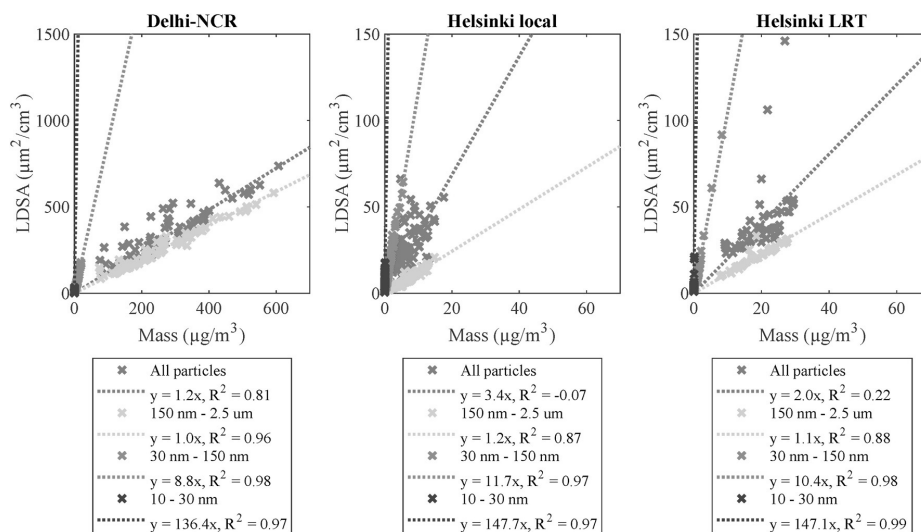

Fig. 4. Correlation plots of LDSA vs mass concentration for different particle size bins. The different colors represent the different size groups, and a best fit line has been calculated for each group, equations listed in the legend. Note the different axes used in the subfigures. (For interpretation of the references to color in this figure legend, the reader is referred to the Web version of this article.)
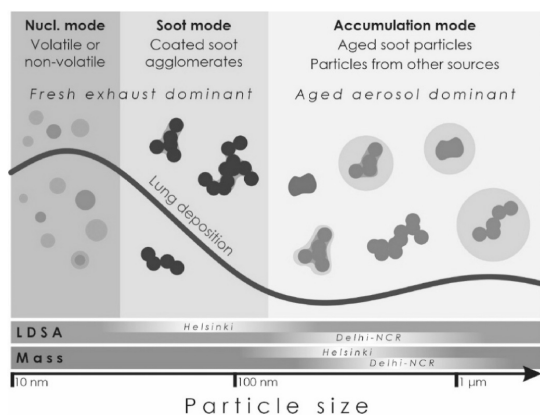
Fig. 5. Schematic of traffic environment particle types in different sizes and their lung-deposition probability. The blue lung-deposition curve shows that small particles have the highest lung deposition probability, but deposition probability increases again around 1 μm. The largest surface area of lung-depositing particles in Helsinki (Local) belongs to the medium particle size range (30–150 nm), while in Delhi NCR the largest LDSA of particles belongs to the largest particle size range (150 nm–2.5 μm), these are shown by the lighter color intensity in the LDSA strip towards the bottom. (For interpretation of the references to color in this figure legend, the reader is referred to the Web version of this article.)

the accumulation mode size range dominates the particulate mass concentrations both in Helsinki and in Delhi-NCR. These size ranges, i.e., the nucleation mode size range, soot mode size range and the accumulation mode size range, are shown in the figure as separate parts, overlaid with the bi-modal alveolar lung-deposition curve. The Figure also shows the different particle types dominating each size range. The first size range (<30 nm) is dominated by nucleation mode particles from precursor gases or tiny solid particles emitted directly from engines (Rönkkö et al., 2017). The second size range is affected mainly by freshly emitted soot agglomerates from combustion. This soot can be coated with harmful substances, such as oxidative species or polycyclic hydrocarbons (PAHs) (Biswas et al., 2009; Surawski et al., 2011). The largest particles, referred to here as the accumulation mode particles, consist typically of more aged particles, which can originate from distant sources, and e.g. biomass burning can contribute their concentrations (Tissari, 2008; Obaidullah et al., 2012). Some road dust can also be found in this size range (Zhao et al., 2017; Wang et al., 2005). Due to their different physical and chemical characteristic, particles in different size ranges can have different effects on human health, which should also be taken into account in air pollution monitoring and pollution mitigation actions.

3.3. Sources of uncertainty in the LDSA results

In this study, we assumed particles to be spherical with unit density, and to not grow due to hygroscopicity when entering the lungs. These assumptions were required to conduct the analyses above, but they led to some uncertainties in the results, as discussed below.

Many studies report on the effective densities of urban ambient particles, for example, a study at a Helsinki traffic site gives soot mode particles an effective density of 1.5 g/cm^3 in the summertime (Virtanen et al., 2006). Another study conducted at a street canyon in Copenhagen (Rissler et al., 2014) found 75 nm particles grouped into two categories of effective density: approximately 1 g/cm^3 and 1.5 g/cm^3, with the higher density particles identified as LRT aerosol, and the lower density as locally emitted soot. In the same study, particles sized 350 nm

contained some very low-density soot agglomerates (0.3 g/cm^3) but were mostly LRT aerosol with a density close to 1.5 g/cm^3. Considering these previous studies, perhaps a density between 1.0 and 1.5 g/cm^3 is closer to the true mean densities of the ambient aerosols studied here. To examine the effects of density on the LDSA distribution, we calculated two additional distributions for the Delhi-NCR, Helsinki Local and Helsinki LRT data sets (Fig. S11). Assuming a higher density decreased the LDSA of accumulation mode particles, while increasing the LDSA of soot mode particles. Overall, increasing the effective density from 1.0 to 1.5 g/cm^3 did not significantly affect the total LDSA, but the relative importance of local emissions increased.

Highly fractal particles have a larger surface area than corresponding spherical particles, but they are also charged more efficiently by the diffusion charger in the ELPI+ (Ouf and Sillon, 2009)—in that sense the surface area is expected to be somewhat accurately represented. From a deposition perspective, a fractal particle is less likely to deposit by impaction, but more likely to deposit by diffusion than its counterpart sphere of equal mobility. In a previous study, the relative standard error for soot particle deposition was 1.2–3.8% when taking into account uncertainties in both shape and effective density (Vu et al., 2018).

Hygroscopicity determines how much a particle grows due to water uptake in a humid environment. Lungs have high humidity, and thus the hygroscopicity of particles is important in determining their lung-deposition fraction. Vehicle exhaust particles are mostly hydrophobic (Henning et al., 2012), but accumulation mode particles can be hygroscopic (Swietlicki et al., 2008). In our study, the effect of including hygroscopicity into calculations would likely be to increase the fraction of depositing accumulation mode particles in both Helsinki (LRT period) and Delhi-NCR, assuming that the soot mode particles are hydrophobic.

Finally, as was noted in the introduction, particle surface area has been shown to be a health-relevant metric for insoluble particles, but studies with soluble particles have not yet been conducted. Typically, in the ambient atmosphere approximately 30–60% of submicron particulate matter consist of organic compounds, 30–40% of inorganic ions and 5–20% of black carbon, depending on the particle sources and aging stage of particles (e.g. (Jimenez et al., 2009; Gani et al., 2019; Barreira et al., 2020)). Black carbon is water insoluble, approximately 50% of organic mass is water-soluble (e.g. (Timonen et al., 2010)) and inorganic ions are mostly water-soluble. Thus, the ambient aerosol contains both insoluble and soluble compounds forming as a complex internally and externally mixed aerosol. Due to that, results for ambient aerosol cannot be directly compared to laboratory studies made with purely water insoluble particles, when evaluating the potential health effects of the studied aerosols.

4. Conclusions

In this study, we conducted experiments in a relatively clean traffic environment and in a highly polluted traffic environment, i.e., in Helsinki and in Delhi-NCR. We focused the experiments on the lung-depositing surface area (LDSA) of ambient particles, aiming to understand the differences in LDSA concentrations and size distributions between the measurement sites. We observed vast differences in LDSA, both in the LDSA concentrations and in particles' LDSA size distributions. The LDSA of particles in Helsinki was mostly in the size range of the freshly emitted soot particles, but during the LRT event a second mode appeared in the larger particles. In Delhi-NCR, only a small fraction of the LDSA came from freshly emitted particles, but for most of the measurement period the larger, aged particles contributed an overwhelming majority of the LDSA, despite the lower lung deposition probability of larger particles (Fig. 5). Additionally, The LDSA to mass ratio of particles was significantly smaller in Delhi-NCR than in Helsinki, which may be one reason for the previously observed location-based differences in toxicity of ambient particulate matter (Li et al., 2019; Ritchie, 2019).

Our study indicates that if health effects of particulate pollution were

estimated based on PM mass only, they would be significantly different than if information on particle number and LDSA size distributions are considered, and further, the largest differences in this study were observed specifically in the LDSA distributions.

Here, we presented the first measured evidence that the size of lung-deposited particles differs on average by a factor of five between clean and polluted traffic environments. This implies that particle sources and expected health implications are different as well. Further toxicological and epidemiological studies along with long-term LDSA measurement data in several locations across the globe are needed to establish the detailed relationship between health and LDSA.

CRediT authorship contribution statement

Laura Salo: Data curation, Formal analysis, Measurements were designed, The measurements were conducted, Data was analyzed, The manuscript was initially written. **Antti Hyvärinen:** Measurements were designed, The measurements were conducted. **Pasi Jalava:** The manuscript was initially written. **Kimmo Teinilä:** The measurements were conducted. **Rakesh K. Hooda:** Measurements were designed, The measurements were conducted. **Arindam Datta:** The measurements were conducted. **Sanna Saarikoski:** Data curation, Formal analysis, Data was analyzed. **Henna Lintusaari:** Measurements were designed, The measurements were conducted. **Teemu Lepistö:** Data curation, Formal analysis, The measurements were conducted, Data was analyzed. **Sampsa Martikainen:** The measurements were conducted. **Antti Rostedt:** The measurements were conducted. **Ved Prakash Sharma:** The measurements were conducted. **Md. Hafizur Rahman:** The measurements were conducted. **Sanjukta Subudhi:** Measurements were designed. **Eija Asmi:** Measurements were designed. **Jarkko V. Niemi:** Measurements were designed. **Heikki Lihavainen:** Measurements were designed. **Banwari Lal:** Measurements were designed. **Jorma Keskinen:** Measurements were designed. **Heino Kuuluvainen:** Measurements were designed, The measurements were conducted, The manuscript was initially written. **Hilkka Timonen:** Measurements were designed, The manuscript was initially written. **Topi Rönkkö:** Measurements were designed, The manuscript was initially written, further discussed, edited and commented on by all authors.

Declaration of competing interest

The authors declare that they have no known competing financial interests or personal relationships that could have appeared to influence the work reported in this paper.

measurements in Gwal Pahari.

Appendix A. Supplementary data

Supplementary data to this article can be found online at https://doi.org/10.1016/j.atmosenv.2021.118421.

References

Aguilera, I., Dratva, J., Caviezel, S., Burdet, L., De Groot, E., Ducret-Stich, R.E., et al., 2016. Particulate matter and subclinical atherosclerosis: associations between different particle sizes and sources with carotid intima-media thickness in the SAPALDIA study. Environ. Health Perspect. 124 (11), 1700–1706.

Aufderheide, M., Mohr, U., 1999 Nov. CULTEX–a new system and technique for the cultivation and exposure of cells at the air/liquid interface. Exp Toxicol Pathol Off J Gesellschaft fur Toxikologische Pathol 51 (6), 489–490.

[Internet] Bakand, S., Hayes, A., 2016 Jun 14. Toxicological considerations, toxicity assessment, and risk management of inhaled nanoparticles [cited 2020 Apr 21] Int. J. Mol. Sci. 17 (6), 929. Available from: http://www.mdpi.com/1422-0067/17/6/929.

[Internet] Balakrishnan, K., Dey, S., Gupta, T., Dhaliwal, R.S., Brauer, M., Cohen, A.J., et al., 2019 Jan 1. The impact of air pollution on deaths, disease burden, and life expectancy across the states of India: the Global Burden of Disease Study 2017 [cited 2020 May 29] Lancet Planet Health 3 (1), e26–39. Available from: http://www.ncbi.nlm.nih.gov/pubmed/30528905.

Barreira, L.M.F., Helin, A., Aurela, M., Teinilä, K., Friman, M., Kangas, L., et al., 2020. In-depth characterization of submicron particulate matter inter-annual variations at a street canyon site in Northern Europe [Internet] Atmos. Chem. Phys. Discuss. 2020, 1–34. Available from: https://acp.copernicus.org/preprints/acp-2020-908/.

Biswas, S., Verma, V., Schauer, J.J., Cassee, F.R., Cho, A.K., Sioutas, C., 2009 May 15. Oxidative potential of semi-volatile and non volatile particulate matter (PM) from heavy-duty vehicles retrofitted with emission control technologies [Internet] Environ. Sci. Technol. 43 (10), 3905–3912. https://doi.org/10.1021/es9000592. Available from:

Cheristanidis, S., Grivas, G., Chaloulakou, A., 2020 Sep. Determination of total and lung-deposited particle surface area concentrations, in central Athens, Greece. Environ. Monit. Assess. 192 (10), 627.

Cohen, A.J., Brauer, M., Burnett, R., Anderson, H.R., Frostad, J., Estep, K., et al., 2017. Estimates and 25-year trends of the global burden of disease attributable to ambient air pollution: an analysis of data from the Global Burden of Diseases Study 2015 [Internet] Lancet 389 (10082), 1907–1918. https://doi.org/10.1016/S0140-6736(17)30505-6. Available from:

Daellenbach, K.R., Uzu, G., Jiang, J., Cassagnes, L.-E., Leni, Z., Vlachou, A., et al., 2020. Sources of particulate-matter air pollution and its oxidative potential in Europe [Internet] Nature 587 (7834), 414–419. https://doi.org/10.1038/s41586-020-2902-8. Available from:

de Jesus, A.L., Rahman, M.M., Mazaheri, M., Thompson, H., Knibbs, L.D., Jeong, C., et al., 2019. Ultrafine particles and PM2.5 in the air of cities around the world: are they representative of each other? [Internet] Environ. Int. 129, 118–135. Available from: http://www.sciencedirect.com/science/article/pii/S0160412019311110.

Delhi, India Population, 2019. Population Stat [Internet]. Available from: https://populationstat.com/india/delhi.

[Internet] Enroth, J., Saarikoski, S., Niemi, J., Kousa, A., Ježek, I., Močnik, G., et al., 2016 May 3. Chemical and physical characterization of traffic particles in four different highway environments in the Helsinki metropolitan area [cited 2020 Apr 21] Atmos. Chem. Phys. 16 (9), 5497–5512. Available from: https://www.atmos-chem-phys.net/16/5497/2016/.

Fierz, M., Meier, D., Steigmeier, P., Burtscher, H., 2014. Aerosol measurement by induced currents [Internet] Aerosol. Sci. Technol. 48 (4), 350–357. https://doi.org/10.1080/02786826.2013.875981. Available from:

Fröhlich, R., Cubison, M.J., Slowik, J.G., Bukowiecki, N., Prévôt, A.S.H., Baltensperger, U., et al., 2013. The ToF-ACSM: a portable aerosol chemical speciation monitor with TOFMS detection. Atmos. Meas. Technol. 6 (11), 3225–3241.

[Internet] Gani, S., Bhandari, S., Seraj, S., Wang, D.S., Patel, K., Soni, P., et al., 2019 May 22. Submicron aerosol composition in the world's most polluted megacity: the Delhi Aerosol Supersite study [cited 2020 Apr 21] Atmos. Chem. Phys. 19 (10), 6843–6859. Available from: https://www.atmos-chem-phys.net/19/6843/2019/.

Gaschen, A., Lang, D., Kalberer, M., Savi, M., Geiser, T., Gazdhar, A., et al., 2010 Feb 15. Cellular responses after exposure of lung cell cultures to secondary organic aerosol particles [Internet] Environ. Sci. Technol. 44 (4), 1424–1430. https://doi.org/10.1021/es902261m. Available from:

Habre, R., Zhou, H., Eckel, S.P., Enebish, T., Fruin, S., Bastain, T., et al., 2018. Short-term effects of airport-associated ultrafine particle exposure on lung function and inflammation in adults with asthma. Environ. Int. 118, 48–59. https://doi.org/10.1016/j.envint.2018.05.031.

Hennig, F., Quass, U., Hellack, B., Küpper, M., Kuhlbusch, T.A.J., Stafoggia, M., et al., 2018 Feb 15. Ultrafine and fine particle number and surface area concentrations and daily cause-specific mortality in the ruhr area, Germany, 2009–2014 [Internet] Environ Health Perspect. 126 (2), 27008. https://doi.org/10.1289/EHP2054. Available from:

Henning, S., Ziese, M., Kiselev, A., Saathoff, H., Möhler, O., Mentel, T.F., et al., 2012. Hygroscopic growth and droplet activation of soot particles: uncoated, succinic or

sulfuric acid coated [Internet] Atmos. Chem. Phys. 12 (10), 4525–4537. Available from: https://acp.copernicus.org/articles/12/4525/2012/.

Hinds, W.C., 1999. Aerosol Technology: Properties, Behavior, and Measurement of Airborne Particles, second ed. Wiley-Interscience Publication, New York: Wiley, p. 504.

Hooda, R.K., Hyvärinen, A.-P., Vestenius, M., Gilardoni, S., Sharma, V.P., Vignati, E., et al., 2016. Atmospheric aerosols local–regional discrimination for a semi-urban area in India [Internet] Atmos. Res. 168, 13–23. Available from: http://www.sciencedirect.com/science/article/pii/S0169809515002598.

Human respiratory tract model for radiological protection. A report of a task group of the international commission on radiological protection. Ann. ICRP 24 (1–3), 1994, 1–482.

Hyvärinen, A.P., Lihavainen, H., Komppula, M., Panwar, T.S., Sharma, V.P., Hooda, R.K., et al., 2010. Aerosol measurements at the Gual Pahari EUCAARI station: preliminary results from in-situ measurements. Atmos. Chem. Phys. 10 (15), 7241–7252.

Ihalainen, M., Jalava, P., Ihantola, T., Kasurinen, S., Uski, O., Sippula, O., et al., 2019 Feb 1. Design and validation of an air-liquid interface (ALI) exposure device based on thermophoresis [Internet] Aerosol. Sci. Technol. 53 (2), 133–145. https://doi.org/10.1080/02786826.2018.1556775. Available from:

Ihantola, T., Di Bucchianico, S., Happo, M., Ihalainen, M., Uski, O., Bauer, S., et al., 2020. Influence of wood species on toxicity of log-wood stove combustion aerosols: a parallel animal and air-liquid interface cell exposure study on spruce and pine smoke [Internet] Part. Fibre Toxicol. 17 (1), 27. https://doi.org/10.1186/s12989-020-00355-1. Available from:

Jalava, P.I., Salonen, R.O., Hälinen, A.I., Penttinen, P., Pennanen, A.S., Sillanpää, M., et al., 2006. In vitro inflammatory and cytotoxic effects of size-segregated particulate samples collected during long-range transport of wildfire smoke to Helsinki [Internet] Toxicol. Appl. Pharmacol. 215 (3), 341–353. Available from: http://www.sciencedirect.com/science/article/pii/S0041008X06001062.

[Internet] Järvinen, A., Aitomaa, M., Rostedt, A., Keskinen, J., Yli-Ojanperä, J., 2014 Mar 1. Calibration of the new electrical low pressure impactor (ELPI+) [cited 2018 Jan 10] J. Aerosol Sci. 69, 150–159. https://doi.org/10.1016/j.jaerosci.2013.12.006. Available from:

Jia, B., Gao, M., Zhang, S., Lam Yung, K.K., 2020. Rapid increase in mortality attributable to PM2.5 exposure in India over 1998-2015 [Internet] Chemosphere 128715. Available from: http://www.sciencedirect.com/science/article/pii/S004565352003 29131.

Jimenez, J.L., Canagaratna, M.R., Donahue, N.M., Prevot, A.S.H., Zhang, Q., Kroll, J.H., et al., 2009 Dec. Evolution of organic aerosols in the atmosphere. Science 326 (5959), 1525–1529.

Joshi, H., Naja, M., Singh, K.P., Kumar, R., Bhardwaj, P., Babu, S.S., et al., 2016. Investigations of aerosol black carbon from a semi-urban site in the Indo-Gangetic Plain region [Internet] Atmos. Environ. 125, 346–359. https://doi.org/10.1016/j.atmosenv.2015.04.007. Available from:

Keller, J., Wohlleben, W., Ma-Hock, L., Strauss, V., Gröters, S., Küttler, K., et al., 2014. Time course of lung retention and toxicity of inhaled particles: short-term exposure to nano-Ceria [Internet] Arch. Toxicol. 88 (11), 2033–2059. https://doi.org/10.1007/s00204-014-1349-9. Available from:

Keskinen, J., Pietarinen, K., Lehtimäki, M., 1992. Electrical low pressure impactor. J. Aerosol Sci. 23 (4), 353–360.

Kittelson, D.B., 1998. Engines and nanoparticles: a review. J. Aerosol Sci. 29 (5–6), 575–588.

Korhonen, S., Loukkola, K., Portin, H., 2020. Air Quality in the Helsinki Metropolitan Area in 2019. (in Finnish with an abstract in English), Helsinki.

[Internet] Kuula, J., Kuuluvainen, H., Niemi, J.V., Saukko, E., Portin, H., Kousa, A., et al., 2020 Feb 1. Long-term sensor measurements of lung deposited surface area of particulate matter emitted from local vehicular and residential wood combustion sources [cited 2020 Apr 17] Aerosol. Sci. Technol. 54 (2), 190–202. Available from: https://www.tandfonline.com/doi/full/10.1080/02786826.2019.1668909.

Kuuluvainen, H., Rönkkö, T., Järvinen, A., Saari, S., Karjalainen, P., Lähde, T., et al., 2016. Lung deposited surface area size distributions of particulate matter in different urban areas [Internet] Atmos. Environ. 136, 105–113. https://doi.org/10.1016/j.atmosenv.2016.04.019. Available from:

Kuuluvainen, H., Poikkimäki, M., Järvinen, A., Kuula, J., Irjala, M., Dal Maso, M., et al., 2018. Vertical profiles of lung deposited surface area concentration of particulate matter measured with a drone in a street canyon. Environ. Pollut. 241, 96–105.

Lelieveld, J., Evans, J.S., Fnais, M., Giannadaki, D., Pozzer, A., 2015. The contribution of outdoor air pollution sources to premature mortality on a global scale. Nature 525 (7569), 367–371.

Lelieveld, J., Klingmüller, K., Pozzer, A., Pöschl, U., Fnais, M., Daiber, A., et al., 2019. Cardiovascular disease burden from ambient air pollution in Europe reassessed using novel hazard ratio functions. Eur. Heart J. 40 (20), 1590–1596.

Lepistö, T., Kuuluvainen, H., Juuti, P., Järvinen, A., Arffman, A., Rönkkö, T., 2020. Measurement of the human respiratory tract deposited surface area of particles with an electrical low pressure impactor [Internet] Aerosol. Sci. Technol. 1–21. https://doi.org/10.1080/02786826.2020.1745141. Available from:, 0(0).

Li, X., Jin, L., Kan, H., 2019. Air pollution: a global problem needs local fixes. Nature 570 (7762), 437–439.

Lovett, C., Baasiri, M., Atwi, K., Sowlat, M.H., Shirmohammadi, F., Shihadeh, A.L., et al., 2019. Comparison of the oxidative potential of primary (POA) and secondary (SOA) organic aerosols derived from ?-pinene and gasoline engine exhaust precursors [version 2; peer review: 2 approved] [Internet] F1000Research 7 (1031). Available from: http://openr.es/fn2.

Lu, F., Xu, D., Cheng, Y., Dong, S., Guo, C., Jiang, X., et al., 2015. Systematic review and meta-analysis of the adverse health effects of ambient PM2.5 and PM10 pollution in

the Chinese population [Internet] Environ. Res. 136, 196–204. https://doi.org/10.1016/j.envres.2014.06.029. Available from:

Marjamäki, M., Keskinen, J., Chen, D.-R., Pui, D.Y.H., 2000. Performance evaluation of the electrical low-pressure impactor [Internet] J. Aerosol Sci. 31, 249–261. Available from: http://www.sciencedirect.com/science/article/pii/S002185029900052X.

[Internet] Moshammer, H., Neuberger, M., 2003 Apr 1. The active surface of suspended particles as a predictor of lung function and pulmonary symptoms in Austrian school children [cited 2020 Apr 17] Atmos. Environ. 37 (13), 1737–1744. Available from: https://www.sciencedirect.com/science/article/pii/S1352231003000736.

Mostafavi, N., Jeong, A., Vlaanderen, J., Imboden, M., Vineis, P., Jarvis, D., et al., 2019. The mediating effect of immune markers on the association between ambient air pollution and adult-onset asthma. Sci. Rep. 9 (1), 1–11.

Mülhopt, S., Dilger, M., Diabaté, S., Schlager, C., Krebs, T., Zimmermann, R., et al., 2016. Toxicity testing of combustion aerosols at the air–liquid interface with a self-contained and easy-to-use exposure system [Internet] J. Aerosol Sci. 96, 38–55. Available from: http://www.sciencedirect.com/science/article/pii/S0021850 216300647.

Nair, V.S., Moorthy, K.K., Alappattu, D.P., Kunhikrishnan, P.K., George, S., Nair, P.R., et al., 2007. Wintertime aerosol characteristics over the Indo-Gangetic Plain (IGP): impacts of local boundary layer processes and long-range transport. J. Geophys. Res. Atmos. 112 (13), 1–15.

[Internet] Niemi, J.V., Saarikoski, S., Aurela, M., Tervahattu, H., Hillamo, R., Westphal, D.L., et al., 2009 Feb 1. Long-range transport episodes of fine particles in southern Finland during 1999–2007 [cited 2020 Apr 17] Atmos. Environ. 43 (6), 1255–1264. Available from: https://www.sciencedirect.com/science/article/pii/S1 35223100801090X.

Obaidullah, M., Bram, S., Verma, V.K., De Ruyck, J., 2012. A review on particle emissions from small scale biomass combustion [Internet] Energy Resour. 2 (1), 147–159. Available from: http://www.ijrer.net/index.php/ijrer/article/view/147.

Oberdörster, G., 1996. Significance of particle parameters in the evaluation of exposure-dose-response relationships of inhaled particles [Internet] Inhal. Toxicol. 8 (Suppl. L), 73–89. Available from: https://www.scopus.com/inward/record.uri?eid=2-s2. 0-0030308101&partnerID=40&md5=6586fe5aace37ad374f1deaaeeae5573.

Oberdörster, G., Oberdörster, E., Oberdörster, J., 2005. Nanotoxicology: an emerging discipline evolving from studies of ultrafine particles. Environ. Health Perspect. 113 (7), 823–839.

Ouf, F.-X., Sillon, P., 2009 Jun 19. Charging efficiency of the electrical low pressure impactor's corona charger: influence of the fractal morphology of nanoparticle aggregates and uncertainty analysis of experimental results [Internet] Aerosol. Sci. Technol. 43 (7), 685–698. https://doi.org/10.1080/02786820902878245. Available from:

Pañella, P., Casas, M., Donaire-Gonzalez, D., Garcia-Esteban, R., Robinson, O., Valentín, A., et al., 2017. Ultrafine particles and black carbon personal exposures in asthmatic and non-asthmatic children at school age. Indoor Air 27 (5), 891–899.

Park, M., Joo, H.S., Lee, K., Jang, M., Kim, S.D., Kim, I., et al., 2018. Differential toxicities of fine particulate matters from various sources [Internet] Sci. Rep. 8 (1), 17007. https://doi.org/10.1038/s41598-018-35398-0. Available from:

Patel, S., Leavey, A., Sheshadri, A., Kumar, P., Kandikuppa, S., Tarsi, J., et al., 2018. Associations between household air pollution and reduced lung function in women and children in rural southern India. J. Appl. Toxicol. 38 (11), 1405–1415.

Pelucchi, C., Negri, E., Gallus, S., Boffetta, P., Tramacere, I., La Vecchia, C., 2009. Long-term particulate matter exposure and mortality: a review of European epidemiological studies. BMC Publ. Health 9, 1–8.

Pirjola, L., Niemi, J.V., Saarikoski, S., Aurela, M., Enroth, J., Carbone, S., et al., 2017. Physical and chemical characterization of urban winter-time aerosols by mobile measurements in Helsinki, Finland. Atmos. Environ. 158, 60–75.

Pohjola, M.A., Kousa, A., Kukkonen, J., Härkönen, J., Karppinen, A., Aarnio, P., et al., 2002. The spatial and temporal variation of measured urban PM10 and PM2.5 in the helsinki metropolitan area. Urban Air Qual — Recent Adv. 189–201.

[Internet] Population, 2019. Statistics Finland. Available from: https://www.stat.fi/tup/suoluk/suoluk_vaesto_en.html.

[Internet] Puthussery, J.V., Zhang, C., Verma, V., 2018 Oct 19. Development and field testing of an online instrument for measuring the real-time oxidative potential of ambient particulate matter based on dithiothreitol assay [cited 2020 May 29] Atmos. Meas. Technol. 11 (10), 5767–5780. Available from: https://www.atmos-meas-tech.net/11/5767/2018/.

Puthussery, J.V., Singh, A., Rai, P., Bhattu, D., Kumar, V., Vats, P., et al., 2020 May 18. Real-time measurements of PM2.5 oxidative potential using a dithiothreitol assay in Delhi, India [Internet] Environ. Sci. Technol. Lett. 7 (7), 504–510. https://doi.org/10.1021/acs.estlett.0c00342. Available from:

Raatikainen, T., Hyvärinen, A.-P.P., Hatakka, J., Panwar, T.S., Hooda, R.K., Sharma, V. P., et al., 2014. The effect of boundary layer dynamics on aerosol properties at the Indo-Gangetic plains and at the foothills of the Himalayas [Internet] Atmos. Environ. 89, 548–555. https://doi.org/10.1016/j.atmosenv.2014.02.058. Available from:

Reche, C., Viana, M., Brines, M., Perez, N., Beddows, D., Alastuey, A., et al., 2015 Jun. Determinants of aerosol lung-deposited surface area variation in an urban environment. Sci. Total Environ. 517, 38–47.

Rissler, J., Nordin, E.Z., Eriksson, A.C., Nilsson, P.T., Frosch, M., Sporre, M.K., et al., 2014 Jun 3. Effective density and mixing state of aerosol particles in a near-traffic urban environment [Internet] Environ. Sci. Technol. 48 (11), 6300–6308. https://doi.org/10.1021/es5000353. Available from:

Ritchie, H., 2019. Outdoor air pollution [Internet] Our World Data. Available from: https://ourworldindata.org/outdoor-air-pollution.

Rönkkö, T., Timonen, H., 2019. Overview of sources and characteristics of nanoparticles in urban traffic-influenced areas. J. Alzheimers Dis. 72 (1), 15–28.

Rönkkö, T., Kuuluvainen, H., Karjalainen, P., Keskinen, J., Hillamo, R., Niemi, J.V., et al., 2017. Traffic is a major source of atmospheric nanocluster aerosol [Internet] Proc. Natl. Acad. Sci. Unit. States Am. 114 (29), 7549–7554. Available from: http://www.pnas.org/lookup/doi/10.1073/pnas.1700830114.

Saffari, A., Daher, N., Shafer, M.M., Schauer, J.J., Sioutas, C., 2014 Jul 1. Global perspective on the oxidative potential of airborne particulate matter: a synthesis of research findings [Internet] Environ. Sci. Technol. 48 (13), 7576–7583. https://doi.org/10.1021/es500937x. Available from:

Samet, J.M., Dominici, F., Curriero, F.C., Coursac, I., Zeger, S.L., 2000 Dec 14. Fine particulate air pollution and mortality in 20 U.S. Cities, 1987–1994 [Internet] N. Engl. J. Med. 343 (24), 1742–9. Available from: http://www.nejm.org/doi/abs/10.1056/NEJM200012143432401.

Schmid, O., Stoeger, T., 2016. Surface area is the biologically most effective dose metric for acute nanoparticle toxicity in the lung [Internet] J. Aerosol. Sci. 99, 133–143. https://doi.org/10.1016/j.jaerosci.2015.12.006. Available from:

Song, C., He, J., Wu, L., Jin, T., Chen, X., Li, R., et al., 2017. Health burden attributable to ambient PM2.5 in China. Environ. Pollut. 223, 575–586. https://doi.org/10.1016/j.envpol.2017.01.060.

Stoeger, T., Reinhard, C., Takenaka, S., Schroeppel, A., Karg, E., Ritter, B., et al., 2006. Instillation of six different ultrafine carbon particles indicates a surface area threshold dose for acute lung inflammation in mice. Environ. Health Perspect. 114 (3), 328–333.

Surawski, N.C., Miljevic, B., Ayoko, G.A., Roberts, B.A., Elbagir, S., Fairfull-Smith, K.E., et al., 2011 Jul 1. Physicochemical characterization of particulate emissions from a compression ignition engine employing two injection technologies and three fuels [Internet] Environ. Sci. Technol. 45 (13), 5498–5505. https://doi.org/10.1021/es200388f. Available from:

Swietlicki, E., Hansson, H.-C., Hämeri, K., Svenningsson, B., Massling, A., Mcfiggans, G., et al., 2008 Jan 1. Hygroscopic properties of submicrometer atmospheric aerosol particles measured with H-TDMA instruments in various environments—a review [Internet] Tellus B 60 (3), 432–469. https://doi.org/10.1111/j.1600-0889.2008.00350.x. Available from:

Teinilä, K., Aurela, M., Niemi, J.V., Kousa, A., Petäjä, T., Järvi, L., et al., 2019. Concentration variation of gaseous and particulate pollutants in the helsinki city centre — observations from a two-year campaign from 2013–2015. Boreal Environ. Res. 24 (September), 115–136.

[Internet] Timonen, H., Saarikoski, S., Tolonen-Kivimäki, O., Aurela, M., Saarnio, K., Petäjä, T., et al., 2008 Sep 26. Size distributions, sources and source areas of water-soluble organic carbon in urban background air [cited 2020 Apr 17] Atmos. Chem.

Phys. 8 (18), 5635–47. Available from: https://www.atmos-chem-phys.net/8/5635/2008/.

Timonen, H., Aurela, M., Carbone, S., Saarnio, K., Saarikoski, S., Mäkelä, T., et al., 2010. High time-resolution chemical characterization of the water-soluble fraction of ambient aerosols with PILS-TOC-IC and AMS [Internet] Atmos. Meas. Technol. 3 (4), 1063–1074. Available from: https://amt.copernicus.org/articles/3/1063/2010/.

Tissari, J., 2008. Fine Particle Emissions from Residential Wood Combustion.

Tiwari, S., Srivastava, A.K., Bisht, D.S., Parmita, P., Srivastava, M.K., Attri, S.D., 2013. Diurnal and seasonal variations of black carbon and PM2.5 over New Delhi, India: influence of meteorology [Internet] Atmos. Res. 125–126, 50–62. https://doi.org/10.1016/j.atmosres.2013.01.011. Available from:

Tran, P.T.M., Ngoh, J.R., Balasubramanian, R., 2020. Assessment of the integrated personal exposure to particulate emissions in urban micro-environments: a pilot study. Aerosol. Air Qual. Res. 20 (2), 341–357.

Verma, V., Fang, T., Xu, L., Peltier, R.E., Russell, A.G., Ng, N.L., et al., 2015 Apr 7. Organic aerosols associated with the generation of reactive oxygen species (ROS) by water-soluble PM2.5 [Internet] Environ. Sci. Technol. 49 (7), 4646–4656. https://doi.org/10.1021/es505577w. Available from:

Virtanen, A., Rönkkö, T., Kannosto, J., Ristimäki, J., Mäkelä, J.M., Keskinen, J., et al., 2006. Winter and summer time size distributions and densities of traffic-related aerosol particles at a busy highway in Helsinki. Atmos. Chem. Phys. 6 (9), 2411–2421.

Vu, T.V., Zauli-Sajani, S., Poluzzi, V., Harrison, R.M., 2018. Factors controlling the lung dose of road traffic-generated sub-micrometre aerosols from outdoor to indoor environments [Internet] Air Qual. Atmos. Health 11 (6), 615–625. https://doi.org/10.1007/s11869-018-0568-2. Available from:

Wang, C.-F., Chang, C.-Y., Tsai, S.-F., Chiang, H.-L., 2005. Characteristics of road dust from different sampling sites in northern taiwan [Internet] J. Air Waste Manag. Assoc. 55 (8), 1236–1244. https://doi.org/10.1080/10473289.2005.10464717. Available from:

Wang, L., Slowik, J.G., Tripathi, N., Bhattu, D., Rai, P., Kumar, V., et al., 2020. Source characterization of volatile organic compounds measured by PTR-ToF-MS in Delhi, India [Internet] Atmos. Chem. Phys. Discuss. 2020, 1–27. Available from: https://www.atmos-chem-phys-discuss.net/acp-2020-11/.

Zhao, G., Chen, Y., Hopke, P.K., Holsen, T.M., Dhaniyala, S., 2017. Characteristics of traffic-induced fugitive dust from unpaved roads [Internet] Aerosol. Sci. Technol. 51 (11), 1324–1331. https://doi.org/10.1080/02786826.2017.1347251. Available from:

PAPER IV

Inherently Charged Particle (ICP) Sensor Design

Salo, L., Rostedt, A., Kuuluvainen, H., Teinilä, K., Hooda, R.K., Rahman, Md. H., Datta, A., Sharma, V.P., Subudhi, S., Hyvärinen, A., Timonen, H., Asmi, E., Martikainen, S., Karjalainen, P., Lal, B., Keskinen, J., Rönkkö, T.

Inherently Charged Particle (ICP) Sensor Design

Laura Salo[ID], Antti Rostedt, Heino Kuuluvainen, Kimmo Teinilä, Rakesh K. Hooda, Md. Hafizur Rahman,
Arindam Datta, Ved Prakash Sharma, Sanjukta Subudhi, Antti Hyvärinen, Hilkka Timonen, Eija Asmi,
Sampsa Martikainen[ID], Panu Karjalainen, Banwari Lal, Jorma Keskinen, and Topi Rönkkö[ID]

Abstract—Ambient particles from natural and anthropogenic sources are a major cause of premature deaths globally. While there are many instruments suitable for scientific measurements of aerosols, better methods for long-term monitoring purposes are still needed, especially low-maintenance, affordable solutions for ultrafine particles. In this article, we present a new sensor design and prototype, the inherently charged particle (ICP) sensor, which uses the preexisting electrical charge of particles to measure particle concentration, instead of employing a charging mechanism, as is typical for instruments based on electrical detection. When the ICP-sensor is employed in conjunction with another instrument, information on the particle charge state can also be derived.

We present the results of a laboratory characterization as well as two measurements in suggested applications: 1) engine exhaust measurements and 2) ambient measurements in a traffic environment, where we compare the sensor response to three particle concentration metrics: 1) number; 2) surface area; and 3) mass. The sensor proved suitable for both applications, the signal correlated best with number concentration in the engine emission measurements and with particle surface area in the ambient measurements. The measured charge concentrations were well-correlated ($R^2 > 0.8$) with theoretical values calculated from the number size distribution assuming an equilibrium charge distribution.

Index Terms— Air pollution, air quality monitoring, ultrafine particles.
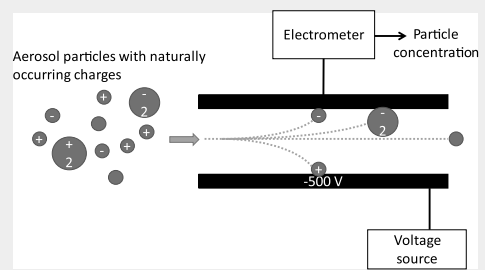
I. INTRODUCTION

PARTICLES in the air are known to contribute to cloud formation and atmospheric radiative forcing [1], [2] and they have adverse effects on human health [3]. High particle pollution levels are a problem, especially in large cities, as cities bring together particle sources (traffic and heating)

and large numbers of people. The risk of major wildfires is also growing with the increased temperature due to changes in land use and global warming [4]. The World Health Organization (WHO) has set targets for particle concentration levels and air quality monitoring is key in making sure that those targets are met. In addition to well-equipped monitoring stations with a variety of gaseous and particle measurement instruments, sensor-type monitoring is needed for a denser measurement network. Long-term monitoring with sensor networks can expose particle sources and show particle dispersion patterns. In addition, sensor data are used to inform air quality modeling, e.g., The Finnish Meteorological Institute's ENvironmental information FUsion SERvice (FMI-ENFUSER), which is used to show real time and predicted urban air quality (https://en.ilmatieteenlaitos.fi/environmental-information-fusion-service).

Different types of particle sensors give different information. For example, the most common and inexpensive solutions rely on optical detection of particles sized ~0.3 μm and larger–smaller particles cannot be detected because their size is close to the wavelength of light [5]. Optical measurement gives a signal that correlates with the mass concentration of particles. Some optical sensors target specific compounds such as black carbon (BC); these sensors operate by collecting particles on a filter and measuring the attenuation of light through the filter [6]. Electrical measurement of diffusion-charged (DC) particles can detect much smaller particles, down to approximately 10 nm, and the signal of DC particles

is closely correlated with the lung-deposited surface area (LDSA) [7], [8]. To get a full picture of an aerosol population, many particle sizes and metrics must be covered.

Because aerosol particles are small, the electrostatic forces affecting them can be much stronger than the gravitational force [9]. This property is used in many aerosol applications, for example, to remove unwanted particles from a flow with an electrical field or to classify them by size, as in the differential mobility analyzer (DMA), where particles are selected based on their electrical mobility (charge to diameter ratio). Electrical particle sensors do not (usually) rely on the preexisting charge, but instead charge particles by ionizing the surrounding air. A common method is diffusion charging, where particles pass through a chamber with a high-voltage corona needle creating ions. The ions attach to the particle surfaces mainly through movement caused by diffusion [9]. Diffusion charging is employed in many existing commercial particle sensors: 1) nanoparticle surface area monitor (NSAM) (TSI); 2) Partector (Naneos); and 3) AQ Urban (Pegasor), for instance. There are also some examples of sensors employing bipolar charging methods, for example, with a radioactive source [10], [11]. While particles are usually intentionally charged in aerosol instruments based on particle electrical detection, Bilby et al. [12] presented a particle emission sensor utilizing the existing charge on the particles in the engine exhaust. This design, however, is based on the current amplification effect caused by the fragmentation of the collected conductive soot particles inside the sensor. To differentiate between particles charged intentionally for detection or classification and particles charged naturally, the latter will be referred to as indigenously or inherently charged (IC) hereafter. This terminology is also used by Eastwood [13].

In our study, we present a prototype of a new electrical particle sensor, the IC particle (ICP)-sensor, which relies on the IC of particles in the atmosphere or in exhaust. Our study shows that IC can easily be used to monitor particle concentrations, thus removing the necessity of a diffusion charger, at least for some applications. We share our results from two test measurements, first in an engine laboratory where we measured the (diluted) emissions of a heavy-duty truck and second from ambient measurements in a roadside environment with heavy air pollution. We also compare the measured charge concentrations to number, surface area, and mass concentrations of particles as well as theoretical charge concentrations calculated from the particle number distribution.

II. THEORETICAL BACKGROUND

Particle charge is the net charge of all electrons and protons contained in a particle. The number of elementary charges is often reported instead of the absolute charge. Negatively charged particles have more electrons than protons and vice versa. In equilibrium conditions, the charge distribution of particles depends on the ambient temperature, as well as the size of the particles [14]. The equilibrium ambient particle charge distribution can be calculated based on Fuchs' limiting-sphere theory, most conveniently using the formulation by Wiedensohler [15]. The net charge of an ambient particle population is close to zero, but negatively charged particles are

slightly more common [16]. The charge distribution of freshly emitted combustion-originated particles is indicative of the temperature when the particles were formed and tend to follow a Boltzmann distribution, although the emitted particles will eventually neutralize to the ambient charge distribution [17], [18]. The time it takes aerosol particles to reach an equilibrium state depends on the availability of gaseous ions, and how far from equilibrium the aerosol population is to begin with. Ambient ion concentrations are typically around 10^3 ions/cm^3 [16], but polluted air tends to have fewer ions, as they either grow into larger ions (particles) or are scavenged by existing particles [19]. Jayaratne et al. [20] showed that cluster ions near a road were rapidly scavenged by particles, but highly charged particles were detected up to 400 m from the road, giving some indication of the timeframe it takes for particles to reach an equilibrium charge distribution.

Previous studies have shown ways in which the particle charge of IC particles can be used to understand particle sources. Burtscher et al. [17] showed that particles produced by combustion had charge distributions, which could be related back to the process that created the particles. Kittelson and Pui [21] studied the charged fraction of particles (by mass) from exhaust and found a range of 72% during idle to 88% at full load. They also measured the charge distribution by electrical mobility and found that there were equal amounts of positive and negative particles. Maricq [18] also measured particle charge distributions from a motor vehicle and determined that the distributions corresponded to Boltzmann distributions at temperatures of 800–1100 K. Like Kittelson and Pui, he also found there to be equal amounts of positive and negative charges. In addition, Lähde et al. [22] reported on the ion number concentration distribution in heavy-duty diesel engine exhaust, finding that far fewer ions were present in the exhaust when using a diesel particulate filter (DPF), compared to no after treatment, or a diesel oxidation catalyst (DOC). Large amounts of charged particles (ions) have also been observed when measuring near busy roads [20], [23], [24] and the number of charges carried by ultrafine particles has been found to be larger near traffic than in background locations [24] or near powerlines [23]. Other types of combustion also produce charged particles, for example, natural gas engines [25], mixed pulverized coal and wood pellets in power plant boilers [26], and cooking on a gas stove [27].

Fig. 1 shows the average number of charges per particle for 10-nm-to-1-μm particles at temperatures of 20 °C–1000 °C. Even at high temperatures, many particles are neutral, which is why the average number of charges can remain below one. The black line represents a typical diffusion charger, this one is the electrical low-pressure impactor (ELPI+, Dekati Ltd.) Pn-curve [28], and the other lines show how temperature affects the charge distribution. A Pn-curve describes the efficiency of a charger, giving the average charge per particle as a function of particle size. Diffusion charging imparts a much higher charge to the particles than they would have otherwise.

The Boltzmann charge distribution is symmetrical around 0, i.e., the number of charges is the same for negative and positive charges, and therefore, only one line is shown in Fig. 1
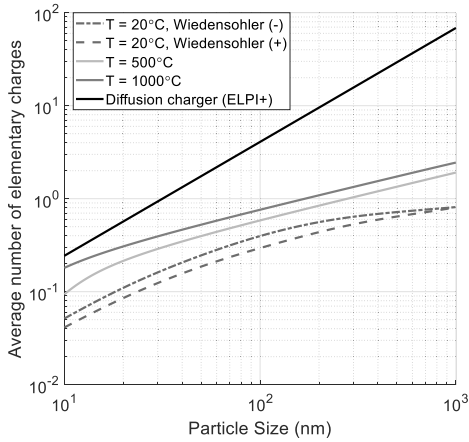
Fig. 1. Boltzmann equilibrium mean particle charge as a function of particle size at two different temperatures, as well as the Wiedensohler mean charge at $T = 20$ °C. The Pn curve of the ELPI+ charger is also shown (black line).

for each temperature (the other line can be imagined to be on top). The Wiedensohler distribution charge distribution is more accurate at ambient temperatures, especially at the lower particle sizes where the Boltzmann distribution underestimates the mean charge [15]. Unlike the Boltzmann distribution, it is not symmetrical, and thus, both the negative and positive charge numbers are shown. Later in this article, we will use the Wiedensohler distribution for the negative charge fraction when comparing our measurements to a theoretical ambient charge distribution and the Boltzmann distributions when comparing exhaust aerosol measurements

III. SENSOR DESIGN

For our sensor design, we used a zeroth-order mobility analyzer, or electrostatic collector, with annular geometry. A cross-sectional drawing of the mobility analyzer is shown in Fig. S1. The inner electrode is connected to a voltage source and the outer electrode is connected to an electrometer. The basic principle of any mobility analyzer is that particles travel through an electric field, and particles with a high enough electrical mobility Z are collected, while low mobility particles travel through. This type of an analyzer can be characterized by the smallest electrical mobility (Z_0) that has a 100% collection efficiency [29], and for an annular geometry, it is given by (1), where Q is the volumetric air flow rate, d_{outer} and d_{inner} are the diameters of the electrodes, L is their length, and V is the voltage difference across the electrodes. The ratio of a particle's mobility to the limiting mobility is the collection efficiency η (2) when the flow is laminar

$$Z_0 = \frac{Q \ln\left(\frac{d_{outer}}{d_{inner}}\right)}{2\pi L V} \qquad (1)$$

$$\eta = \frac{Z}{Z_0}. \qquad (2)$$

The electrical mobility of a particle is given by (3), where n is the number of elementary charges, e is equal to one elementary charge (1.602×10^{-19} C), $C(d_p)$ is the Cunningham slip

TABLE I
IMPORTANT DIMENSIONS AND OTHER PARAMETERS OF THE SENSOR

Parameter	Value
L	48 mm
L_{outer}	50 mm
d_{outer}	32 mm
d_{inner}	28 mm
Q	1 Lpm
V	±500 V
Z_0	1.466×10^{-4} cm²/(V·s)

correction factor, $\eta(T)$ is the viscosity of the surrounding gas, dependent on the gas temperature T, and d_p is the particle diameter. As can be seen from the equation, particles have high electrical mobility if they are small and highly charged. Ignoring the slip correction, a singly charged particle has the same mobility as a twice charged particle of double the diameter (including the slip correction would increase the mobility of the smaller particle compared to the larger)

$$Z = \frac{neC(d_p)}{3\pi \eta(T) d_p}. \qquad (3)$$

The dimensions and other constant parameters used in our sensor are shown in Table I. The measurement electrode was slightly longer than the opposing high-voltage electrode to minimize particle losses caused by the edge effects of the electric field. The L value shown and used for calculation is for the shorter electrode.

The Z_0 value above corresponds to a singly charged particle with a diameter of 140 nm or a doubly charged particle with a diameter of 220 nm, which is suitable for measuring most urban particles or engine emitted particles. The same sensor geometry can easily be changed to target various mobility sizes, either by changing the flow rate or the collection voltage. When characterizing the sensor efficiency, we also used lower voltages to change the Z_0 value.

In addition to the mobility analyzer, the ICP-sensor consisted of an ion trap to prevent the measurement of gaseous ions; a voltage source, electrometer, and computer connected to the mobility analyzer; a critical orifice to control the flow rate; and a pump. In the engine laboratory and ambient measurements, we also used a cyclone to prevent coarse dust from entering the sensor.

IV. METHODS

We measured the sensor's detection efficiency dependency on particle mobility, size, and number concentration in a laboratory. We then tested the ICP-sensor for two applications: measuring particles from engine exhaust from a heavy-duty truck as well as ambient aerosol in an urban traffic environment. Correlations with different metrics were calculated using simple linear regression with ordinary least squares method.

A. Laboratory Measurement of Detection Efficiency

The laboratory characterization was conducted at the Tampere University Aerosol Physics Calibration Laboratory.

To measure the detection efficiency of the ICP-sensor, we built the setup shown in Fig. S2 and used the singly charged aerosol reference (SCAR) system to produce a monodisperse aerosol of unipolar, singly charged particles [30]. Our main reference for the detection efficiency was a Faraday cup and electrometer (FCAE) (Keithley 6430 Sub-femtoamp Remote Sourcemeter, Keithley Inc.), FCAE. In addition, particles penetrating through the sensor were measured with a condensation particle counter (CPC 3750, by TSI).

For the most part, only the mobility analyzer portion of the ICP was characterized, but we also conducted a few measurement points with the ion trap in place, in order to characterize the losses in the ion trap for small particles.

B. Engine Laboratory Measurements

The engine laboratory measurements were conducted at Indian Oil Corporation (IOCL) facilities in Faridabad, using a chassis dynamometer. The test subject was a typical Indian heavy-duty truck, registered in 2017 and equipped with a DOC, but DPF, and it was driven following a transient driving cycle. The exhaust sampling was conducted using a constant volume sampler (CVS), and we alternated between measuring all particles and solid particles. A thermodenuder was used to remove the semivolatile particle fraction in the latter case, as shown in the simple schematic (Fig. S3). The measurement matrix included three different fuels and two lubricating oils. The three fuels were Bharat Stage VI (BSVI) fossil fuel, and two fuels blended with Bharat Stage IV (BSIV): 1) renewable paraffinic diesel (RPD) and renewable fatty acid Methyl Ester (r-FAME). The test cycle was the Delhi Bus Driving Cycle, which includes accelerations, decelerations, and idling. One cycle lasts 7 min, and the maximum speed is 50 km/h. For two fuels, the "All particles" measurements were conducted twice, and we were able to measure both the positively and negatively charged particle fractions by changing the collection voltage from $+500$ to -500 V. The measurement matrix is included in Table S1. Results from the measurement campaign have been previously published [31], and more details on the vehicle, fuels, oils, driving cycle, and so on can be found there.

We used an ELPI+ [28], [32] to measure the particle number and size distribution as well as to compare the ICP to. ELPI+ is a cascade impactor, where each impactor stage is separately connected to an electrometer. The particles are positively charged using diffusion charging. The particles going through the ICP-sensor were measured with an eFilter (by Dekati Ltd., presented in [33]), which also employs diffusion charging. eFilter also allows for collecting particles onto a filter, which can then be weighed to interpret the mass concentration of the sample, but we only used the electrical portion of the instrument. The data output of the instrument is simply the current measured from the DC particles. The sample dilution was calculated using CO_2 as a tracer gas.

C. Ambient Air Measurements on a Roadside

The ambient measurements were conducted in Gual Pahari, located south of New Delhi, in December 2018. During the measurements, the days were sunny, there was almost no wind
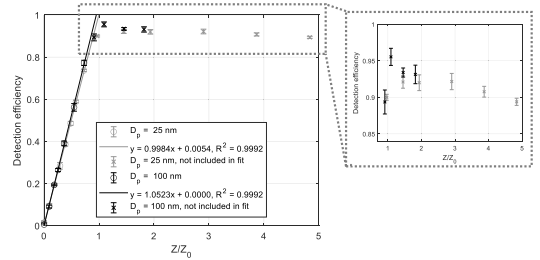

Fig. 2. Detection efficiency of the sensor prototype as a function of particles' electrical mobility divided by the minimum electrical mobility. The variation in the ratio $Z/Z_0(V)$ was achieved by varying the collection voltage. Two particle sizes were used, 25 and 100 nm.

(<1 m/s), and the temperature ranged between 10 °C and 25 °C. The instruments were housed in a mobile laboratory parked adjacent to a busy road with approximately 800 vehicles per hour during daytime. Fig. S4 shows a simplified schematic of the measurement setup. All instruments sampled air through a PM2.5 inlet, and the ICP had an additional cyclone to prevent the accumulation of coarse dust. The cutoff diameter (d_{50}) of the cyclone was 2.239 μm. The sensor collection voltage was set to -500 V; thus, the measured particles were also negatively charged. Again, ELPI+ was used for comparison and to calculate the theoretical charge concentration. The ELPI+ sample was diluted with 5 L/min of clean air to lessen the accumulation of particles. The total flow for the ELPI+ is 10 L/min, and thus, the dilution ratio was 2 (results corrected to represent ambient concentrations in the data analysis). The measurements are described in more detail in a previous article [34].

V. RESULTS

In this section, we present the results from each measurement separately, and the three experiments are interpreted together in Section VI.

A. Mobility Analyzer Characterization

We determined the detection efficiency for the mobility analyzer portion of the ICP by employing (2) for two different particle sizes, 25 and 100 nm, and varied the Z/Z_0 ratio by changing the collection voltage of the analyzer.

Fig. 2 shows the detection efficiency of the ICP-sensor as a function of electrical mobility ratio. The ratio Z/Z_0 was changed by changing the voltage used to collect particles, V in (1). Ideally, the relationship between detection efficiency and the mobility ratio should be one-to-one, as shown in (2), and the measurements show that this is the case. The fit for 100-nm particles is slightly steeper than the fit for 25-nm particles, due to greater diffusional and electrical losses for the smaller particles. The results for mobility ratios greater than one show that the detection efficiency begins to go down. This is most likely due to the increased electrical field causing losses in the area before the detection plates. We also measured the detection efficiency for the whole sensor (including an ion trap and additional tubing to connect it to the analyzer) in
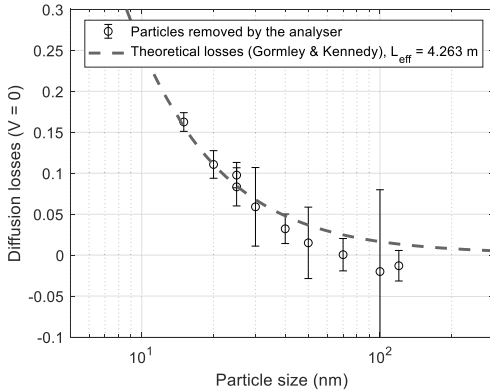
Fig. 3. Particles lost due to diffusion as a function of particle size. Collection voltage V was set to 0 V. The error bars represent the standard deviation of measured variables combined into a total standard deviation using error propagation. The fit line represents theoretical diffusion losses for a tube of length 4.263 m (L_{eff}).
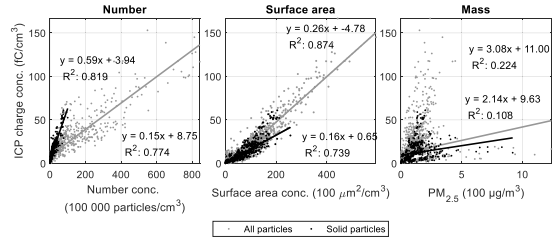

Fig. 4. Charge concentration measured with ICP compared to particle number and mass concentrations during the engine laboratory measurement campaign. These values are corrected for dilution and losses in the thermodenuder, representing the concentrations in the CVS. Each data point is a 5-s average.

a similar measurement but changed particle size (instead of the collection voltage) to vary the mobility ratio (see Fig. S5). As expected, the detection efficiency was slightly lower due to additional diffusion losses (fit line $y = 0.8976x + 0.0582$ and $R^2 = 0.9988$). Here, we also observed that the detection efficiency began to decrease when Z/Z_0 increased past one, due to the increased diffusion losses of smaller particles.

Fig. 3 shows the particle losses due to diffusion in the mobility analyzer inlet, outlet, and annular flow geometry before and after the electrodes. Particles deposited onto the detection cylinder were not counted as losses, i.e., the measured values were calculated as

$$\text{diffusion losses} = 1 - \frac{\text{penetrating particles} + \text{detected particles}}{\text{total concentration}}.$$

The d_{50} value for the lower limit of the mobility analyzer is 5.5 nm, but in practice, the d_{50} size will be larger, and the overall losses greater, as diffusion losses due to the ion trap and tubing are not accounted for here. To compare to a theoretical value, we used Gormley and Kennedy's equation for diffusion losses in a tube [35], calculating the effective length to best match the measured values. We used the form given by Cheng [36]. The diffusion losses for a tube resulted in a good fit, with an effective length of 4.26 m, and this equation is used to correct the theoretical current from the ELPI+ number size distribution. An even better fit might have been achieved by dividing the mobility analyzer into regions and using a combination of equations; however, we preferred this approach due to its simplicity.

Fig. S6 shows the effect of particle concentration on detection efficiency. In theory, high particle number could lower the detection efficiency due to space charge losses. The space charge is caused by our test aerosol, in which all particles are either positively or negatively charged (in this test, they were negatively charged). Consequently, the particles repel each other, and if the particle concentration is large enough,

particles may be lost inside the sensor due to movement caused by the space charge. However, we calculated an approximate value for space charge losses inside the sensor, and even with a concentration of 10^7 particles/cm^3, the space charge losses were less than 0.5%. Thus, it is unlikely that the lowering detection efficiency seen in Fig. S6 has to do with this effect. In addition, the space charge losses should continue to reduce detection efficiency with increasing particle concentration, whereas in our results, the detection efficiency levels off at 10 000 particles/cm^3, settling at approximately 0.93. In the previous results for detection efficiency, particle concentrations were between 10 and 15 $\times$ 10^3 particles/cm^3 and thus in the level area.

B. Engine Laboratory Measurements

The engine exhaust particles were small but numerous. Based on the data measured by ELPI+, the count median diameters (CMDs) of the particles were below 30 nm in all cases and the measured number concentration of particles ranged from 50 000 to 800 000 particles/cm^3 (after dilution). The median current measured by the ICP ranged from 20 to 70 fA, depending mostly on the phase of the driving cycle. Median values for each measurement point are shown in Table S2 and the particle size distributions of the exhaust sample are presented in Fig. S7. There was no statistical difference between the charge concentrations of different fuels and oils and the in-group variation was large, i.e., if a difference exists, the sample size would need to be larger.

Fig. 4 shows the correlation of the charge concentration to three different particle metrics: 1) number; 2) geometric surface area; and 3) mass (PM$_{2.5}$, mass concentration of sub 2.5 μm particles). Number, surface area, and mass were chosen for comparison because they are common metrics for particle measurements. Number concentration was highly correlated with the charge concentration, but the fit was different for solid particles versus all particles. This demonstrates that solid particles have a larger charge concentration than nucleation particles, which are included in the "all particles" case, and agrees with previous research showing that particles originating from inside the engine (solid particles) are more highly charged than particles formed when the exhaust dilutes (e.g., [22]), which have been found to carry little to no charges [37],
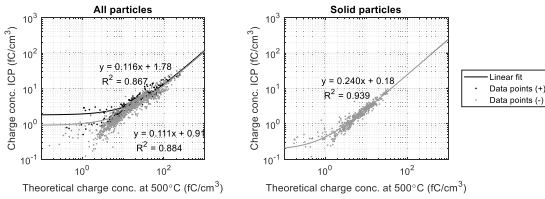
Fig. 5. Current measured with ICP compared to a theoretical current, calculated based on the data measured by the ELPI+ and assuming a Boltzmann charge distribution at 500 °C. The left plot shows the correlation for "all particle" test points, while the right plot shows solid particle test points. The data were averaged into 5-s sections from the original 1-Hz data and charge concentrations smaller than 0.1 fC/cm^3 were filtered out.
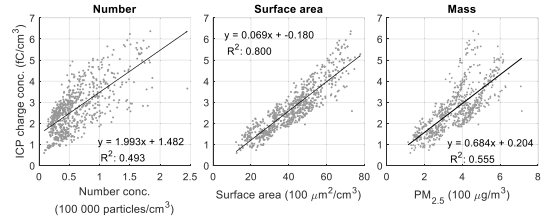

Fig. 6. Charge concentration measured with ICP compared to particle number and mass concentrations measured with ELPI+ during the ambient air measurement campaign. Each data point represents a 5-min average.
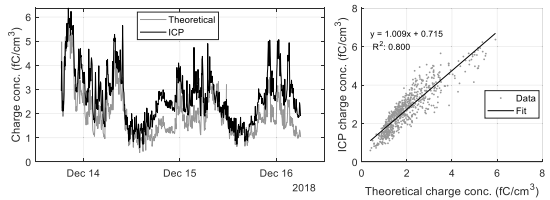

Fig. 7. Measured current from ambient charged particles, and the theoretical charge concentration calculated by assuming a Wiedensohler charge distribution and using ELPI+ size-distributed particle number concentration data. The data in both plots have been averaged into 5-min sections. Tick marks in the time series are placed at midnight.

[38]. When the aerosol is passed through the thermodenuder, not only are semivolatile particles removed, but solid particles that have been coated by the semivolatile vapors lose their coating, causing them to shrink. As a result, diffusional losses increase. Thus, some of the change in the charge concentration measured with the ICP can be due to higher diffusional losses in the sensor and in the sampling lines, and this effect is not corrected for. Selected time series for ICP current and number concentration are shown in Fig. S8 and time series for ELPI+ current and ICP current for each measurement point are shown in Fig. S9.

Finally, we looked at the charge concentration measured with ICP in comparison to a theoretical concentration derived from the ELPI+ number concentration and a Boltzmann charge distribution at 500 °C. This temperature was chosen based on previous findings that engine exhaust charge distributions match a Boltzmann equilibrium between 800 and 1100 K [18]. All the engine laboratory data are gathered in Fig. 5, which shows the linear fit between the measured current and theoretical charge concentration at 500 °C. The left side plot shows "all particles" cases and the right side plot shows "solid particles" cases. Note that the axes are logarithmic, which is why the linear fit function with a constant term looks nonlinear. In both cases, the correlation between the measured and theoretical charge concentration is very good ($R^2 > 0.8$), but the slope is far from one (0.12 for all particles and 0.24 for solid particles). Positive and negative polarities were not significantly different, which agrees with previous findings [18]. Examining the residuals for the "solid only" data points (Fig. S10) showed that larger CMD values (60–80 nm) were associated with positive residuals and vice versa for small CMD values (<20 nm).

C. Ambient Roadside Measurements

The particle concentration during the roadside measurements was very high and ELPI+ showed signs of overloading, and thus, only the first few days of measurements after cleaning the ELPI+ are analyzed in depth. Many particle concentration metrics have been previously reported and are not repeated here [34].

To investigate the relationship of charge concentration to other particle metrics, Fig. 6 shows the correlation plots com-

paring the measurements with ICP to particle number, surface area, and mass (PM$_{2.5}$). The correlation was similar with number concentration ($R^2 = 0.493$) and mass concentration ($R^2 = 0.555$), while the correlation was highest with surface area ($R^2 = 0.800$).

Fig. 7 shows a time series of the electrical current measured with the ICP and a theoretical current calculated using the particle size distribution data measured with ELPI+ and Wiedensohler equation for the charge distribution at a temperature of 293.15 K or 20 °C. Along with the time series, the correlation between the two is displayed with a line fit to the data.

Fig. 7 shows that the ICP charge concentration is correlated with the theoretical charge concentration, and the difference between the two seems to be the smallest from midday to afternoon (tick marks are placed at midnight). The ICP charge concentration was larger than the theoretical at midnight. The fit line between the two for the whole duration is $y = 1.009x + 0.715$ with a correlation coefficient of $R^2 = 0.800$. We investigated the dependency of the residuals on the time of day, ambient temperature, electrometer temperature, particle size, and particle concentration (Fig. S11) and found that they depended on the time of day, ambient temperature, and particle size. Initially, we worried that the electrometer temperature might be the cause for residual dependence on ambient temperature, but the electrometer temperature had essentially no effect on the residuals. Instead, it seems that the particle size might be the root cause: smaller particles (<40 nm) resulted in negative residuals, while larger (~100 nm) particles resulted in positive residuals. Our interpretation is that when the particle

size distribution is dominated by small particles, they are either newly formed ambient particles or particles nucleated during fresh exhaust cooling and thus have no charge to begin with and have not reached charge equilibrium. Conversely, soot mode particles may still be closer to their initial higher charge, explaining the positive residual associated with them. The correlation coefficient between temperature and particle size was -0.34 (Table S3), which then explains why the ambient temperature seemed to affect the residuals: particle size was smaller and temperatures higher during midday to afternoon times. Surprisingly, hourly traffic counts (shown in Fig. S11) were unrelated to residuals.

We noted that the best fit line in Fig. 7 leaves a relatively large error for smaller values, and thus, we checked whether the analysis would change if the logarithmic values for measured and theoretical charge concentration were compared instead. While the fit improved for the smaller values, the interpretation of the residuals did not change.

VI. DISCUSSION

Comparing the charge concentration measured with ICP to other metrics revealed a high correlation ($R^2 > 0.7$) with number and surface area concentration in the engine laboratory measurements, whereas in the ambient measurement case, the correlation was equally good for number and mass ($R^2 \approx 0.5$) and the highest correlation was with surface area ($R^2 = 0.8$). The expectation was that the surface area would have the best correlation, as ion attachment is governed by Fuchs' surface area. The good agreement with mass concentration in the ambient measurement case was surprising and perhaps somewhat of a coincidence due to the specific aerosol properties at the location.

Previous engine exhaust studies have found particles to match a Boltzmann distribution of much higher temperatures than found here. For example, Maricq [18] observed that particles from a diesel passenger car corresponded to Boltzmann distributions at approximately 500 °C–800 °C. There are, however, a few differences between our studies: in our study, the vehicle was a heavy-duty truck, not a passenger car, and while we used a conventional CVS dilution system, Maricq used a "remote mix tee," which reduces the time from tailpipe to dilution tunnel. In the "All particles" case, the nucleation mode particles were at least partially responsible for the measured current being smaller than predicted, but when measuring only the solid particles, the measured charge concentration relative to the theoretical charge concentration only increased a little. Although the charge per particle (Table S2) is correlated with the CMD, $R^2 = 0.63$, we assume based on previous studies that the main reason for the change in the level of charge between the two cases is the removal of uncharged nucleation particles. The particle size distributions show that the solid particle measurements still included many small particles (Fig. S7). These must either be solid core particles [39], [40] or the thermodenuder was not efficient enough to remove all the semivolatile material. In future measurements, it would be interesting to measure particles directly from the tailpipe, or with less dilution, to see whether the charge per particle would better match previous findings.

In calculating a reference value for the measured ambient charge concentrations, we assumed that the particles had reached an equilibrium distribution described by the Wiedensohler equation. The measured charge concentration was slightly larger than the theoretical one, and we assumed that overcharged traffic-originated soot particles were the cause. When we aimed to verify this by analyzing the residuals of the fit to measured versus theoretical values, it turned out that traffic rates did not correlate with higher positive residuals (or negative residuals, for that matter), as is evident when comparing the hourly residuals to the traffic cycle in Fig. S11. From the analysis, we determined that particles in the soot mode size range were indeed more charged, but also nucleation particles were less charged than the equilibrium distribution predicted. Combustion engines can release particles from both modes, which is why the effect of traffic might be difficult to spot. In addition, other combustion sources nearby, such as cooking or heating, may also have contributed to the soot mode.

One aim of the engine and ambient measurements was to test the sensor performance in different settings and particle concentrations. The sensor's limit of detection is 1.636 fA, equal to three times the standard deviation of the electrometer signal when measuring clean air. This corresponds to a concentration of 4500 particles/cm^3 for 25-nm particles or 1500 particles/cm^3 of 100-nm particles with ambient charge levels. The ICP is, therefore, not a good choice for low particle concentrations. In the ambient measurements, the ICP was employed in a high-pollution environment for two weeks without problems (the data from these measurements were limited due to particle accumulation in the ELPI+), which shows that the geometry tolerates particle accumulation quite well. The highest currents we measured were around 700 fA, in the engine laboratory, but the electrometer can measure far larger currents (up to 400 000 fA); thus, high concentrations are not a problem.

The chosen mobility analyzer dimensions worked quite well in both environments. For these dimensions, many other applications are also possible, as the ICP can easily be modified for different needs by varying the collection voltage and/or flow rate. New versions with different dimensions could also be built to cater to specific needs. For instance, to target low concentrations, a higher flow rate could be used to increase the sensitivity (although the Z_0 value must be checked). Outside of modifying the mobility analyzer, particles in a soot mode size range could be better targeted by increasing the ion trap voltage, thereby removing more of the nucleation mode particles. Large particles with multiple charges could be removed aerodynamically before the sensor (with an impactor or a cyclone). Although we did use a cyclone in the ambient measurements here as well, the dp_{50} was not sufficiently low to impact the measurements (2.2 μm).

We did not have an instrument available to measure the neutral particles penetrating the ICP in the ambient measurements. However, we examined this possibility by simulating the output of the ICP and a subsequent DC sensor (we used the Pn-curve for an eFilter) for different types of particle distributions. Two examples are shared in Fig. S12:

the first is an ambient number size distribution dominated by local emissions and the second is dominated by more aged emissions in the accumulation mode. Assuming that the nucleation and accumulation mode particles have reached an equilibrium state (calculated for negative particles from the empirical Wiedensohler equation [15]) and a Boltzmann distribution at 800 K for the soot mode particles, the IC to DC ratio was 50% for the first case and 30% for the second case. Therefore, this combination of sensors could be used to detect local traffic emissions based on this ratio, but as was seen in the ambient measurements, nucleation mode particles had less inherent charge than in theoretical equilibrium conditions.

VII. Conclusion

In this article, we presented a new electrical sensor type and showed it to be suitable for measuring particles both in an engine laboratory and in ambient measurements in a polluted environment. When used in tandem with other instruments, such as we did here with the ELPI+, it can give information of the charge state of the aerosol. Compared to most previous electrical sensors, the benefit of the ICP is that a charging mechanism, often vulnerable to contamination, is not needed, whereas the downside of the ICP-sensor is that larger particle concentrations are required to produce a detectable current than in DC sensors.

Acknowledgment

References

[1] U. Lohmann and J. Feichter, "Global indirect aerosol effects: A review," *Atmos. Chem. Phys.*, vol. 4, no. 6, pp. 7561–7614, 2004, doi: 10.5194/acpd-4-7561-2004.

[2] M. O. Andreae, C. D. Jones, and P. M. Cox, "Strong present-day aerosol cooling implies a hot future," *Nature*, vol. 435, pp. 1187–1190, Jun. 2005, doi: 10.1038/nature03671.

[3] J. Lelieveld, J. S. Evans, M. Fnais, D. Giannadaki, and A. Pozzer, "The contribution of outdoor air pollution sources to premature mortality on a global scale," *Nature*, vol. 525, no. 7569, pp. 367–371, 2015, doi: 10.1038/nature15371.

[4] *Spreading Like Wildfire—The Rising Threat of Extraordinary Landscape Fires*, United Nations Environment Programme, Nairobi, Kenya, 2022.

[5] P. Kulkarni and P. A. Baron, "An approach to performing aerosol measurements," in *Aerosol Measurement: Principles, Techniques, and Applications*, 3rd ed., P. Kulkarni, K. Willeke, and P. A. Baron, Eds. 2011, pp. 55–65.

[6] J. J. Caubel, T. E. Cados, C. V. Preble, and T. W. Kirchstetter, "A distributed network of 100 black carbon sensors for 100 days of air quality monitoring in west Oakland, California," *Environ. Sci. Technol.*, vol. 53, no. 13, pp. 7564–7573, Jul. 2019, doi: 10.1021/acs.est.9b00282.

[7] M. Fierz, D. Meier, P. Steigmeier, and H. Burtscher, "Aerosol measurement by induced currents," *Aerosol Sci. Technol.*, vol. 48, no. 4, pp. 350–357, Apr. 2014, doi: 10.1080/02786826.2013.875981.

[8] J. Kuula et al., "Long-term sensor measurements of lung deposited surface area of particulate matter emitted from local vehicular and residential wood combustion sources," *Aerosol Sci. Technol.*, vol. 54, no. 2, pp. 190–202, Feb. 2020, doi: 10.1080/02786826.2019.1668909.

[9] W. C. Hinds, *Aerosol Technology: Properties, Behavior, and Measurement of Airborne Particles*, 2nd ed. New York, NY, USA: Wiley, 1999.

[10] R. T. Nishida, T. J. Johnson, J. S. Hassim, B. M. Graves, A. M. Boies, and S. Hochgreb, "A simple method for measuring fine-to-ultrafine aerosols using bipolar charge equilibrium," *ACS Sensors*, vol. 5, no. 2, pp. 447–453, Feb. 2020, doi: 10.1021/acssensors.9b02143.

[11] S. Jakubiak and P. Oberbek, "Determination of the concentration of ultrafine aerosol using an ionization sensor," *Nanomaterials*, vol. 11, no. 6, p. 1625, Jun. 2021, doi: 10.3390/nano11061625.

[12] D. Bilby, D. J. Kubinski, and M. M. Maricq, "Current amplification in an electrostatic trap by soot dendrite growth and fragmentation: Application to soot sensors," *J. Aerosol Sci.*, vol. 98, pp. 41–58, Aug. 2016, doi: 10.1016/j.jaerosci.2016.03.003.

[13] P. Eastwood, *Particle Emissions From Motor Vehicles*. Hoboken, NJ, USA: Wiley, 2008.

[14] D. Keefe, P. Nolan, and T. Rich, "Charge equilibrium in aerosols according to the Boltzmann law," *Proc. Roy. Irish Acad. Sect. A, Math. Phys. Sci.*, vol. 60, pp. 27–45, Jul. 1959.

[15] A. Wiedensohler, "An approximation of the bipolar charge distribution for particles in the submicron size range," *J. Aerosol Sci.*, vol. 19, no. 3, pp. 387–389, Jun. 1988, doi: 10.1016/0021-8502(88)90278-9.

[16] P. Kulkarni, P. A. Baron, and K. Willeke, *Aerosol Measurement: Principles, Techniques, and Applications*. Hoboken, NJ, USA: Wiley, 2011.

[17] H. Burtscher, A. Reis, and A. Schmidt-Ott, "Particle charge in combustion aerosols," *J. Aerosol Sci.*, vol. 17, no. 1, pp. 47–51, Jan. 1986.

[18] M. M. Maricq, "On the electrical charge of motor vehicle exhaust particles," *J. Aerosol Sci.*, vol. 37, no. 7, pp. 858–874, Jul. 2006, doi: 10.1016/j.jaerosci.2005.08.003.

[19] V. Jokinen, *Aerosolinhiukkasten Ja Ilman Ionien Mittaus Differentiaalisella Liikkuvuusanalysaatorilla*. Helsinki: Aerosolitutkimusseura, 1995.

[20] E. R. Jayaratne, X. Ling, and L. Morawska, "Observation of ions and particles near busy roads using a neutral cluster and air ion spectrometer (NAIS)," *Atmos. Environ.*, vol. 84, pp. 198–203, Feb. 2014, doi: 10.1016/j.atmosenv.2013.11.045.

[21] D. B. Kittelson and D. Y. H. Pui, "Electrostatic collection of diesel particles," *SAE Trans.*, vol. 95, no. 1, pp. 51–62, 1986.

[22] T. Lähde et al., "Heavy duty diesel engine exhaust aerosol particle and ion measurements," *Environ. Sci. Technol.*, vol. 43, no. 1, pp. 163–168, 2009, doi: 10.1021/es801690h.

[23] E. R. Jayaratne, X. Ling, and L. Morawska, "Comparison of charged nanoparticle concentrations near busy roads and overhead high-voltage power lines," *Sci. Total Environ.*, vol. 526, pp. 14–18, Sep. 2015, doi: 10.1016/j.scitotenv.2015.04.074.

[24] E. S. Lee, B. Xu, and Y. Zhu, "Measurements of ultrafine particles carrying different number of charges in on- and near-freeway environments," *Atmos. Environ.*, vol. 60, pp. 564–572, Dec. 2012, doi: 10.1016/j.atmosenv.2012.06.085.

[25] J. Alanen et al., "The formation and physical properties of the particle emissions from a natural gas engine," *Fuel*, vol. 162, pp. 155–161, Dec. 2015, doi: 10.1016/j.fuel.2015.09.003.

[26] F. Mylläri et al., "Physical and chemical characteristics of flue-gas particles in a large pulverized fuel-fired power plant boiler during co-combustion of coal and wood pellets," *Combustion Flame*, vol. 176, pp. 554–566, Feb. 2017, doi: 10.1016/j.combustflame.2016.10.027.

[27] L. Stabile, E. R. Jayaratne, G. Buonanno, and L. Morawska, "Charged particles and cluster ions produced during cooking activities," *Sci. Total Environ.*, vols. 497–498, pp. 516–526, Nov. 2014, doi: 10.1016/j.scitotenv.2014.08.011.

[28] A. Järvinen, M. Aitomaa, A. Rostedt, J. Keskinen, and J. Yli-Ojanperä, "Calibration of the new electrical low pressure impactor (ELPI+)," *J. Aerosol Sci.*, vol. 69, pp. 150–159, Mar. 2014, doi: 10.1016/J.JAEROSCI.2013.12.006.

[29] H. Tammet, *The Aspiration Method for the Determination of Atmospheric-Ion Spectra*, vols. 195–2. Jerusalem: Israel Program for Scientific Translations, 1970.

[30] J. Yli-Ojanperä, J. M. Mäkelä, M. Marjamäki, A. Rostedt, and J. Keskinen, "Towards traceable particle number concentration standard: Single charged aerosol reference (SCAR)," *J. Aerosol Sci.*, vol. 41, no. 8, pp. 719–728, Aug. 2010, doi: 10.1016/j.jaerosci.2010.04.012.

[31] S. Martikainen et al., "Reducing particle emissions of heavy-duty diesel vehicles in India: Combined effects of diesel, biodiesel and lubricating oil," *Atmos. Environ., X*, 2023, Art. no. 100202, doi: 10.1016/j.aeaoa.2023.100202.

[32] J. Keskinen, K. Pietarinen, and M. Lehtimäki, "Electrical low pressure impactor," *J. Aerosol Sci.*, vol. 23, no. 4, pp. 353–360, 1992.

[33] L. Salo et al., "Emission measurements with gravimetric impactors and electrical devices: An aerosol instrument comparison," *Aerosol Sci. Technol.*, vol. 53, no. 5, pp. 526–539, May 2019, doi: 10.1080/02786826.2019.1578858.

[34] L. Salo et al., "The characteristics and size of lung-depositing particles vary significantly between high and low pollution traffic environments," *Atmos. Environ.*, vol. 255, Jun. 2021, Art. no. 118421, doi: 10.1016/j.atmosenv.2021.118421.

[35] P. G. Gormley and M. Kennedy, "Diffusion from a stream flowing through a cylindrical tube," *Proc. Roy. Irish Acad. Sect. A, Math. Phys. Sci.*, vol. 52, pp. 163–169, Sep. 1948. [Online]. Available: http://www.jstor.org/stable/20488498

[36] Y.-S. Cheng, "Instruments and samplers based on diffusional separation," in *Aerosol Measurement: Principles, Techniques, and Applications*, 3rd ed., P. Kulkarni, K. Willeke, and P. A. Baron, Eds. 2011, pp. 365–379.

[37] H. Jung and D. B. Kittelson, "Measurement of electrical charge on diesel particles," *Aerosol Sci. Technol.*, vol. 39, no. 12, pp. 1129–1135, Dec. 2005.

[38] H. Ma, H. Jung, and D. B. Kittelson, "Investigation of diesel nanoparticle nucleation mechanisms," *Aerosol Sci. Technol.*, vol. 42, no. 5, pp. 335–342, Mar. 2008.

[39] T. Rönkkö, A. Virtanen, J. Kannosto, J. Keskinen, M. Lappi, and L. Pirjola, "Nucleation mode particles with a nonvolatile core in the exhaust of a heavy duty diesel vehicle," *Environ. Sci. Technol.*, vol. 41, no. 18, pp. 6384–6389, Sep. 2007, doi: 10.1021/es0705339.

[40] A. D. Filippo and M. M. Maricq, "Diesel nucleation mode particles: Semivolatile or solid?" *Environ. Sci. Technol.*, vol. 42, no. 21, pp. 7957–7962, Nov. 2008, doi: 10.1021/es8010332.

Rakesh K. Hooda is a Senior Scientist and the Coordinator of Indo-Finnish Research at the Aerosol Composition research Group, Finnish Meteorological Institute, Helsinki, Finland. He works for the last 20 years on aerosols' physicochemical and optical properties; quantifying sources and emission inventories; boundary layer dynamics, atmospheric aging, and transformation due to physicochemical processes; direct, semidirect, and indirect effect studies of aerosol; and particle climate and health impacts.

Md. Hafizur Rahman received the M.Tech. degree in environmental biotechnology from Jadavpur University, Kolkata, India, in 2017.
He is one of the research professionals at The Energy and Resources Institute (TERI), New Delhi, India. His research interests include air quality monitoring and assessment, development of air pollutant emission inventory, and developing innovative solutions for air quality management.

Arindam Datta received the Ph.D. degree in environmental sciences from the University of Kalyani, Kalyani, India, in 2008.
He was a Fulbright Fellow at the Ohio State University, Columbus, OH, USA, and a Postdoctoral Research Fellow at the University of Aberdeen, Aberdeen, U.K. He is one of the senior professionals at The Energy and Resources Institute (TERI), New Delhi, India. His research interests include sector-specific air pollution and GHG emission inventory and emission factor development.

Ved Prakash Sharma has more than 24 years of experience in environmental management, on air quality management monitoring, laboratory analysis, including black carbon monitoring in association with the Finnish metrological institute. He was responsible for aerosol monitoring center in the central Himalayas from 2005 to 2018. His other areas of expertise are in monitoring biomass heat exposure, workplace exposure, water quality and wastewater quality, solid waste characteristics, and OSHA auditing. He is the Laboratory Head of the Air Quality Laboratory and the Radiological Safety officer (RSO) of The Energy and Resources Institute (TERI), New Delhi, India, responsible for nucleonic Gauge facility of the aerosol monitoring instruments. He has published about 25 research papers in various international and national journals.

Laura Salo is pursuing the Ph.D. degree in aerosol physics with Tampere University, Tampere, Finland.
She is with the Aerosol Physics Laboratory, Faculty of Engineering and Natural Sciences, Tampere University. She began her studies in 2017 and since has been involved with air quality, aerosol emissions, and instrument development.

Sanjukta Subudhi received the Ph.D. degree from the University of Delhi, New Delhi, India, in 2001.
She was a Postdoctorate at the National Center for Genetic Engineering and Biotechnology, National Science and Technology Development Agency (NSTDA), Bangkok, Thailand. She is a Senior Scientist and the Group Leader at the Microbial Biofuels and Biochemical Group, The Energy and Resources Institute (TERI), New Delhi. Her subject domain spans technology development and demonstration for production of biofuels (gaseous and liquid biofuels: biohydrogen, bioethanol, biodiesel, and biomethane) and value-added industry platform biochemical, including high-value biopigments, in a biorefinery approach through microbial interventions.

Antti Rostedt is a Staff Scientist with the Aerosol Physics Laboratory, Faculty of Engineering and Natural Sciences, Tampere University, Tampere, Finland. His main research interests are aerosol measurement technology and instrument development.

Heino Kuuluvainen was born in Hämeenlinna, Finland, in 1985.
He currently works as a University Instructor in Physics and is involved in aerosol physics research with the Aerosol Physics Laboratory, Faculty of Engineering and Natural Sciences, Tampere University, Tampere, Finland. His research interests include surface interaction of aerosol particles, urban air quality, and particulate emissions.

Antti Hyvärinen is the Head of the Atmospheric Composition Research Unit, Finnish Meteorological Institute, Helsinki, Finland. His expertise lies in measurements of aerosol properties in various field environments around global hotspots for aerosol research, including India.

Kimmo Teinilä is working as a Senior Research Scientist at the Aerosol Composition Research Group, Finnish Meteorological Institute, Helsinki, Finland. His research interests include ambient aerosol measurements, especially particle chemical composition measurements.

Hilkka Timonen is a Senior Scientist and a Leader of the Aerosol Composition Research Group, Finnish Meteorological Institute, Helsinki, Finland. She has long-term experience on chemical and physical characterization of ambient aerosol as well as emissions originating from different anthropogenic emission sources.

Eija Asmi received the Ph.D. degree in aerosol physics from the University of Helsinki, Helsinki, Finland, in 2010.

She has been a Senior Scientist and the Head of the Group Aerosols and Climate, Finnish Meteorological Institute, Helsinki, since 2008. Her main research interests are aerosol particle climate impacts. She is a specialist on in situ experimental studies of absorbing aerosols and aerosol–cloud interactions.

Banwari Lal is currently heading the Environmental and Industrial Biotechnology Division in the capacity of Senior Director at The Energy and Resources Institute (TERI), New Delhi, India. He is also the Managing Director at ONGC TERI Biotech Ltd (OTBL), New Delhi, a joint venture of ONGC and TERI. He is having more than 35 years of research experience in the field of petroleum biotechnology. He has developed three technologies, namely, "oilzapper (for bioremediation of oil spill)," "microbial enhanced oil recovery," and "prevention of paraffin deposition in oil well tubing and flow lines." All the three technologies are patented and commercialized.

Sampsa Martikainen is pursuing the Ph.D. degree with the Aerosol Physics Laboratory, Faculty of Engineering and Natural Sciences, Tampere University, Helsinki, Finland.

His research is on engine emissions, focusing especially on the smallest particles.

Jorma Keskinen is the Head of the Aerosol Physics Laboratory, Faculty of Engineering and Natural Sciences, Tampere University, Helsinki, Finland. His research interests cover aerosol measurement techniques, emissions of engines, vehicles, and ships—especially nanoparticles, volatility, and secondary aerosol formation potential.

Panu Karjalainen is a Senior Research Fellow at the Institute for Advanced Study and the Aerosol Physics Laboratory, Faculty of Engineering and Natural Sciences, Tampere University, Helsinki, Finland. His experimental research focuses on aerosol measurement method development and in-depth characterization of emission aerosols.

Topi Rönkkö is the Leader of the Aerosol Emissions and Air Quality Research Group, Aerosol Physics Laboratory, Faculty of Engineering and Natural Sciences, Tampere University, Helsinki, Finland. His research focuses on particle emissions from anthropogenic sources and their effects on air quality, human health, and climate.